ON THE DYNAMICS OF SHALLOW WATER CURRENTS IN

MASSACHUSETTS BAY AND ON THE NEW ENGLAND CONTINENTAL SHELF

by

BRADFORD BUTMAN

A.B., Cornell University
(1969)

SUBMITTED IN PARTIAL FULFILLMENT OF THE
REQUIREMENTS FOR THE DEGREE OF
DOCTOR OF PHILOSOPHY

at the

MASSACHUSETTS INSTITUTE OF TECHNOLOGY

and the

WOODS HOLE OCEANOGRAPHIC INSTITUTION

April, 1975

Signature of Author..
          Joint Program in Oceanography, Massachusetts Institute
          of Technology - Woods Hole Oceanographic Institution,
          and Department of Earth and Planetary Sciences, and
          Department of Meteorology, Massachusetts Institute of
          Technology, April, 1971

Certified by..
                                                  Thesis Supervisor

Accepted by...
          Chairman, Joint Oceanography Committee in the Earth
          Sciences, Massachusetts Institute of Technology -
          Woods Hole Oceanographic Institution

ON THE DYNAMICS OF SHALLOW WATER CURRENTS IN
MASSACHUSETTS BAY AND ON THE NEW ENGLAND CONTINENTAL SHELF

BRADFORD BUTMAN

Submitted to the Massachusetts Institute of
Technology — Woods Hole Oceanographic Institution
Joint Program in Oceanography on April 7, 1975, in
partial fulfillment of the requirements for the degree
of Doctor of Philosophy.

ABSTRACT

Massachusetts Bay is a coastal Bay 100 km long and 40 km wide
located in the western Gulf of Maine. The Bay is closed by land to
the north, west and south, but is open to the Gulf to the east; the
opening is partially blocked by a shallow bank. The bottom sediment
distribution in the Bay is complex; fine grained material is found
in the deep basin, sand and gravel on the shallow bank, and mixtures
of sand, gravel and fine material nearshore. Richardson current
meters were moored 1 m from the bottom over a one year period at
several locations in the Bay to study the bottom currents and the
equilibrium between current and sediments. The current measurements
suggest that the bottom sediments can be expected to move only
occasionally in certain areas. The maximum bottom speeds are prin-
cipally determined by the strong tidal currents in the basin.

In winter, the near bottom currents are dominated by wind stress
associated with strong storms. Bottom currents in the shallow areas
are generally in the direction of the wind while currents in the deep
portion of the basin are often opposite to the direction of the wind.
Sea surface setup in the direction of the wind is observed, as well as
absolute changes in sea level as the Bay adjusts to changes in the
level of the adjacent Gulf of Maine. Adjustment of the bottom currents
to wind events requires approximately 12 hours.

Moored current meter measurements and synoptic hydrographic
observations made in Massachusetts Bay show that freshening from the
spring runoff dominates the low frequency currents and the hydrography
of the Bay in the spring months. The major freshening is attributed
to the Merrimack River which empties into the Gulf of Maine 30 km to
the north of the Bay; discharge of the Merrimack increases by at least
a factor of two in spring. Flow directly into the basin from several
smaller rivers is not important. Two major features are found: a
fresh surface plume confined to the upper 10 m of the water column
which becomes more distinct as the seasonal thermocline develops, and
a large deep fresh lens. Flow is clockwise around the deep lens and
is consistent with the thermal wind relation. Sustained currents of
10 - 20 cm sec^{-1} with time scales of 5 - 10 days were observed as the
deep lens (or lenses) slowly advected through the basin. Current
observations made in the previous spring show similar low frequency
behavior.

Two simple linear models of the semidiurnal tide on the continental shelf are used to estimate the vertical turbulent eddy viscosity, a linear bottom drag coefficient, and the change in the bottom drag coefficient during storms. The analytic solution for the response of a homogeneous water column with constant eddy viscosity to a sinusoidal body force with a slip bottom boundary condition is presented. With measurements of the tidal current at two depths, four parameters are shown to be independent of the body force: the ratio of the clockwise current at two depths, the ratio of counterclockwise current at two depths, the change in the tidal ellipse orientation, and the change in phase of the tidal ellipse. Observations of the semidiurnal tidal current on the New England continental shelf are consistent with a vertical eddy viscosity of 20 - 50 cm^2sec^{-1} and a bottom drag coefficient of .02 - .05 $cm\ sec^{-1}$. The Ekman depth is thus 10 m and the integrated adjustment time is approximately 28 hours.

An integrated linear model with linear damping of the semidiurnal tide on the continental shelf, forced uniformly at the shelf edge, shows an increasing phase lag of the tide at the coast with increased damping; amplitude remains relatively constant over a wide range of damping coefficient. Observations of the tide at the coast during storms shows a phase lag of as much as 10 degrees for the semidiurnal tide. For approximate dimensions of the New England shelf, this implies an increase by a factor of 3 - 5 of the bottom drag coefficient and an integrated motion adjustment time of 6 - 9 hours. Waves may be an important contribution to the increased bottom stress.

Thesis Supervisor: Dr. Robert C. Beardsley
Associate Professor of Oceanography
Massachusetts Institute of Technology

ACKNOWLEDGMENTS

TABLE OF CONTENTS

LIST OF FIGURES

LIST OF TABLES

INTRODUCTION

This thesis investigates several physical processes which are important in the dynamics of currents in shallow water. Among oceanographers, coastal or continental shelf oceanography has generally been of less interest than study of the deep oceans. However, the need to understand the biological and physical environment of the nearshore coastal areas has increased in the last several years as use and development of coastal resources have grown. To assess the environmental consequences of these activities requires knowledge of the processes which mix and transport substances in the water and on the bottom.

Perhaps the slow development of coastal physical oceanography is a result of the complexity of the coastal physical environment. In shallow water meteorological forcing (heating, cooling, and wind stress), the physical boundaries of the coast and bottom topography, the flux of fresh water from rivers, and the fluxes of mass and momentum at the shelf boundary will be important factors affecting the currents. On the northeast coast of the United States, much of our knowledge of the circulation has come from studies of drift bottle and seabed drifter returns (Bumpus, 1973) which do not adequately resolve short time and space scale phenomena. However, short time scale (periods of days) and space scale (horizontal scales of several tens of kilometers) currents associated with meteorological forcing or with the seasonal density distribution may in fact dominate the nearshore flow. The objective of this thesis is to identify, describe and understand several of these short time and space scale physical processes.

Chapter One, prepared in collaboration with Dr. John Schlee of the
U.S. Geological Survey, reports the results of a study of the equilibrium
between the near bottom currents and the bottom sediments and the factors
which drive the bottom currents in Massachusetts Bay, a semi-enclosed basin
located in the western Gulf of Maine. Bottom currents were monitored over
a one year period using Richardson current meters in areas of widely
different bottom sediment types. The study suggests that the bottom sedi-
ments can be expected to move only occasionally in certain areas, and that
the strong tidal currents in the Bay basically determine the bottom current
speed. Strong storms dominate the net near bottom flow pattern in winter.

Chapter Two is a study of the current and density distribution in
Massachusetts Bay during the period of the spring runoff. The Bay is
located 30 km from a major river which discharges into the western Gulf
of Maine. Synoptic hydrographic observations and moored current measure-
ments show that the low frequency current in the spring months is primar-
ily driven by the strong density gradients associated with the increased
spring river discharge and that winds are not important.

Chapter Three is a study of the effects of friction on the currents
on the New England continental shelf, and on the parametrization of the
frictional effects. Two simple dynamical models appropriate for winter
conditions are developed and used to estimate a bottom drag coefficient
and a vertical eddy viscosity, and the change in the bottom drag coeffi-
cient during storms. The bottom drag coefficient determines the bottom
stress for a given current and thus specifies the adjustment or decay time
for integrated motions on the shelf, while the value of the vertical eddy
viscosity determines the vertical distribution of the stress.

A brief chronology of this thesis work explains the author's
interest in these aspects of the physical oceanography of Massa-
chusetts Bay and the continental shelf. When I began thesis work in
1972 I was particularly interested in the field of coastal oceanography
and especially in field observations of important time dependent processes;
unfortunately there was little ongoing research within the community. At
that time, Dr. John Schlee of the U.S. Geological Survey was conducting a
survey of bottom currents in Massachusetts Bay as an extension of his work
on the bottom sediment distribution. I had worked with Dr. Schlee on the
currents in Massachusetts Bay in preparation for this monitoring program,
and he kindly allowed me to work with the bottom current records.
Chapter I presents the results of the bottom monitoring experiment.

The spring current records from the monitoring experiment and
historical data suggested that the freshening associated with the spring
runoff strongly influenced the hydrography and currents in Massachusetts
Bay in spring, and was an important physical process. To study the
importance of the spring runoff in the low frequency currents, a field
experiment was conducted in the spring of 1973 using moored current meters
and hydrographic observations (Chapter II).

At the same time, the author conducted a pilot experiment with
Prof. R.C. Beardsley on the continental shelf to study the response to
strong winter storms, and to test the feasibility of making current
measurements on the continental shelf using similar mooring techniques as
used in Massachusetts Bay (Beardsley and Butman, 1974). It was clear from
that experiment and from my work on the wind driven currents in Massachu-
setts Bay that an estimate of frictional effects was important in under-

standing shallow water currents. Similar work had been begun using Massachusetts Bay data, but the shelf presented a less complicated geometry with which to work. Dr. Beardsley kindly allowed me to use data from a second more extensive shelf experiment conducted in late winter of 1974 to estimate the vertical eddy viscosity and the bottom drag coefficient using an Ekman model of the bottom boundary layer.

CHAPTER I

NEAR BOTTOM CURRENTS AND THE SEDIMENT DISTRIBUTION

IN MASSACHUSETTS BAY

A. Introduction

Massachusetts Bay and its southeast extension, referred to as Cape

Cod Bay, are bounded on three sides by the Massachusetts coast and open

to the Gulf of Maine on the northeast between Cape Cod and Cape Ann

(Figure 1.1). The opening is partially blocked by Stellwagen Bank which

rises to within 20 m of the surface. Stellwagen Basin, located in the

center of Massachusetts Bay, has a maximum depth slightly in excess of

100 m, though most is about 80 m deep. Depth changes in Cape Cod Bay,

Stellwagen Basin, and on Stellwagen Bank occur gently (grades of .1 - .5%),

except on the western side of Stellwagen Bank (grades of 6%). In contrast,

the bottom along the western side of the Bay from Cape Ann to Plymouth

(42°20'N 70°40'W) is hummocky and rough with depth changes of 5 m in .1 km

(see C&GS chart No. 0808N-50 Cape Cod to Cape Ann).

Although complex, the bottom sediment distribution can be grouped

in four categories by location and sediment type (Schlee and others, 1973;

Oldale and others, 1973; Tucholke and others, 1972). Nearshore adjacent

to the rocky coast from Cape Ann to Plymouth the rough bottom is a patch-

work of gravel, sand, mud, and bedrock, while adjacent to constructional

features (outwash and moraines) from Plymouth around Cape Cod, the

generally smooth bottom is well sorted sand mixed with gravel. Offshore,

the shallow bank is well sorted sand, or sand and gravel. Finest grained

sediment of clay, silt and sand is found in the deep basin and in the

Figure 1.1 Map of Cape Cod and Massachusetts Bays. Smoothed 40 and
            80 m contours show major bathymetric features (Plymouth
            located 42°20'N 70°40'W).
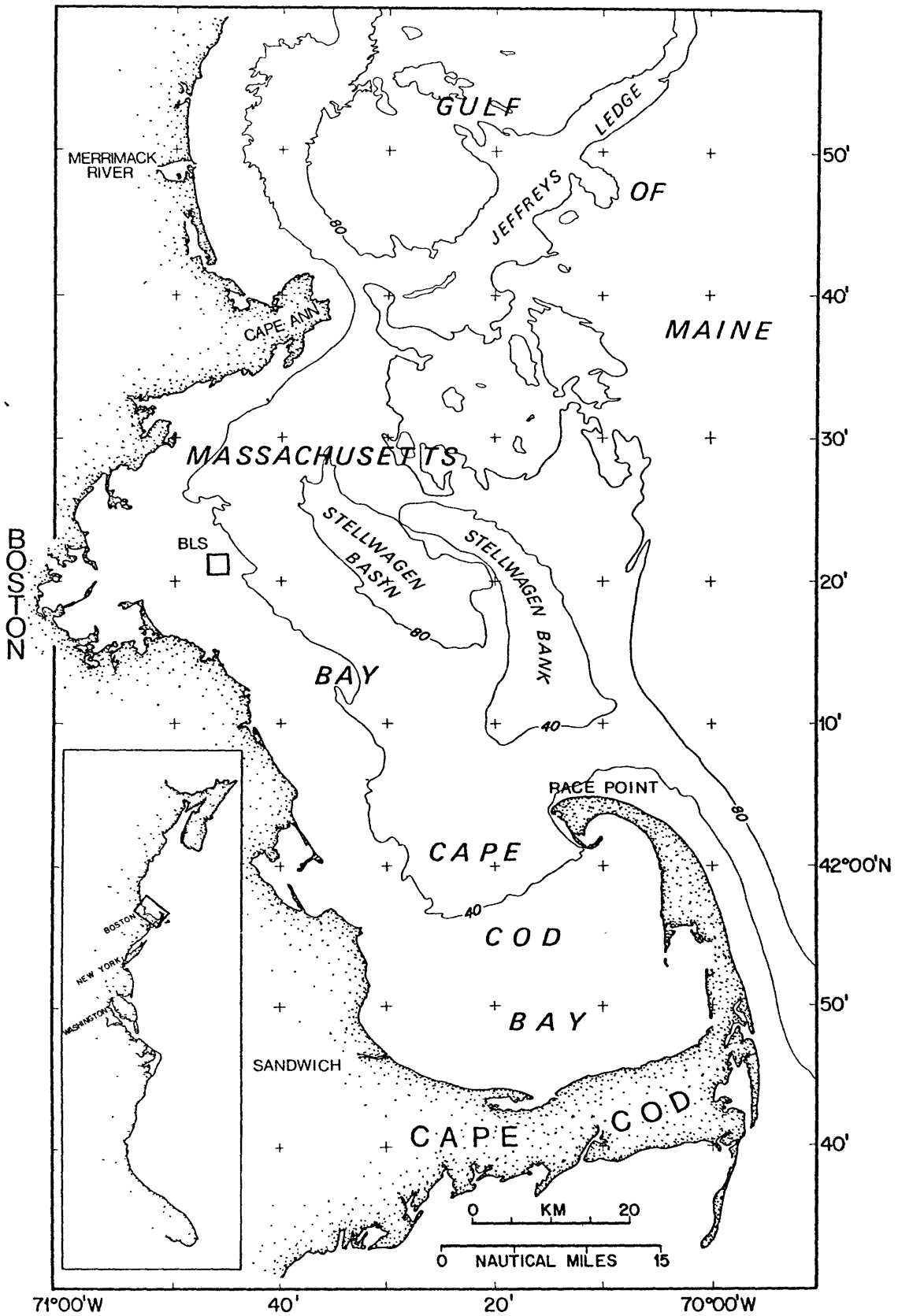
Figure 1.1

Figure 1.2 Bottom sediment distribution (percent by weight) in
            Massachusetts and Cape Cod Bays, after Schlee and
            others (1973).

    a)   Percent sand (2.00 - .062 mm).

    b)   Percent silt (.062 - .004 mm).

Figure 1.2

19
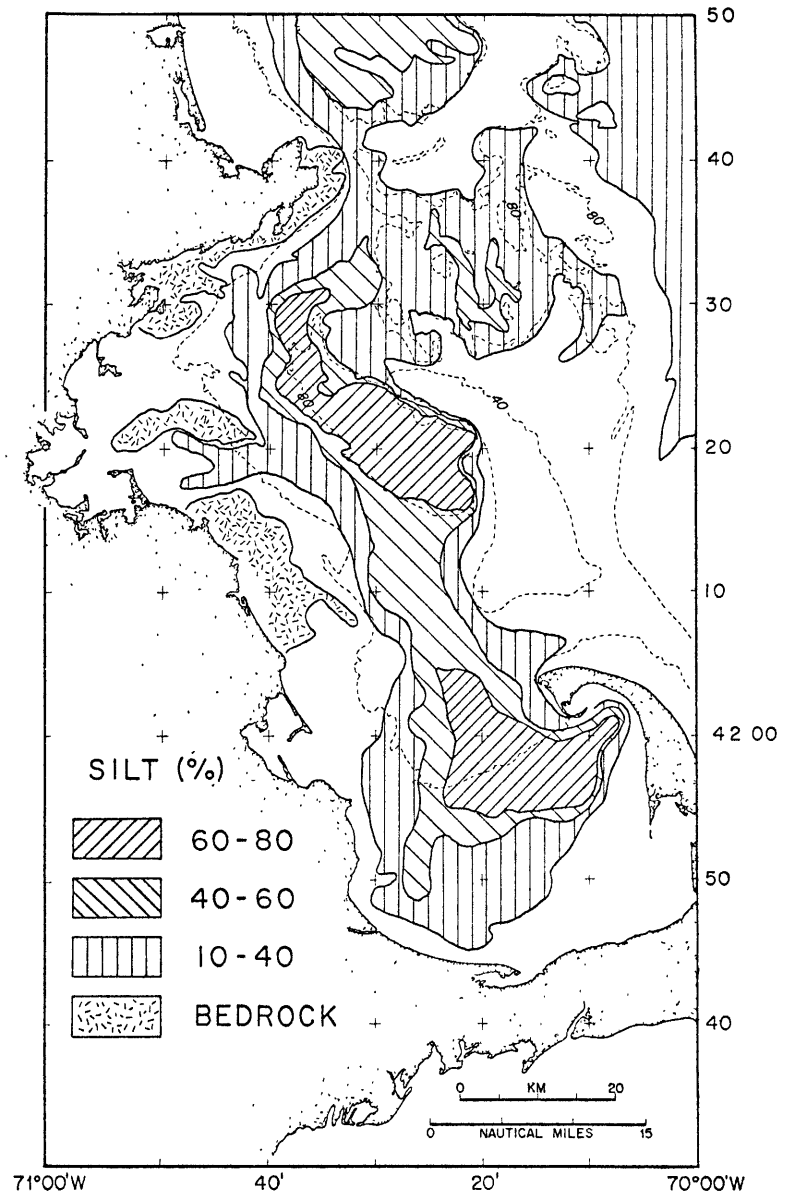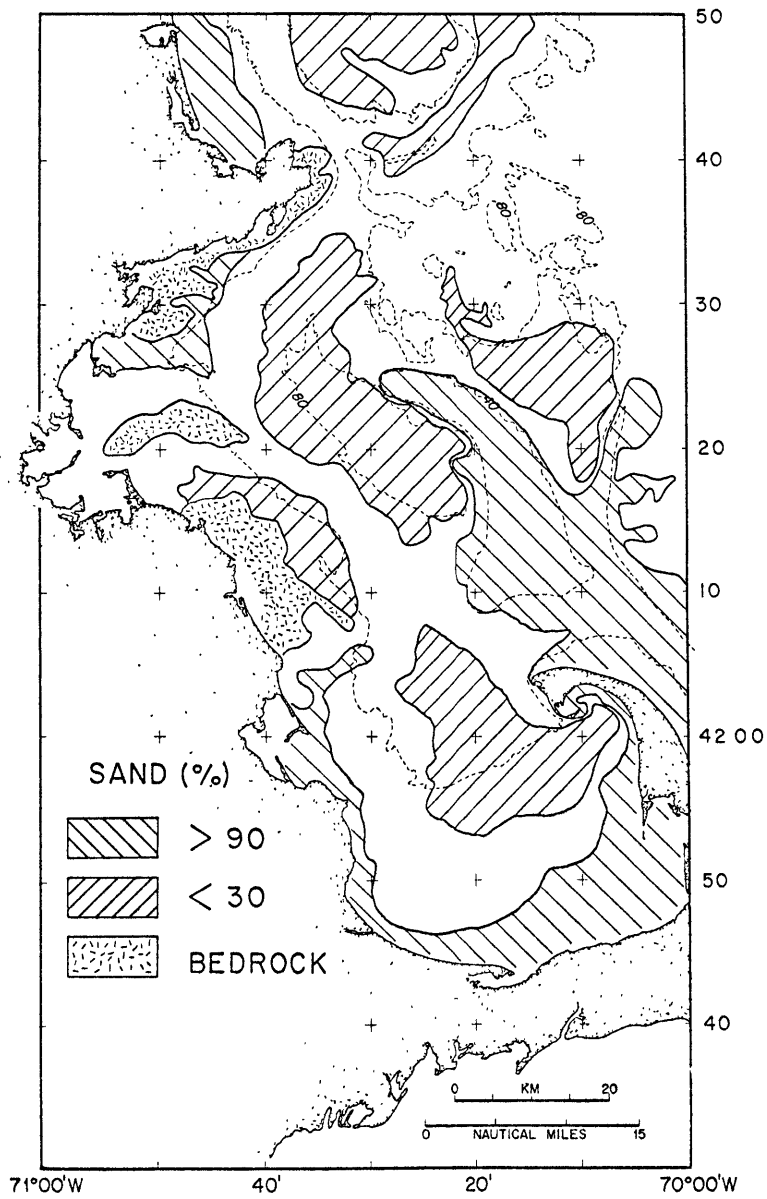
channels entering the Bay (figure 1.2).

In general, the bottom sediment distribution will reflect the present and long term environmental conditions which have deposited, reworked and redistributed existing material (for example, studies by Kranck, 1972), and the diverse agents (ice, rivers, etc.) which have deposited the sediment under entirely different geologic conditions from those of today. The glaciation of the New England coast and the subsequent rise of sea level formed the major bathymetric features and sediment deposits in Massachusetts Bay (Oldale and others, 1973; Tucholke and Hollister, 1973). The accumulation of fine sediments in the deep basin is attributed to winnowing of material from the topographic highs and nearshore and redeposition in the basins, most of the deposition occurring just after glacial retreat. The sedimentation rate has steadily decreased as these sources have become less important and is estimated currently to be 1 - 2 cm per thousand years (Tucholke and Hollister, 1973).

With such a complex sediment distribution and bottom topography, two questions arise: (1) Does movement of the bottom sediment occur in Massachusetts Bay under present conditions and if movement does occur, where and how frequently? (2) What is the pattern of bottom water movement in the Bay which might redistribute sediment if eroded and what are the major factors which drive the bottom currents? This chapter reports the results of a monitoring survey of the bottom currents in Massachsetts Bay using moored current meters. A brief review of the bottom boundary layer is presented, followed by a description of the field experiment.

The equilibrium between bottom sediments and bottom currents at the monitoring locations in the Bay is discussed next. Finally, winds were found to be a major factor in generating net bottom flow in winter, and the bottom flow pattern and associated sea level adjustment in Massachusetts Bay during strong winter storms is presented.

B. The Bottom Boundary Layer and Incipient Sediment Motion

A vast literature exists on the benthic boundary layer and processes of sediment motion and transport. (A review article by Wimbush and Munk (1971), work of Weatherly (1972), and a collection of articles edited by Swift, Duane and Pilkey (1972) were found useful references.) For this study of the adjustment of bottom sediments to currents, an estimate of the stress required to erode the existing material and a method to determine the bottom stress occurring in the marine environment is needed.

Field and laboratory studies have shown that the velocity profile in the bottom boundary layer is logarithmic, extending 1 - 4 m from the bottom (Sternberg, 1971, 1972; Miller and others, 1972; Weatherly, 1972). Thus

$$u(z) = \frac{u^*}{\kappa} \ln (z/z_o) \, , \tag{1}$$

where

κ = VonKarman's constant = .4 ,

u^* = friction velocity = $(\tau/\rho)^{\frac{1}{2}}$,

τ = bottom stress,

z_o = roughness length,

z = height from bottom.

The value of z_o is found empirically to vary with flow characteristics. Specifically, the value of z_o depends on the relative size of the laminar

sublayer and the roughness elements (d) of the boundary. The depth of the laminar sublayer is

$$\delta_\ell \simeq \frac{12\nu}{u*} , \qquad \nu = \text{kinematic viscosity} \quad cm^2 sec^{-1} \quad .$$

For hydrodynamically smooth flow, the roughness elements are enclosed completely within the laminar sublayer, while for rough flow the layer is disrupted by the roughness elements. The conditions for smooth or rough flow are summarized in Table 1.1. For a smooth bottom, velocity measurements at a single height will give an estimate of $u*$ but for a rough bottom an estimate of z_0 is also required. Alternatively, for measurements at a fixed height above the bottom (1) can be written as

$$u*^2 = \rho \ C_D \ u^2 ,$$

where C_D is a property of the bottom roughness and is empirically determined. The drag coefficient is larger for rough bottoms than for smooth bottoms.

Measurements of the logarithmic bottom layer, particularly those of Sternberg (1971) and Weatherly (1972), have shown considerable variability in estimates of z_0. Variability decreased if the velocity profile was averaged over longer times (Weatherly, 1972). It may be that the roughness height is not a physical property of bed, but more a property of the fluid flow. Despite these rather serious reservations, estimates of the bottom stress will be made using bottom photographs to determine roughness, and (1).

Empirical curves of the bottom velocity (Sundborg, 1956; Allen, 1965), or of the bottom stress (Inman, 1963; Bagnold, 1962) required to erode well sorted sediment of a given grain diameter and density have been found to agree roughly with field measurements in a tidal channel (Sternberg,

TABLE 1.1

CONDITIONS FOR FLOW OVER SMOOTH AND ROUGH BOTTOM

<u>Smooth Bottom</u>

$d < \dfrac{4\nu}{u^*}$

$z_0 \sim \dfrac{.1\nu}{u^*}$

$u(z) = \dfrac{u^*}{\kappa} \ln \left(\dfrac{zu^*}{.1\nu}\right)$

<u>Rough Bottom</u>

$d > \dfrac{40\nu}{u^*}$

$z_0 \sim d/30$

$u(z) = \dfrac{u^*}{\kappa} \ln (z/z_0)$

d = characteristic roughness element height

ν = kinematic viscosity

z = height from bottom

z_0 = effective roughness

u^* = friction velocity

κ = VonKarman's constant

1971; Miller and others, 1972). The bottom stress required for movement
is a minimum in the sand range (.1 - 1 mm diameter) and is about 4 dynes
($u*$ = 2 cm sec^{-1}); larger stress is required to move coarser material
($u*$ = 8 cm sec^{-1} for diameter 1 cm). For material in the silt and clay range,
the stress required for incipient movement depends on the degree of
consolidation or 'age' of the sediment after deposition (Postma, 1967;
Southard, Young, Hollister, 1971). The curves of Inman suggest a $u*$
of at least 4 cm sec^{-1} is required to erode consolidated silts and clays,
but there is little experimental data; one exception is the laboratory
study of Southard, Young, Hollister (1971), where a $u*$ of 1.37 cm sec^{-1}
was required to move a deep sea mud.

If the bottom boundary layer is sufficiently turbulent deposition
of fine grained material will not occur, or will be resuspended immediately.
The Sundborg curve indicates no deposition of material less than .05 mm
in diameter (silt) for velocities of 1 cm sec^{-1}. McCave (1972), summa-
rizing laboratory studies, reports deposition of fine material will not
occur for $u*$ in the range of .6 - .9 cm sec^{-1}.

It must be emphasized that the effects of cohesion, biological
reworking and resuspension, aging after deposition, bed form and sorting
on conditions for incipient sediment motion are not well understood.
Rhoads and Young (1971) show intense biological reworking and resuspen-
sion of fine grained bottom sediment in Cape Cod Bay, and biological
activity may be a significant factor in Massachusetts Bay. Also, bedform
contributes to measured shear stress, not just grain diameter. Despite
these problems the approximate bottom stress and velocities required for
incipient motion of material in the sand, silt and clay, and gravel range

TABLE 1.2

ESTIMATES OF BOTTOM STRESS REQUIRED FOR INCIPIENT

SEDIMENT MOTION AND DEPOSITION.

	Required Friction Velocity (U*) cm/sec	Speed 100 cm from bottom[2] cm/sec		
		Smooth	Rough	
Incipient Motion[1]			(a)	(b)
Sand, recently deposited silt and clay	2	61	40	32
Consolidated silt and clay	4	129	80	64
Gravel (1 cm diameter)	8	272	160	128
Deposition[3]				
Silt and clay	.6 - .9	17-26	12-18	10-14

[1]Estimated from Inman (1949), reproduced in Miller and others (1972); Southard, Young and Hollister (1971), Postma (1967).

[2]Velocities estimated from equation 1.1 . For a rough bottom two roughness heights are used: a) d = 1 cm, b) d = 5 cm (z_o = d/30). All estimates to nearest cm/sec.

[3]Estimates from McCave (1972).

are estimated (Table 1.2) using the logarithmic law (1). The estimates

in the sand and gravel range are probably fairly accurate while the

estimates for finer material are somewhat uncertain, primarily because

of uncertainty in the degree of consolidation and cohesion of the sediments

and lack of laboratory and direct field erosion data. Although stress and

velocity estimates in Table 1.2 should be viewed as approximate, they

should provide useful ranges of erosion velocities for this study.

C. Field Program

1. Bottom Current Monitoring

Measurements of the near bottom currents were made in Massachusetts

Bay from May, 1971 through July, 1972 at several locations (figure 1.3)

which were selected to define the bottom current pattern in Massachusetts

and Cape Cod Bays, if possible, and to measure the currents over various

types of bottom sediments. Stations A and F were placed to monitor flow

in the two channels leading into Stellwagen Basin; stations B and E were

selected to monitor circulation on the coastal shelf. Station C was placed

in Stellwagen Basin, and station D was placed to monitor on Stellwagen Bank,

Stations A, C and F are in areas of fine sediments, while B, D and E are in

areas with coarser bottom material. A current meter was deployed through-

out the study at the Boston Lightship to provide continuous measurements at

one location. It was hoped to obtain a one month bottom current record

each season at stations A-F, however temporary loss of one current meter

and malfunctions prevented this objective. The latitude and longitude of

the stations and the dates of the successful measurements are listed in

Appendix A . The time sequence of current meter deployments is shown in

figure 1.4.

Figure 1.3 Location of bottom current monitoring stations and
            bottom photographs.

STATION LOCATIONS

● BOTTOM MOORINGS

▲ PHOTOGRAPHS
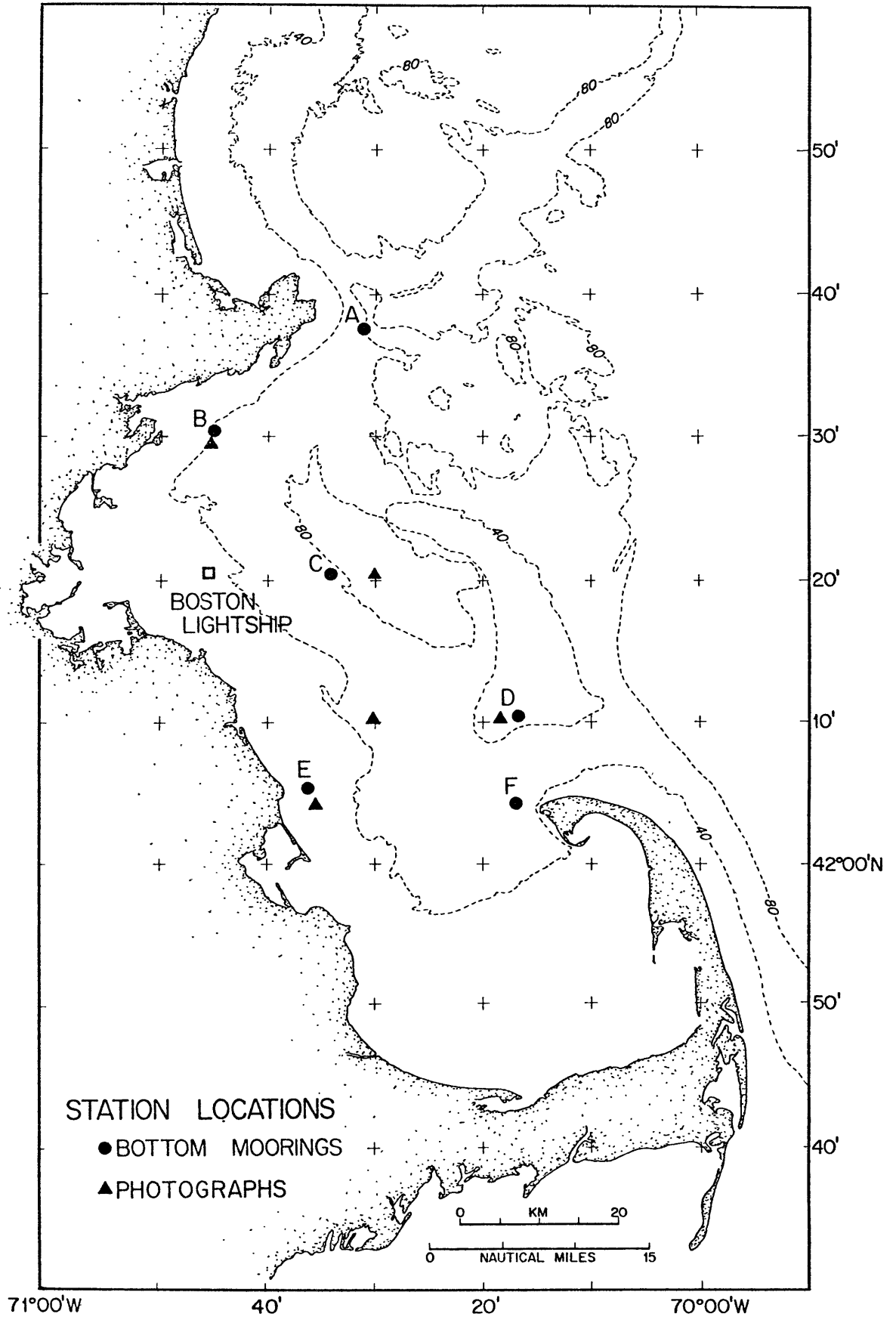
Figure 1.3

Figure 1.4   Schedule of current meter deployment in Massachusetts
            and Cape Cod Bays. Records are numbered sequentially
            at each station and dashed lines indicate records with
            inaccurate sampling rate and time base. See figure 1.3
            for station locations.
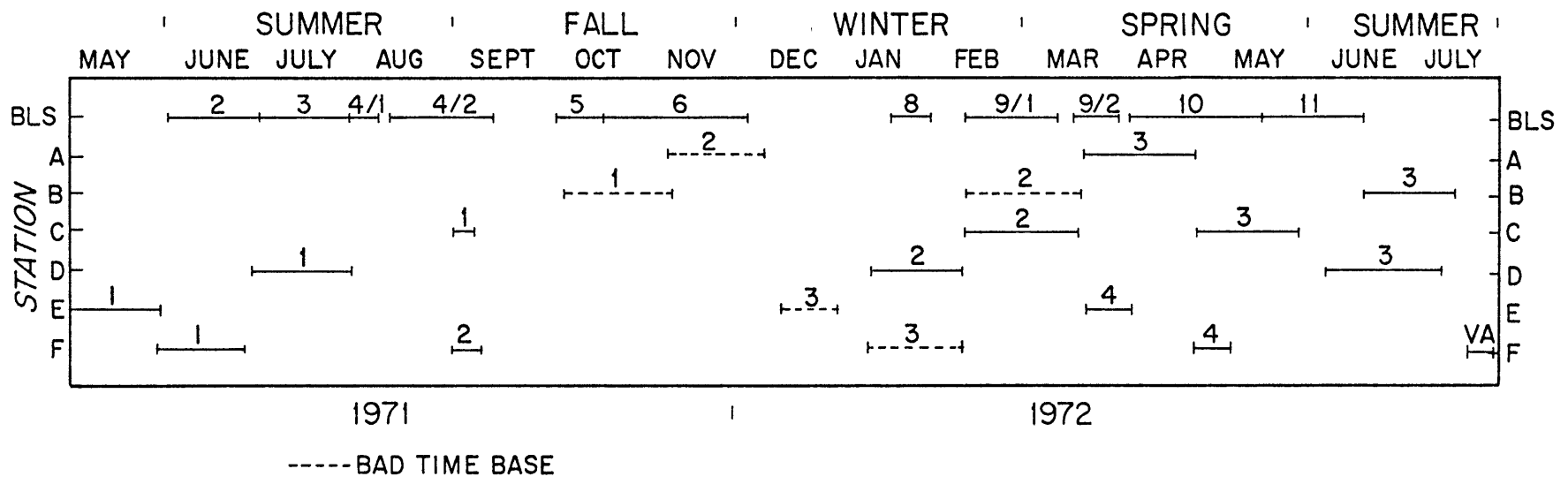
Figure 1.4

The current meters at stations A-F were moored 1 m from the bottom, with all floatation within approximately 5 m of the bottom (figure 1.5). The mooring was designed with groundlines on either side of the main anchor to facilitate recovery of the instrument if the surface marker was lost, and a small acoustic beacon was attached to the meters to aid in locating the instrument. The Boston Lightship meter was suspended from the lightship approximately 8 m from the bottom. One Geodyne model 850 and the two model 102 Richardson type current maters were used in the survey; the 850 current meter was deployed continuously from the Boston Lightship, while the 102 meters were rotated among the offshore stations. No current meters were permanently lost during the program, and approximately 60% of the instruments returned useable data. Instrument malfunction occurred in the 102 current meters which record on film, and was due to film advance problems, malfunction of the circuitry, or to an inaccurate time base. The 850 current meter was found extremely reliable.

2. Bottom Sediment Composition and Texture Near Current Meter Stations

Grain size analysis of the bottom sediment near the current meter stations (Table 1.3) was obtained from an earlier sediment survey (Schlee and others, 1973; Hathaway, 1971). Most of the samples are sandy silt or sand, except at station E where there is a large amount of gravel. At the deeper stations (A,C,F) the bottom composition is similar: 44-47% sand, 32-39% silt, 16-19% clay. At station B and D, the bottom is sand or sand and gravel.

Bottom photographs (see figure 1.2 for locations) obtained from previous studies clearly show the different bottom sediments, sorting and texture. Near Station B a thin layer of fine material overlies gravel

Figure 1.5 Schematic diagram of mooring for near bottom current
measurements.

CURRENT METER MOORING

SURFACE FLOAT

FLOATATION

CURRENT METER

GROUNDLINE   STIMPSON ANCHOR   GROUNDLINE
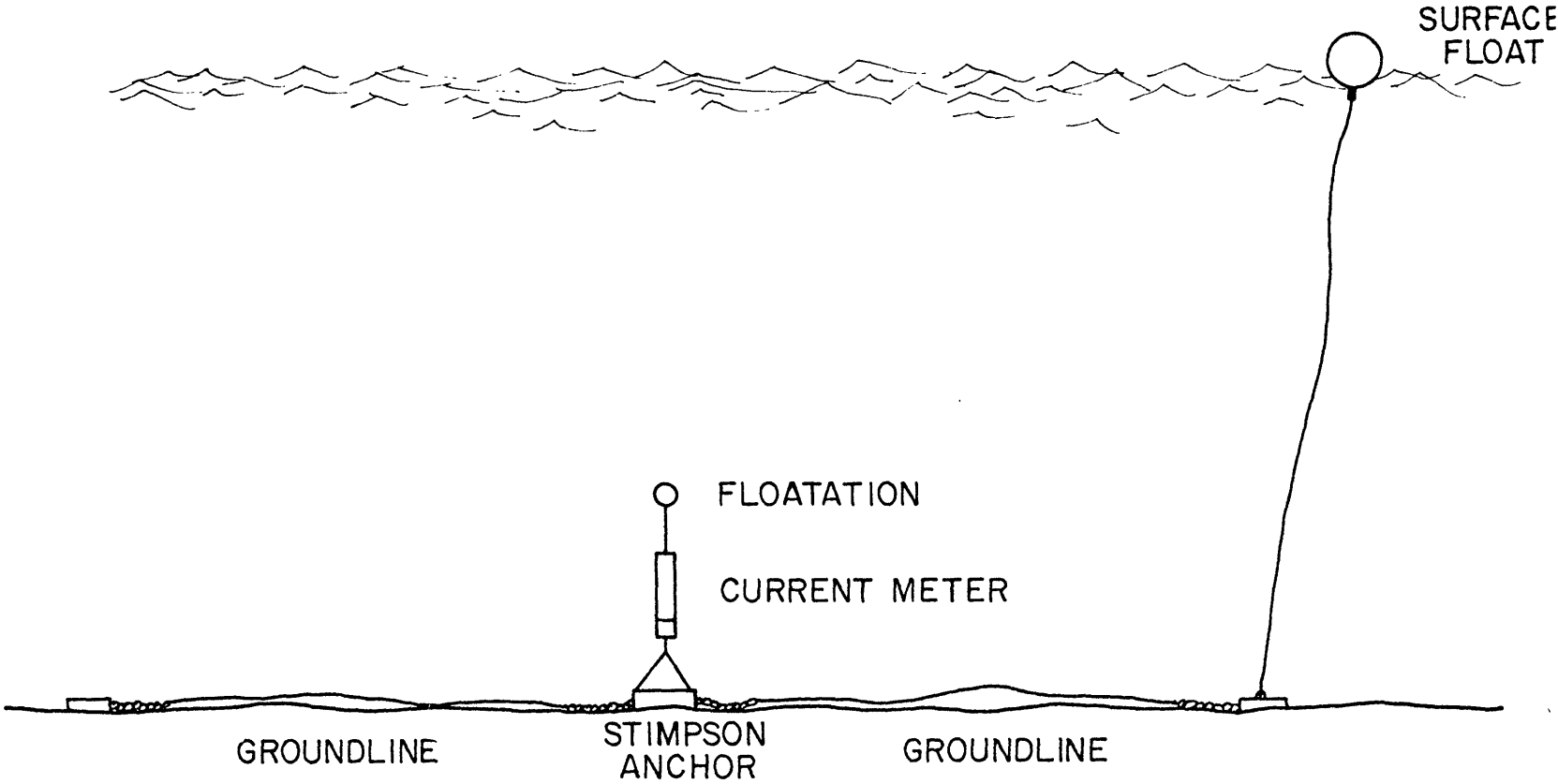
Figure 1.5

TABLE 1.3

SEDIMENT ANALYSES NEAR CURRENT METER STATIONS

PERCENT BY WEIGHT

STATION	GRAVEL[1]	SAND[2]	SILT[3]	CLAY[4]
A	0	49	32	19
B	13	76	10	0
C	0	47	37	16
D	1	99	0	0
E	94	6	0	0
F	1	44	39	16

[1]Gravel   > 2 mm.

[2]Sand   2.00 - .062 mm.

[3]Silt   .062 - .004 mm.

[4]Clay   < .004 mm.

and coarse sand (figures 1.6 a,b) suggesting little active current erosion. The two photographs at station B illustrate the typical patchiness of the bottom sediment distribution and the difficulty in estimating a meaningful roughness height in areas with poor sorting. In the deep basin (figure 1.6 c,d) the bottom is soft silt, sand and clay, much smoother than at station B (roughness elements less than 1 cm), and again there is little evidence for active erosion. In contrast, on Stellwagen Bank (station D, figure 1.6 e) there is no apparent fine material and ripple marks suggest active or recent erosion. Here an approximate roughness height is estimated to be 5 cm. At station E (figure 1.6 f) the bottom is coarse sand with no evidence of active erosion.

In summary, for the purposes of this study the bottom photographs suggest that the bottom in the deep basin (station C) should be considered smooth, while at stations B, D, and E the bottom is rough. No bottom photographs were available at stations A or F, but the bottom sediment is similar to station C suggesting that the bottom might be considered smooth.

D. Speed Statistics and Estimates of Bottom Sediment Movement

The stations may be grouped in three classes by the observed maximum speed and average speed (Table 1.4); the largest maximum and average speeds occur at stations D and F at the southern mouth of the Bay. Nearshore (stations B and E) the maximum and average speeds are weaker, while at the deep stations (A and C) the average speeds are similar to the nearshore stations, but the maximum speeds are somewhat less. The speed distribution in the basin is primarily controlled by the strength of the tidal current and the depth. At the mouth of the Bay the tidal currents are strong and the water is shallow so that wind generated currents and possibly waves contribute to the maximum speed. In the deep basin and on the shallow border of the Bay the tidal currents are substantially weaker, but maximum

Figure 1.6   Bottom photographs in Massachusetts Bay showing bottom
texture.

a)   Station 1200 (near current meter station B)
     42°29.8'N 70°44.7'W   43 m
     Grab sample description: grey silty fine sand
     Composition (%): gvl 13.4; sand 76.3; silt 10.4; clay 0.

b)   Second photograph at station 1200.

c)   Station 1202 (near current meter station C)
     42°20.6'N 70°30.0'W   91 m
     Grab sample description: grey clay
     Composition (%): gvl 0; sand 4.7; silt 49.3; clay 43.0.

d)   Station 1203
     42°10.1'N 70°30.2'W   55 m
     Grab sample description: 5 cm soft brown clay overlying
        stiff grey clay
     Composition (%): gvl 0; sand 39.0; silt 49.5; clay 11.7.

e)   Bottom photograph near station D.   Rod in picture
     approximately 1 m long.

f)   Bottom photograph near station E.

Photographs at stations 1200-1203 from continental margin study
(Hathaway, 1971).   Others from Dr. D. Cooper, U.S. National
Marine Fisheries Service, Woods Hole, Mass.
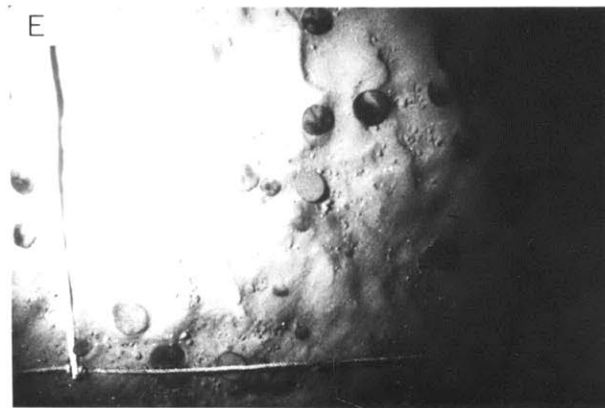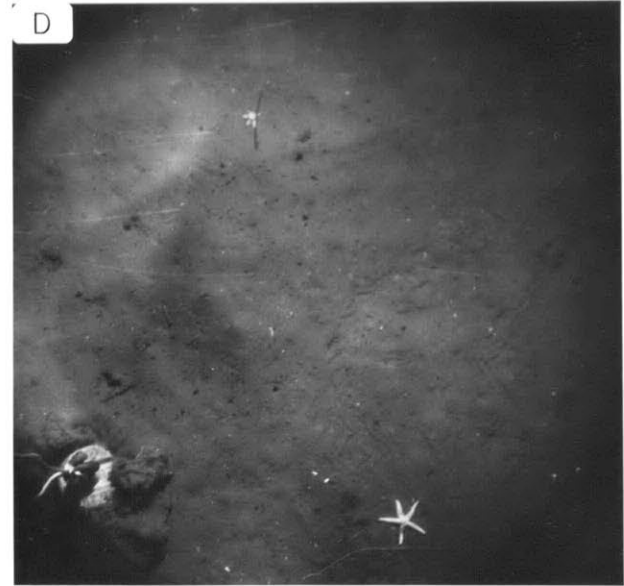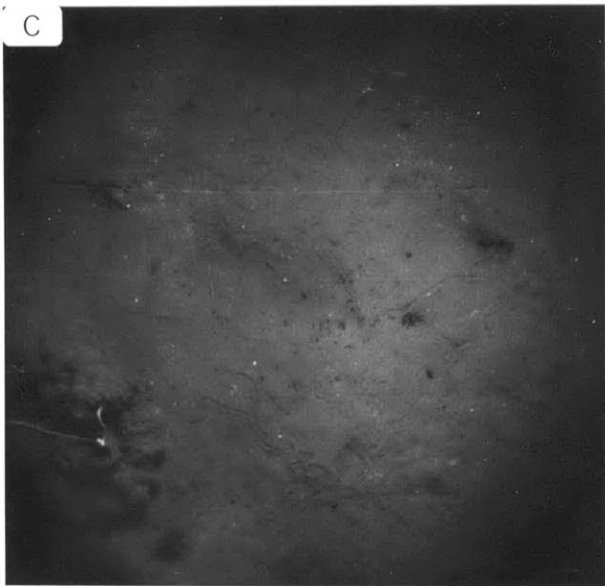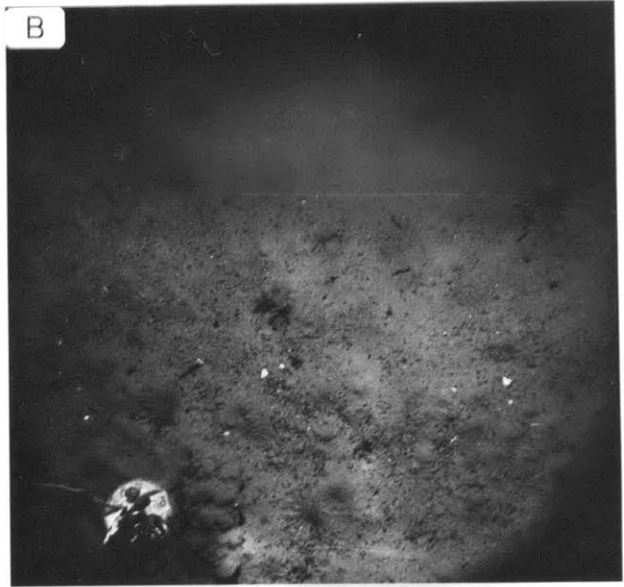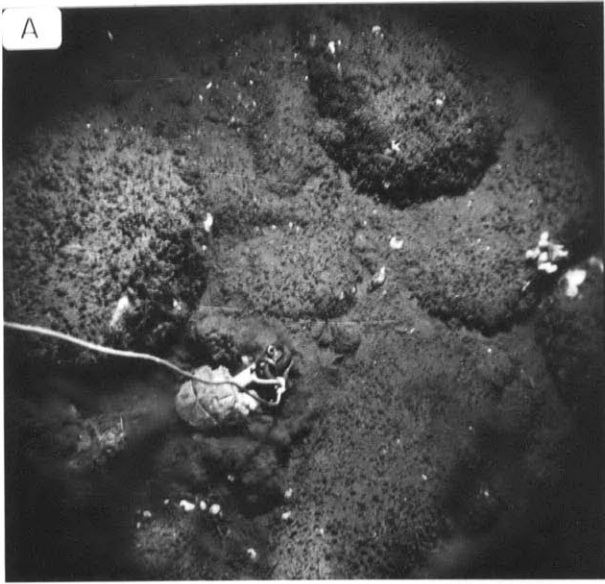
TABLE 1.4

RANGE OF SPEED STATISTICS FOR BOTTOM CURRENT RECORDS[1]

	A	B	C	D	E	F
Maximum Speed	24-34	25-43	26-29	32-47	29-37	35-47
Speed Exceeded 1% of Time	18	14	20	26-36	20-26	27-33
Speed Exceeded 5% of Time	12	10	12-13	23-29	17-21	24-28
Average Speed[2]	5.7	4.7	4.7-6.1	13.1-17.0	4.2-7.9	14.5-15.9
Stand. Dev.	3.2	3.8	3.0-3.5	5.2-8.1	4.2	5.5-7.7
No. Records, Time Base[3]	2,1	3,2	3	3	3,1	2
Days[4]	36	28	66	98	42	44
Semidiurnal Tide[5]						
Major	2.6	3.5	6.2	20.2	5.2	17.5
Minor	.1	2.6	1.2	-3.6	.4	2.2
Orientation	17	5	79	72	170	34

[1] Only records longer than 15 days included except for max. speed. Records not simultaneous, so not directly comparable. All numbers in cm sec^{-1}.

[2] Average speed and stand. deviation for vector averaged 1 hr. samples.

[3] Number of records included (first digit); number with time base error (2nd digit); only max. speeds tabulated for records with time base error.

[4] Total number of days excluding records with time base error.

[5] Computed from 15 day pieces; ellipse orientation with respect to north. Estimated error $\pm$.5 cm sec^{-1} in speed, $\pm5°$ in direction. Positive minor axis indicates vector rotates counterclockwise, negative clockwise.

speeds are larger in the shallow regions probably because of wind and wave action.

At station B, D, and F, the observed maximum speeds are above the estimated minimum critical erosion speeds (Table 1.2), assuming a rough bottom. None of the observed speeds are large enough to move sand if the bottom is smooth. At stations A and C, the maximum speeds are substantially below critical erosion speeds for consolidated or unconsolidated silt and clay. At all stations during most of the measurement period, the current speed was substantially less than the critical erosion speed, and thus bottom movement of sediments, if it occurs at all, is infrequent. There is some suggestion that the maximum bottom speeds occurred in the fall and winter months (Table 1.5); however the data is too sparse to make any generalizations with statistical reliability. The average current at stations D and F is sufficiently high to prevent deposition of fine material, while at the stations A,B,C deposition is possible 95% of the time.

A graph of median grain size versus the maximum one minute average current speed observed during each of the bottom current meter records (figure 1.6) shows that most of the points fall within the limits of the competency curves of Sundborg. It should be noted that these empirical curves do not take into account bottom roughness except through grain diameter. Only at station E do the values fall far below the competency curve, and this is because most of the sample used to characterize the bottom sediments at station E is gravel which is relict glacial material.

In summary in the well sorted sand regions (station B and D), we can expect occasional movement if the bottom is assumed to be rough with roughness elements of at least 1 cm. Estimates of critical erosion stress for the silt-sand bottoms are uncertain, but the data suggest that the

TABLE   1.5

MAXIMUM SPEEDS BY SEASON (cm/sec)

STATION	WINTER	SPRING	SUMMER	FALL
A		24		34
B	43		25	26
C	29	26		27
D	47		32,40	
E	37	29,37		
F	42	41	35	47

Figure 1.7 Maximum one minute average speed observed at current
meter stations A-F and Sundborg (1956) competency
curves (reproduced in Miller and others, 1972).
Note logarithmic velocity scale.
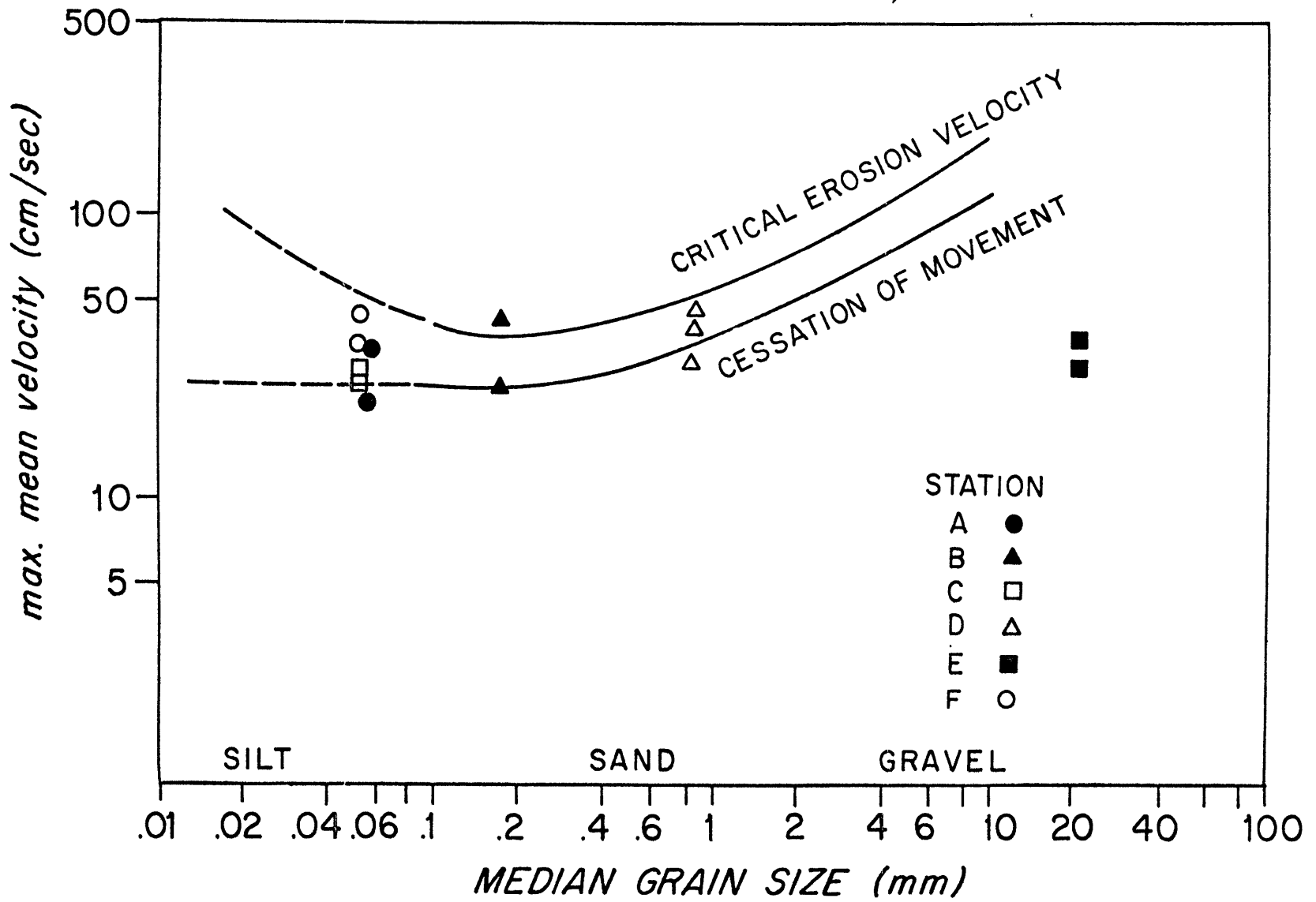
Figure 1.7

observed maximum speeds are not strong enough to move bottom material at

stations A and C. At station F where the bottom is also sandy silt it is

not possible to determine whether occasional incipient motion occurs if

the bottom is unconsolidated without additional information on critical

erosion stress of the material and bottom roughness. For a consolidated

bottom — hard packed clay material retrieved with the current meter

anchor suggests the bottom is consolidated — movement will not occur.

The distinction between smooth and rough bottom is important since at no

station was the maximum speed strong enough to move sand assuming a smooth

bottom. Stresses are low enough to allow deposition of fine material for

a large fraction of the time at stations A, B, C, and E but only for

shorter periods at stations D and F, primarily because of the large tidal

currents at the mouth of the bay.

E. Wind Driven Near Bottom Currents In Winter

One of the most striking features of the winter bottom currents is

that rapid changes in the direction and magnitude of flow occur on time

scales of 1 - 5 days (figure 1.8), with many of the changes associated

with strong wind events. Similar dominance of the low frequency currents

by wind stress on the continental shelf and Great Lakes has been noted

by Beardsley and Butman (1974), Csanady (1973a,b) and Blanton (1974)

among others. Theoretical and numerical studies of flow in closed basins

such as the Great Lakes (Rao and Murty, 1970; Bennett, 1974; Csanady, 1973a)

suggest that topographic variations in a long lake produce a 'two gyre'

flow pattern in response to wind along the major axis; flow is in the

direction of the wind in shallow areas and opposite to the wind in the

deep regions, the return flow being driven by a surface pressure gradient

or setup. The large depth changes and the semi-enclosed geometry of

Figure 1.8   Progressive vector diagram of current at station D
              in January and February, 1972. Two major departures
              from the net southwest flow on Jan. 25-26, and
              Feb. 3-6 are associated with winter storms.

    a)   Progressive vector diagram from hourly data.

    b)   Daily average current and wind stress.

N

0 ⸺⸺⸺⸺⸺⸺ 30

KILOMETERS

STATION D

72 – I – 13 TO 72 – II – 11

Figure 1.8a

KILOMETERS

STATION D

72 − I − 13   TO   72 − II − 11

WINDSTRESS (dynes)

- - - - → <1.0

———→ 1.0-2.0

———→ > 2.0
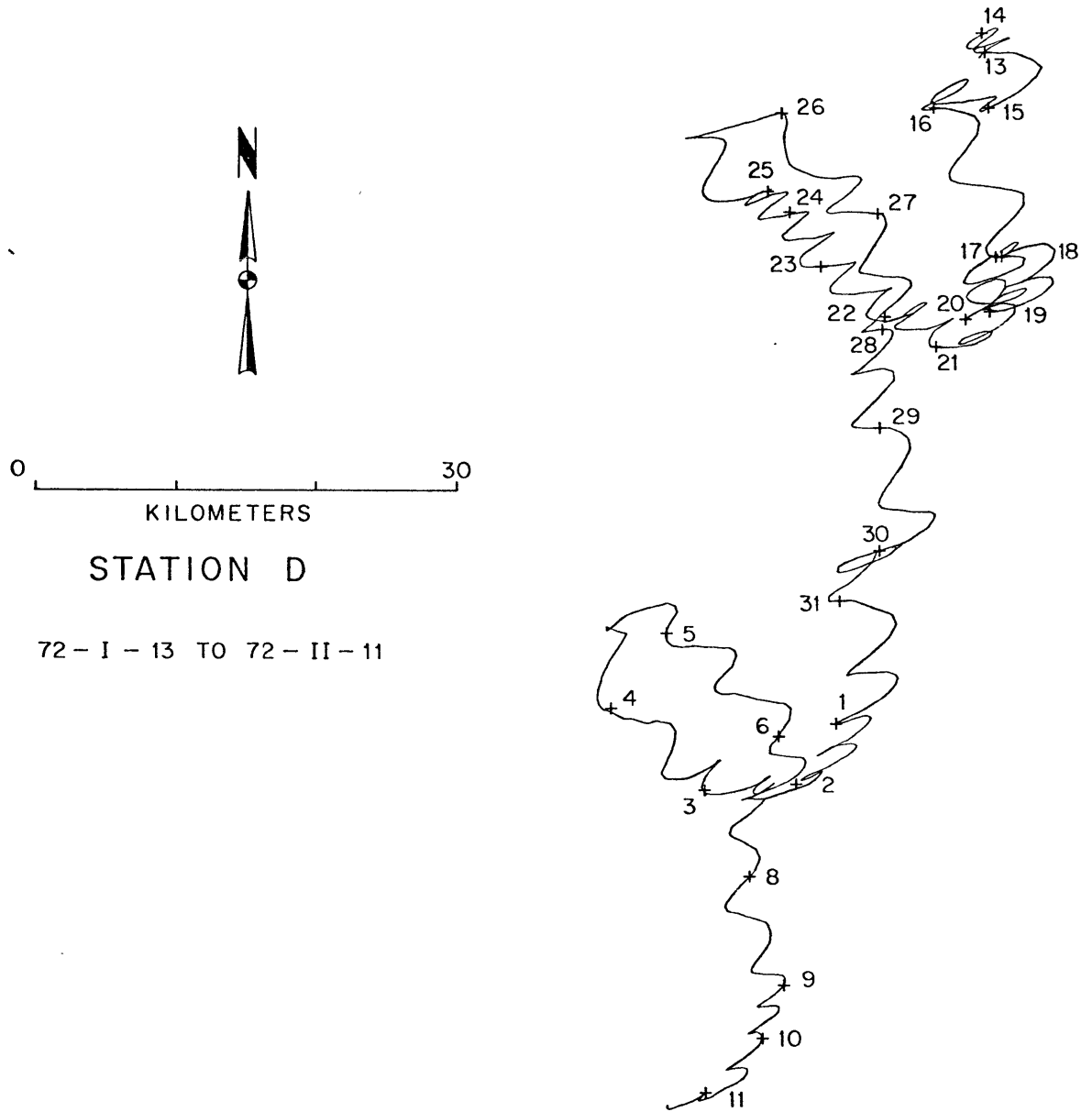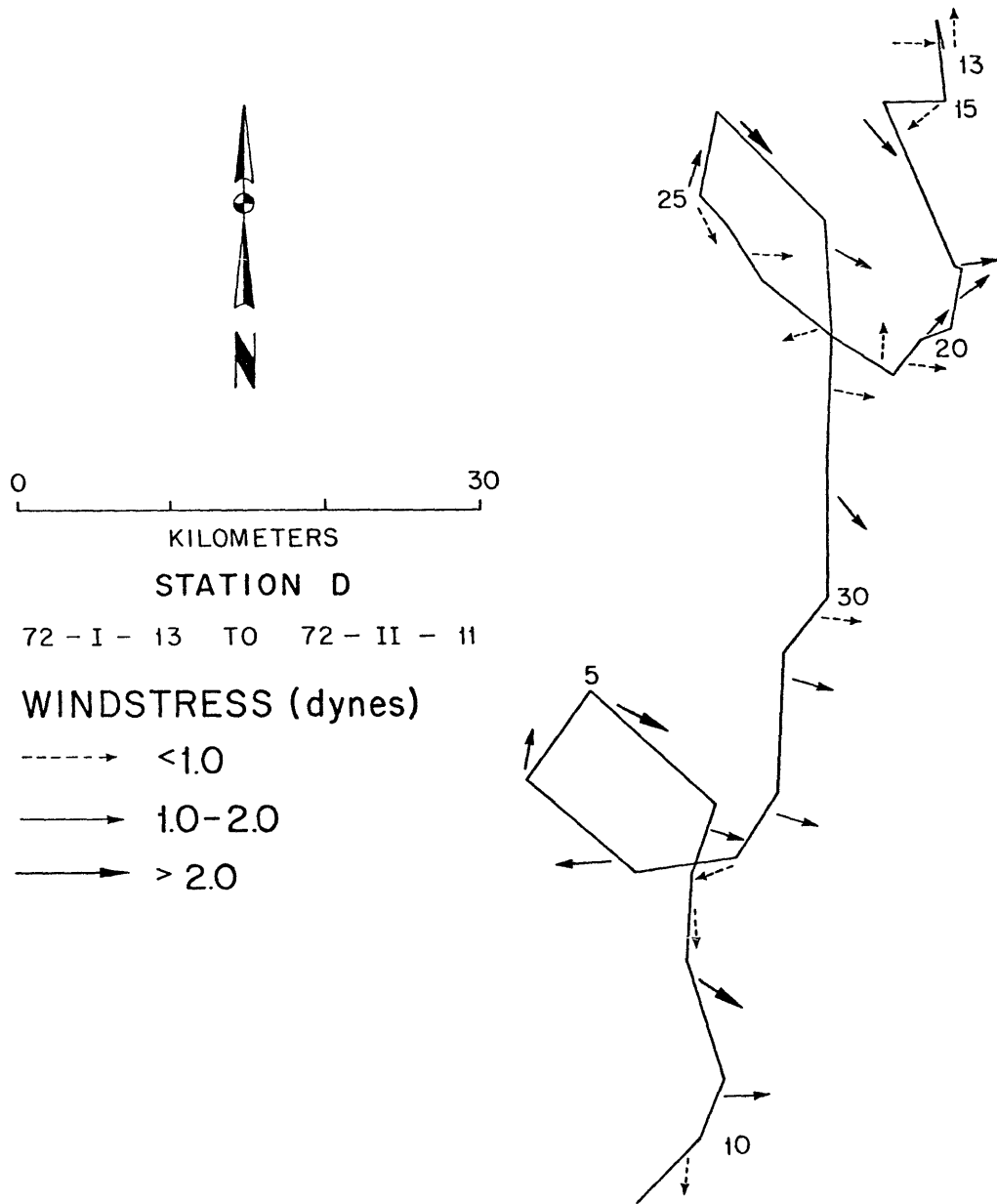
Figure 1.8b

Massachusetts Bay suggests that a similar flow pattern may occur during strong wind events which could be important in redistributing the fine bottom sediments from the nearshore areas and bank to the deep basin. In this section we investigate the response of the bottom currents and sea level in Massachusetts Bay to strong winter storms, using coastal sea level observations and the bottom current measurements made during December - February, 1972 (figure 1.4). Due to the limited nature of the bottom current data set, the discussion is necessarily qualitative.

1. Sea Level Response to Wind

Because Massachusetts Bay is a semi-enclosed basin opening on the east to the Gulf of Maine, sea level will reflect changes in the level of the Gulf at the mouth of the Bay, as well as local changes due to wind stress. The low frequency response of sea level to winds parallel to the major axis of the basin (150° - 330° T, figure 1.9) indicates a setup in the direction of the wind (figure 1.10 a,b). A northwest-southeast wind stress of 1 dyne (using a drag coefficient of 1.1×10^{-3}) results in a change in elevation between Boston and Sandwich of approximately 5 cm, with the setup occurring almost immediately.

The basin response to a wind blowing across the minor axis of the Bay (60 - 240 T, figure 1.10) is more complicated than a simple setup in the direction of the wind. A wind blowing to the northeast results in a large drop in sea level at Boston and Sandwich (order 50 cm for a 1 dyne wind), while a wind blowing to the southwest results in a large rise. Although no sea level observations were made in the outer part of the Bay it is unreasonable to expect that such a large setup (an order of magnitude larger than the setup for winds along the long axis) occurs

Figure 1.9   Map of Massachusetts and Cape Cod Bays showing
              location of tide and meteorological stations,
              and major and minor axes.
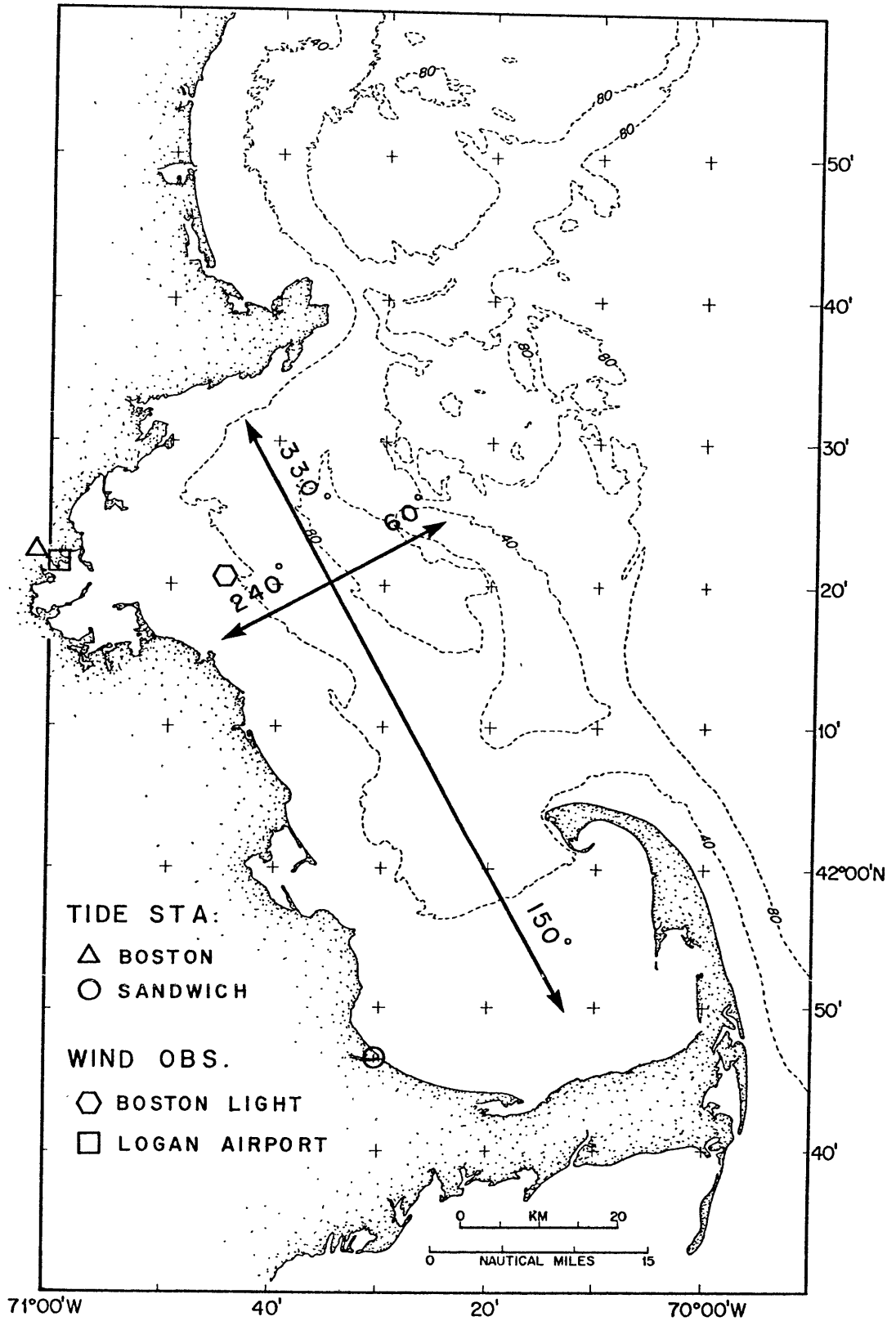
Figure 1.9

Figure 1.10 a,b   Low frequency response of sea level in Massachusetts
                   Bay to wind, Jan.-Feb., 1972.

        Top: Difference in sea level between Sandwich and Boston
                and component of wind stress parallel to major axis
                of the Bay (330°-150°T, figure 1.9).

     Bottom: Deviation of sea level at Boston from mean and
                component of wind stress parallel to minor axis of
                the Bay, and across the open side (60°-240°T).
                Deviation from mean level is corrected for the
                inverse barometer effect using atmospheric pressure
                measured at Logan Airport.

Notes: 1. All series have been filtered with a Gaussian filter
                ($\frac{1}{2}$ power at 56 hr., see Appendix B).

            2. Note difference in sea level scale between top and
                bottom figures; upper scale expanded five times.

            3. Wind stress is computed from Logan wind data using a
                constant drag coefficient of 1.1×10^{-3}. The wind
                stress would be approximately a factor of two higher
                for wind observations from the Boston Lightship. The
                drag coefficient may vary by as much as a factor of
                two - three over the period (Csanady, 1972b; Parker,
                1974) as the stability of the air-water interface
                changes.

            4. Sea level difference between Sandwich and Boston has
                not been corrected for atmospheric pressure differences.
                Parker (1974) indicates that the difference is less
                than 3 mb, and usually less than .5 mb, at least in
                summer.

            5. Wind at Logan and Boston Lightship shown for the
                period Feb. 18-22 where the two observations differed
                significantly (Logan, solid line; Lightship, dotted line).

Figure 1.10a

NW-SE COMPONENT OF WIND STRESS AT LOGAN AIRPORT
SEA LEVEL (SANDWICH - BOSTON)

FROM NW / FROM SE (DYNES)

SAND. HIGH (CM) / BOSTON HIGH

SEA LEVEL --------
WIND STRESS ————

FEBRUARY 1972

NE - SW COMPONENT OF WIND STRESS
   AT LOGAN AIRPORT
   SEA LEVEL AT BOSTON,
CORRECTED FOR ATM. PRESSURE

FROM NE / FROM SW (DYNES)

ABOVE MEAN (CM) / BELOW MEAN

Figure 1.10b

52
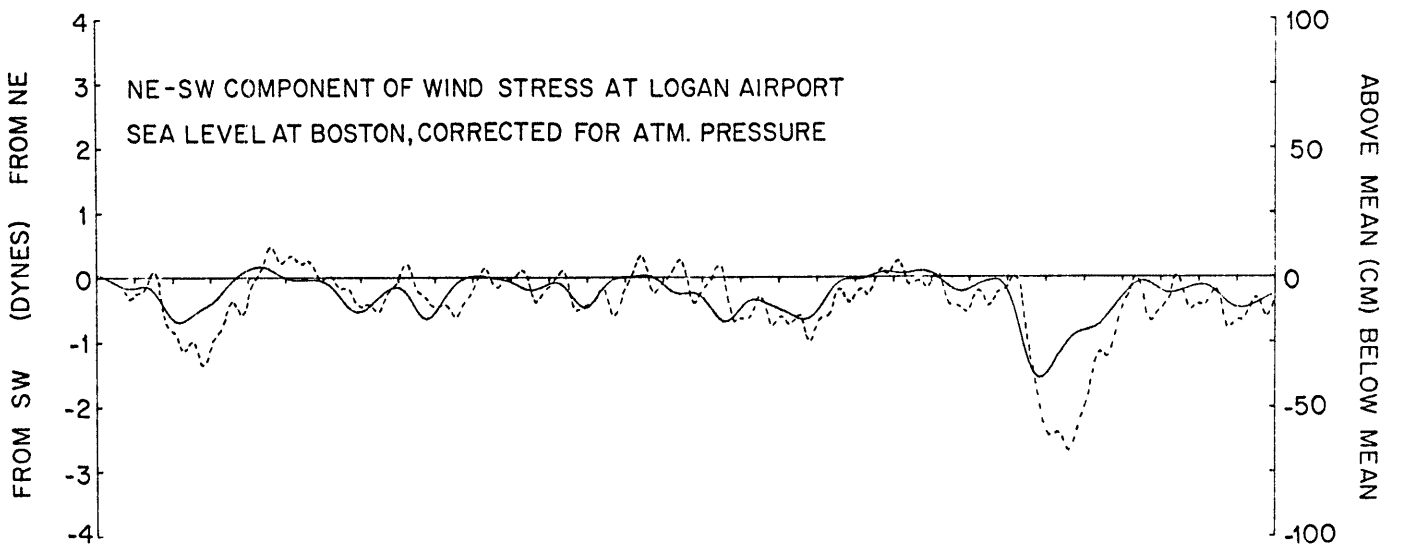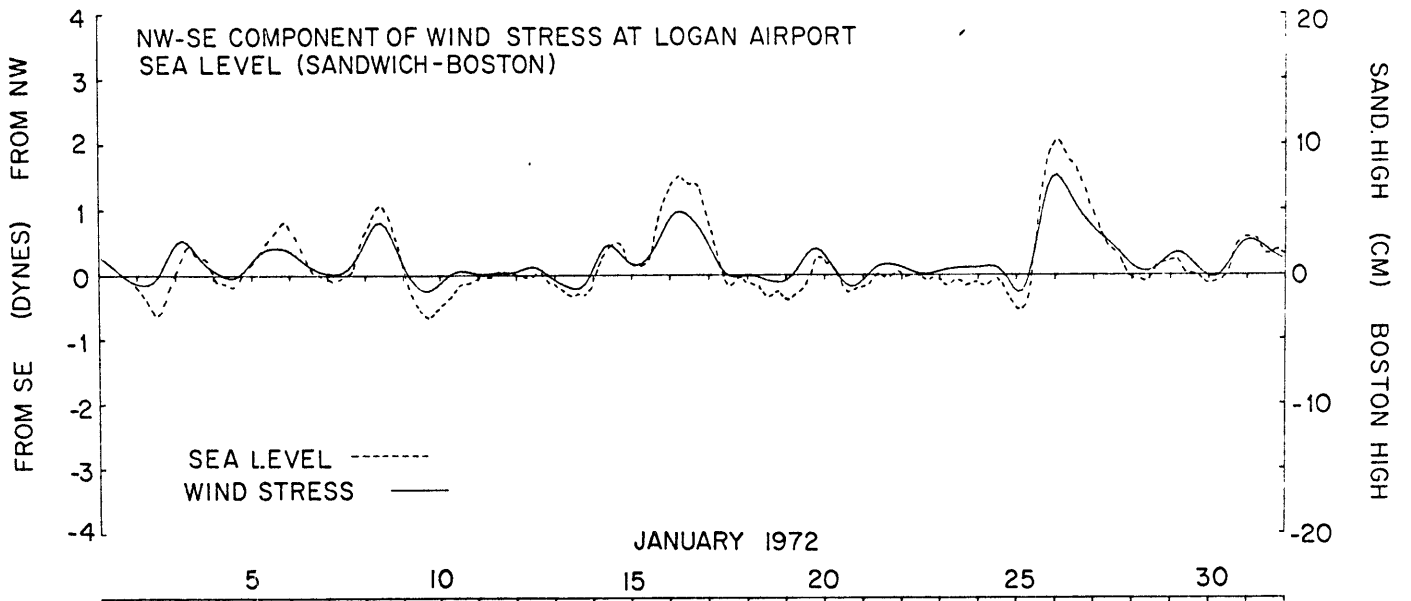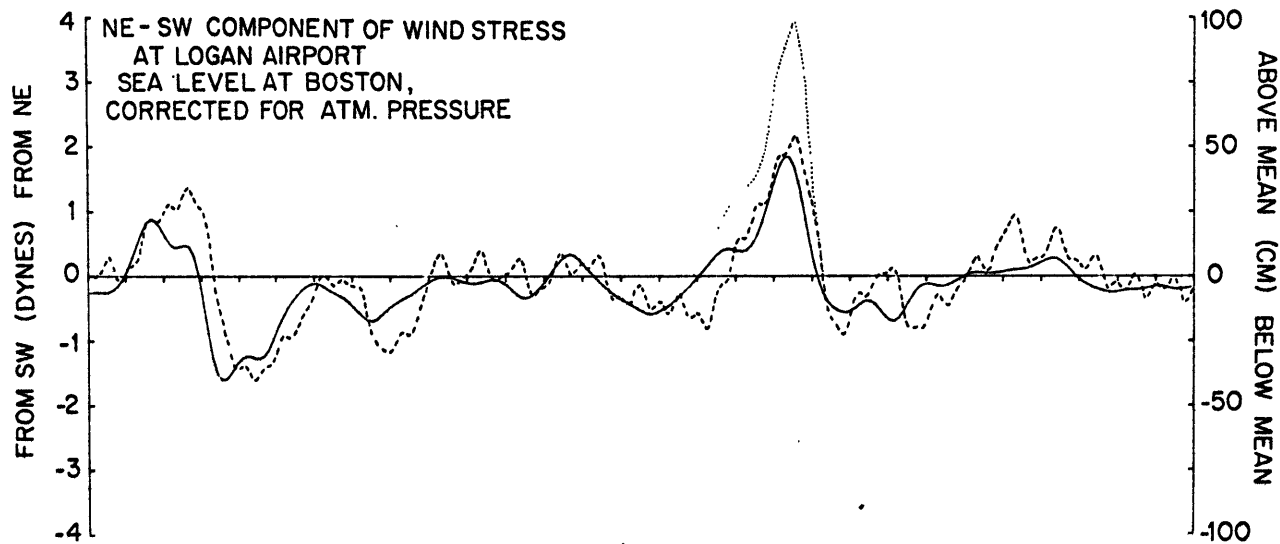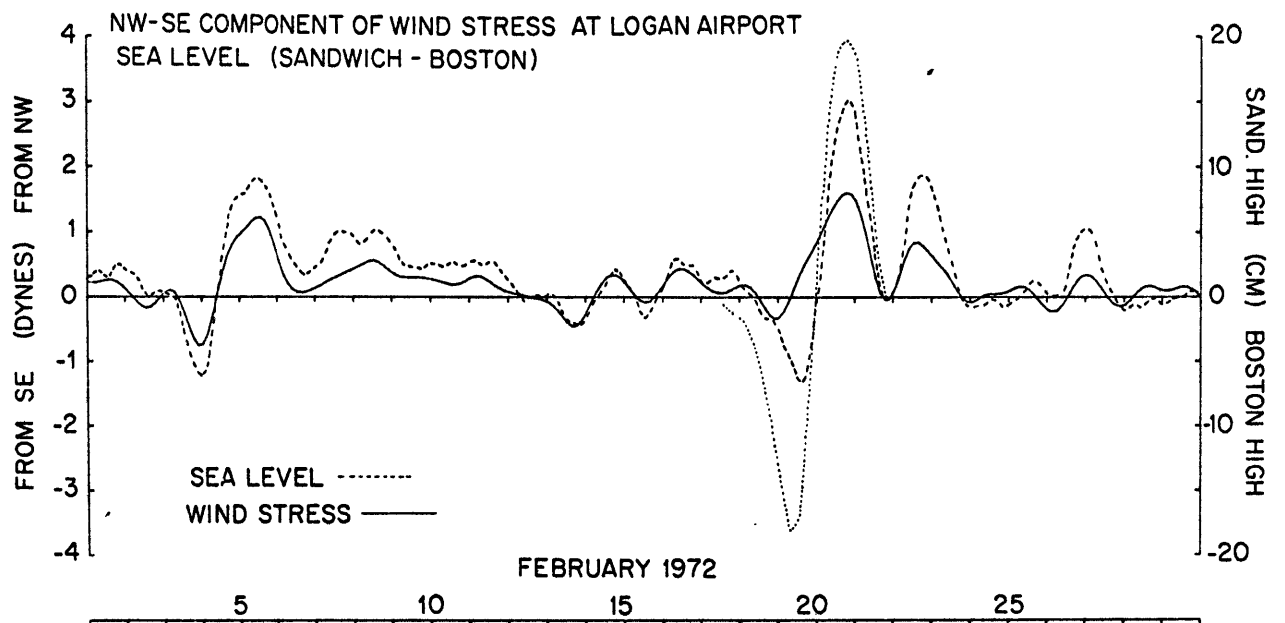
across the short axis of the Bay. The large change in sea level in

response to northeast-southwest winds probably reflects a change in the

level of the Gulf of Maine to which the Bay must adjust. Superimposed

on this change may be a small setup in the direction of the wind

with magnitude similar to the setup observed along the long axis. The

response time for sea level at Boston and Sandwich to northeast-southwest

winds is approximately 6-12 hours (figure 1.10 a,b), significantly longer

than the setup time observed for northwest-southeast winds, which also

suggests that the response of the Gulf of Maine, a larger system than

Massachusetts Bay, controls the elevation. The large change in level

is in agreement with Csanady's (1974) model of the barotropic response of

the Gulf of Maine to wind.

2. Bottom Current and Sea Level Response to Strong Wind Events

a. January 25 - 27, 1972 (Figure 1.10 a,b; 1.11)

During the morning of January 25 winds at Boston were from

the south, became more westerly during the day, and were strongly from

the northwest on January 26 and 27, with a magnitude of 3-5 dynes. On

January 25 the bottom current at station D closely followed the rotation

of the wind stress from north to east to southwest. On January 26 and 27,

the flow was consistently to the southeast, approximately parallel to the

coastline in the western Gulf of Maine. At the Boston Lightship flow was

generally northwest-southeast parallel to the coast in the direction of

the wind. During the 26th and 27th, with constant northwest wind, the

current at Boston Lightship rotated slightly to the west and gradually

decreased. The flow pattern in response to the northwest wind (January 26)

was established within 6 - 12 hours and did not change significantly

throughout the 26th.

Figure 1.11 Wind and near bottom current in Massachusetts Bay
January 25-27, 1972. Current records have been
filtered with a Gaussian filter ($\frac{1}{2}$ power at 33 hours,
see Appendix B) to remove tidal oscillations. Values
of current and wind stress shown every six hours.
Current meter located 1 m from the bottom at station D
and F, 10 m from the bottom at the Boston Lightship.

JAN 25, 1972
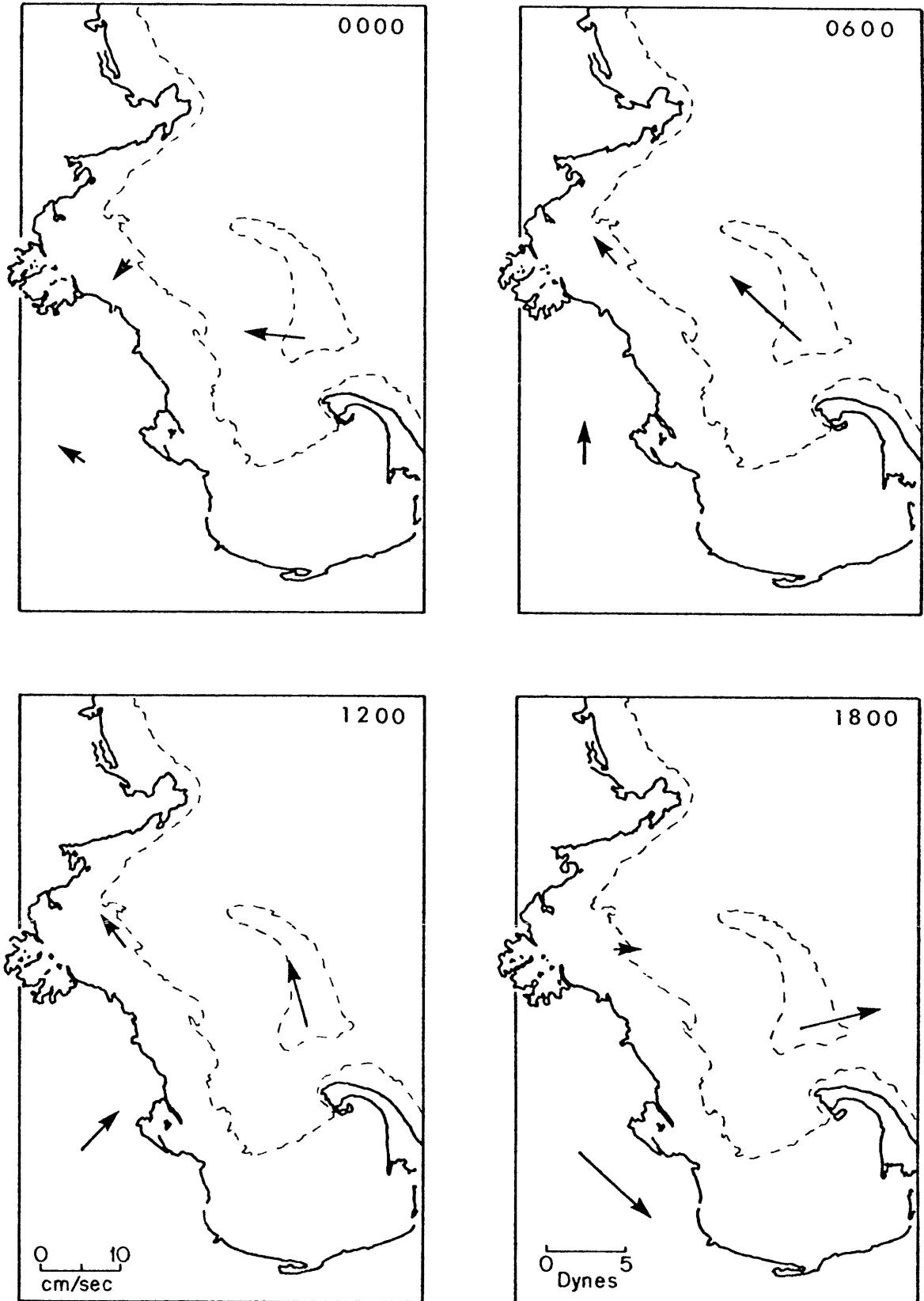
Figure 1.11

JAN 26, 1972
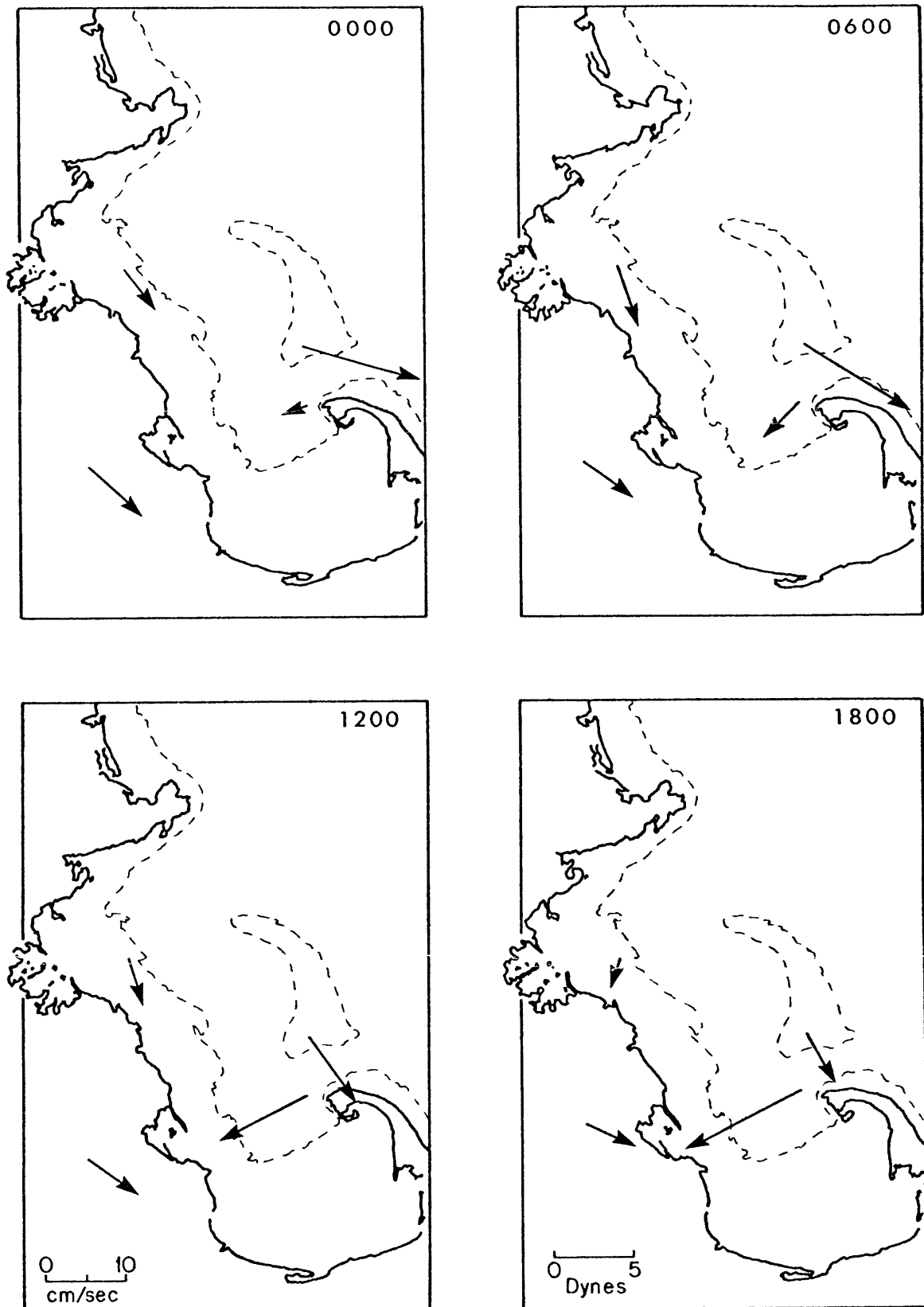
Figure 1.11

JAN 27, 1972
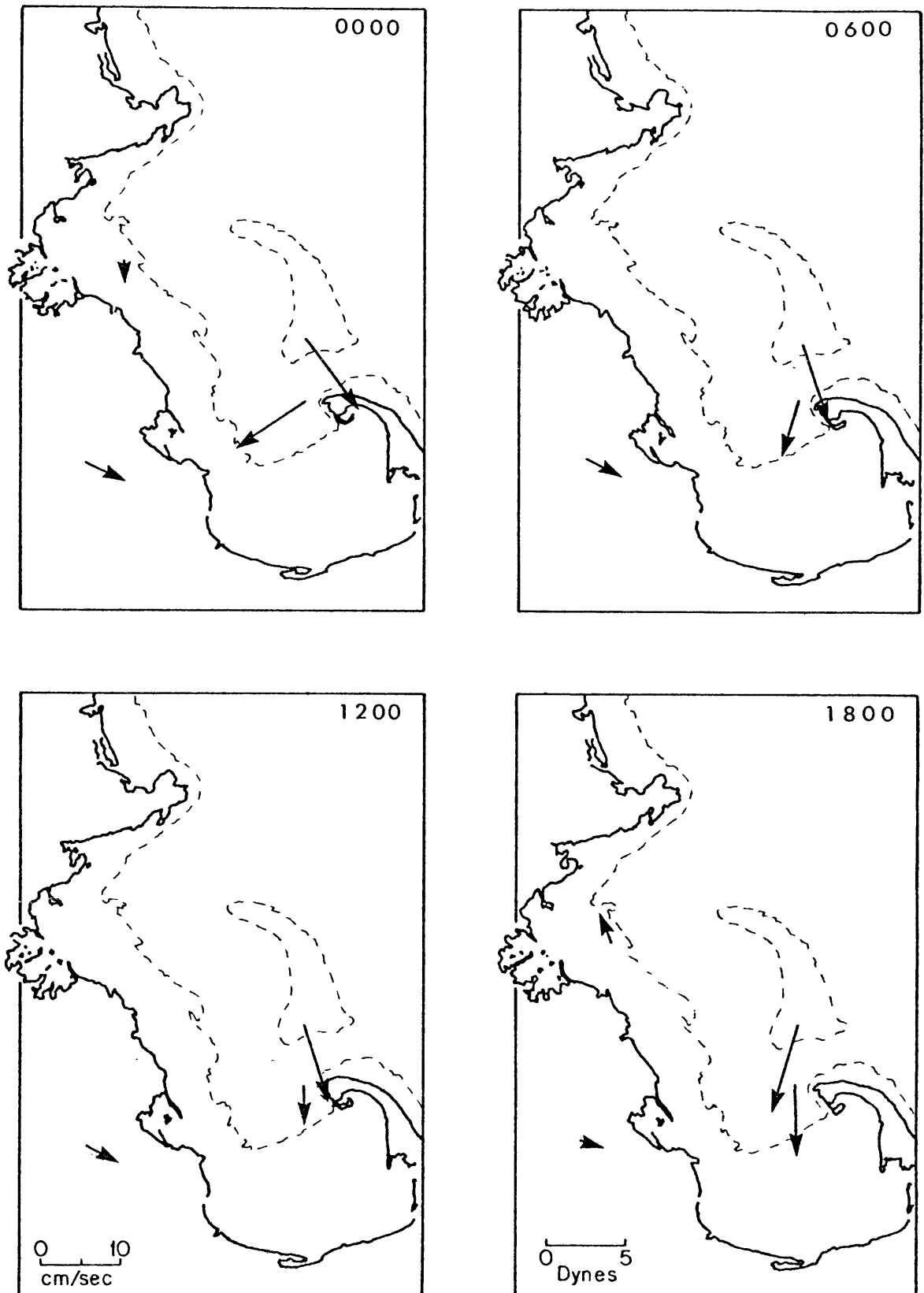
Figure 1.11

Sea level difference between Sandwich and Boston (figure 1.10a)
shows a slight setup on the 24th and early on the 25th in response to
the southerly wind. The strong northwest wind on the 26th and 27th
produced a large setup, with Sandwich higher than Boston by approximately
10 cm. As the wind rotated through north to south, the absolute level
at Boston dropped 65 cm; the outflow is clearly seen at station D at 1800
hr on January 25. The inflow on the 27th is somewhat more gradual and
is not obvious from the current record at station D.

     b.   February 2 - 5, 1972 (Figure 1.10, 1.12)

     Winds over Massachusetts Bay were light on the morning of
the 2nd, gradually became easterly in the afternoon and continued from the
east on the 3rd, then changed to westerly on the 4th. On the 5th, winds
were from the northwest throughout the day. The bottom current at sta-
tion D on the 2nd was to the west into the Bay as sea level at Boston and
Sandwich rose. The flow, at least early on the 2nd does not appear to be
locally wind driven. It is suggested that the flow at stations D and F
was driven by a rise in sea level at the western end of the Gulf of Maine;
wind over most of the Gulf on the morning of the 2nd was to the southwest,
but was only to the southwest at Boston in the afternoon. The flow at
station D became more parallel to the western coast of the Gulf on the 3rd
as the rise in sea level at Boston diminished. Flow at station F late on
the 3rd and early on the 4th was in the direction of the pressure gradient
caused by the slight setup of the bay to the north. On February 4th the
wind changed from southeast to south to southwest to northwest. The
bottom flow at station D closely followed the rotating wind; sea level in
the Bay fell below mean level as the bottom flow at station D passed through
east. The current at station F rotated from south to north as the wind

Figure 1.12   Wind and near bottom current in Massachusetts Bay
February 2-5, 1972. Current records filtered with
a Gaussian filter ($\frac{1}{2}$ power 33 hours, see Appendix B)
and plotted every six hours. Current meters located
1 m from the bottom.

FEB 2, 1972
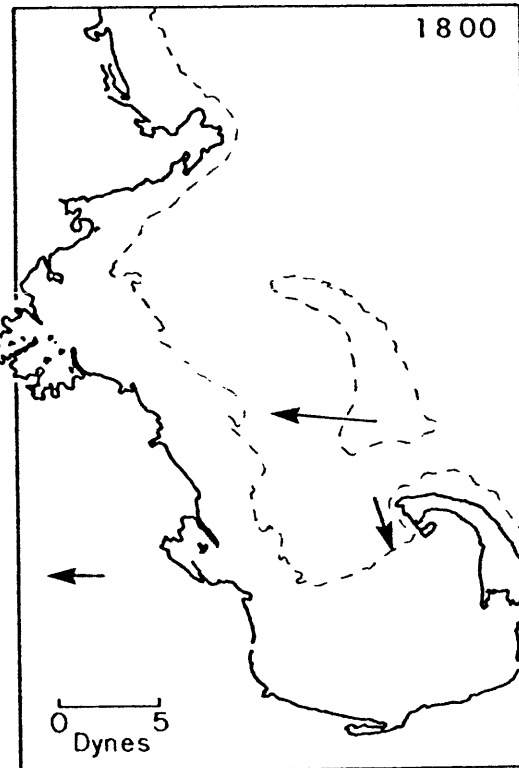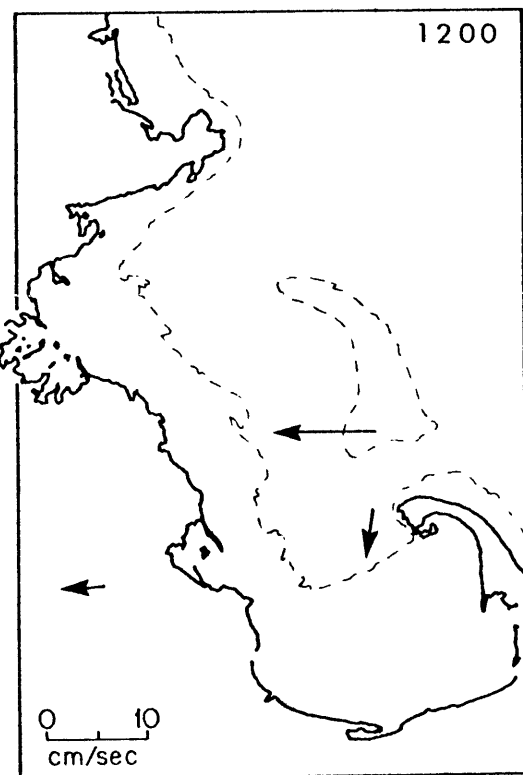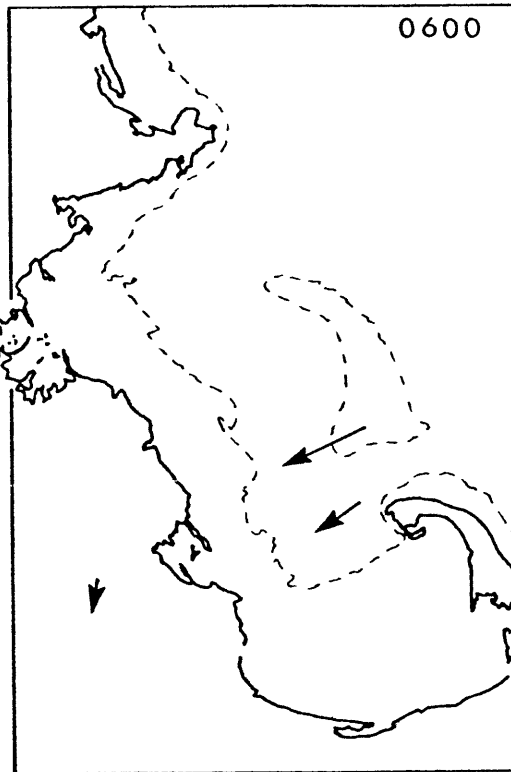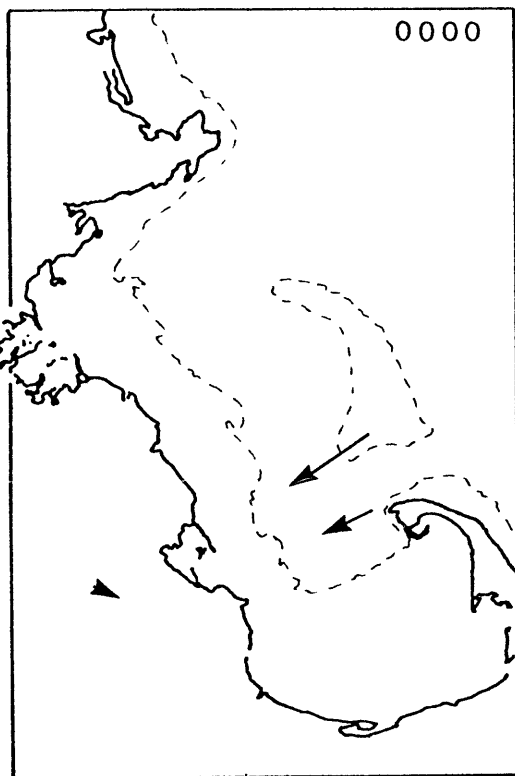
Figure 1.12

FEB 3, 1972
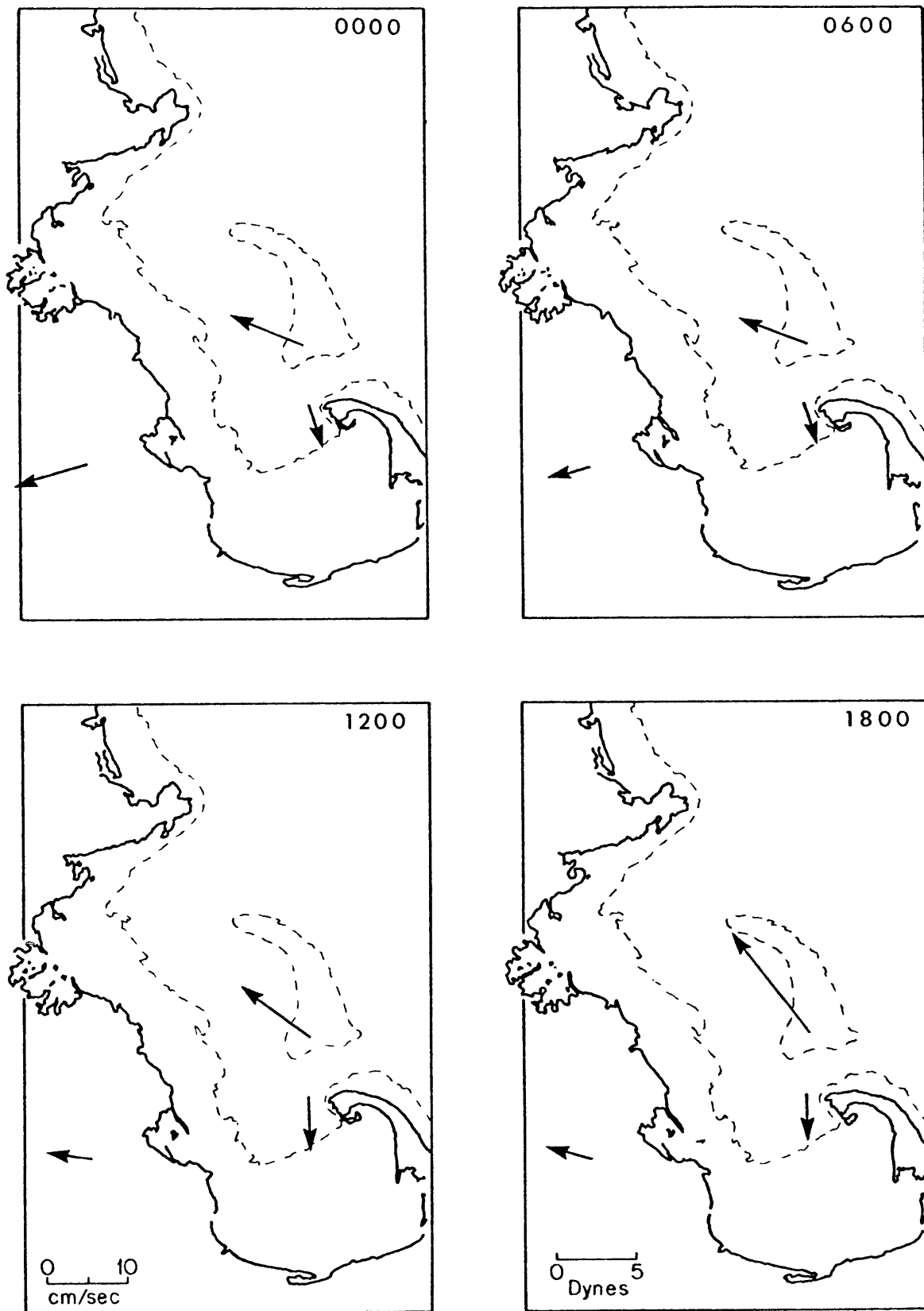
Figure 1.12

FEB 4, 1972
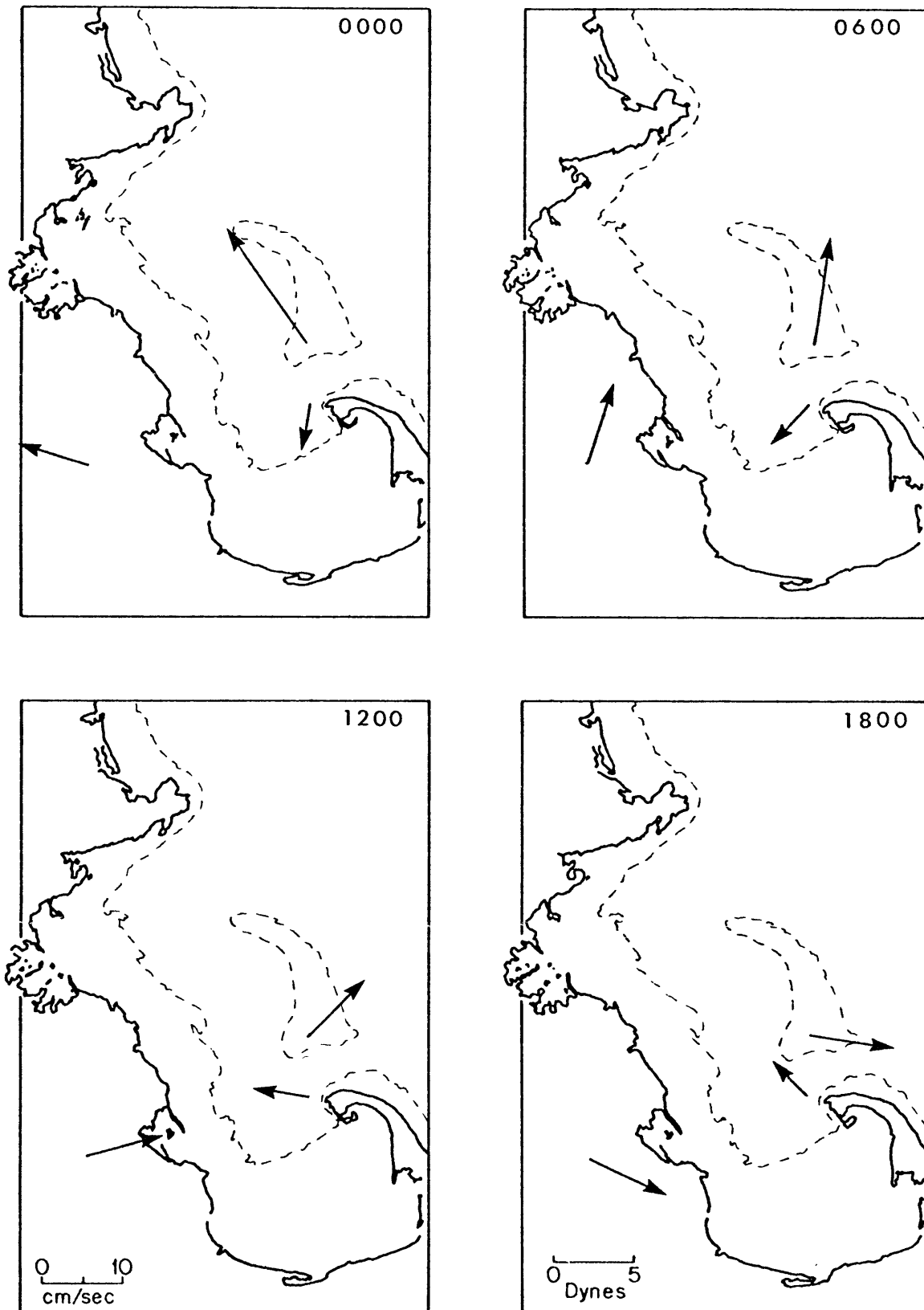
Figure 1.12

FEB 5, 1972
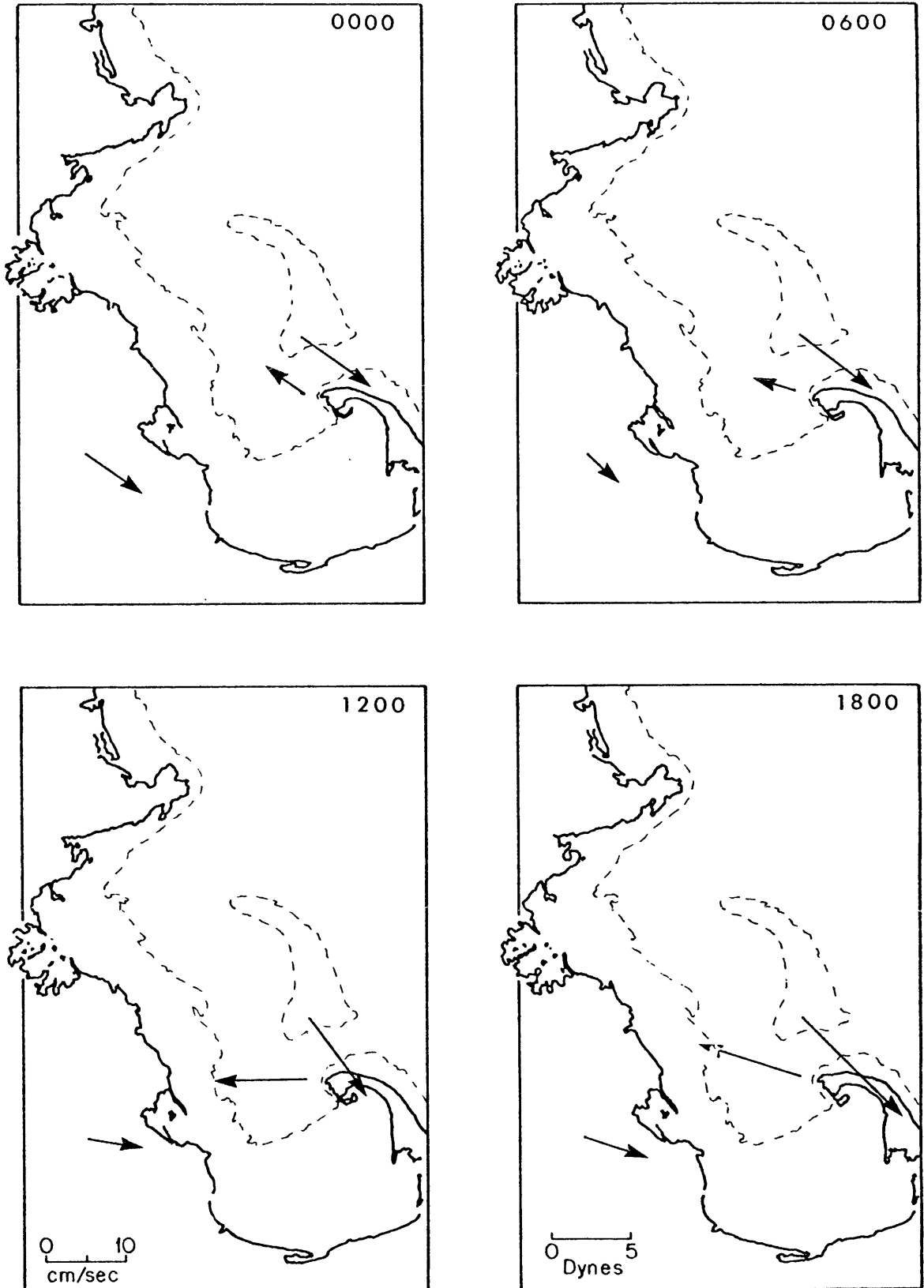
Figure 1.12

shifted. The strong northwest wind continued on the 5th with little

change in the bottom flow pattern.

        c. February 18 - 21, 1972 (Figure 1.10, 1.13)

On February 18, winds over Massachusetts Bay and the Gulf

of Maine were from the east and southeast. Flow at station B and at the

Boston Lightship was southerly parallel to shore while flow at station C

in the deep central basin was to the east, opposite to the direction of

the wind. The wind stress increased from the southeast during the morning

of the 19th; in response the velocities at all stations increased, but the

flow pattern remained basically unchanged. Late on the 19th and early on

the 20th the wind rotated from southeast to northwest. Flow at station C

remained to the south for the first twelve hours of the northwest wind,

but then gradually rotated to the northwest after sea level at Boston

reached equilibrium. Flow at station B was to the northwest at midday on

the 20th and became northeasterly on the 21st. The flow pattern at 0600

on the 21st strongly suggests a double gyre flow pattern, with the north-

west flow at station C feeding both shore parallel flows at station B and

at the Boston Lightship.

     3. Bottom Wind Driven Circulation Pattern

Although the spatial coverage of the currents during any one

storm is sparse, a composite picture of the bottom flow pattern in the

basin in winter for several wind directions can be developed from measure-

ments made at different times but under similar wind conditions (figure

1.14). The composite response suggests near bottom flow in the shallow

parts of the Bay parallel to the wind and flow opposite to the wind in

the deep central basin. Nearshore, flow is parallel to the coast. Flow

on Stellwagen Bank is almost always in the direction of the wind, while

Figure 1.13 Wind and near bottom current in Massachusetts Bay
February 18-21, 1972. Current records filtered with
a Gaussian filter ($\frac{1}{2}$ power at 33 hours, Appendix B)
and plotted every six hours. Flow at station B is
shown only occasionally because of a failure in the
timing circuitry of the current meter. Measurements
at stations B and C 1 m from the bottom, measurements
at Lightship 10 m from the bottom. Wind stress at
both Boston Lightship and Logan Airport shown on
Feb. 19, when direction of the two observations
differ significantly. Scale for Logan stress is
0-2.5 dynes.

FEB. 18, 1972
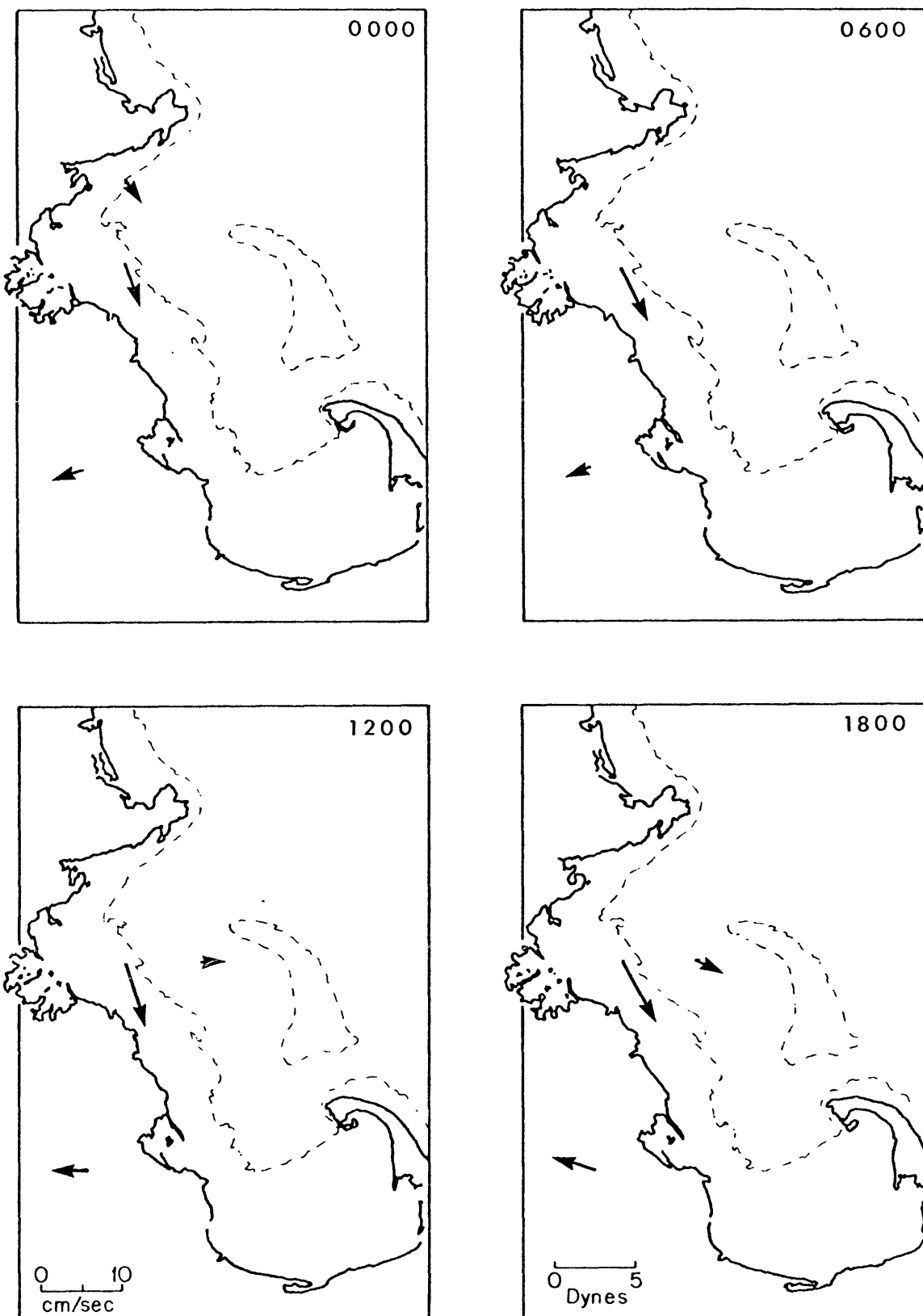
Figure 1.13

FEB. 19, 1972
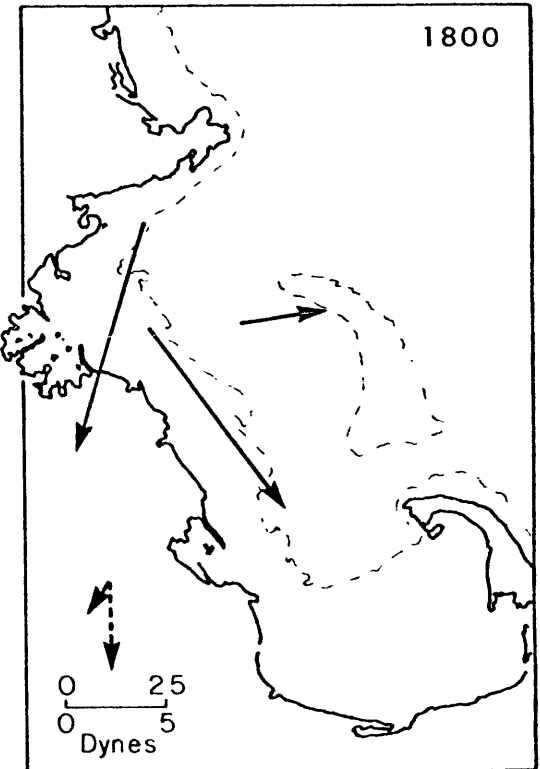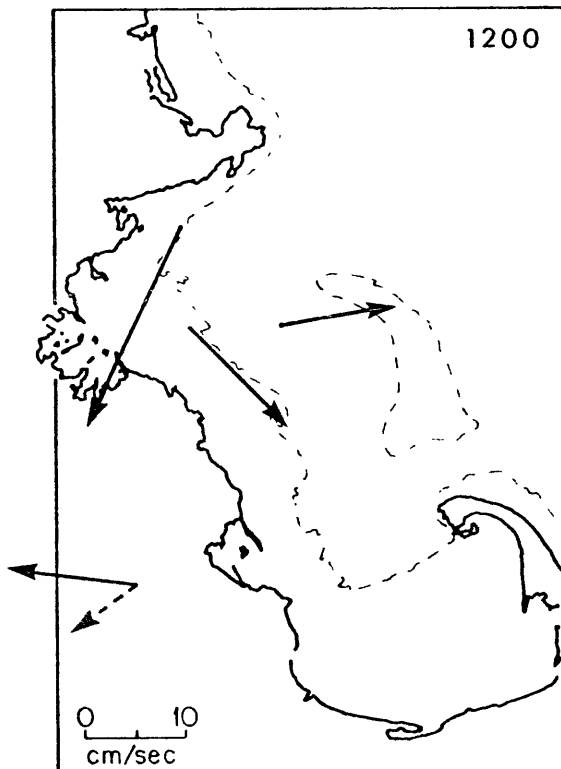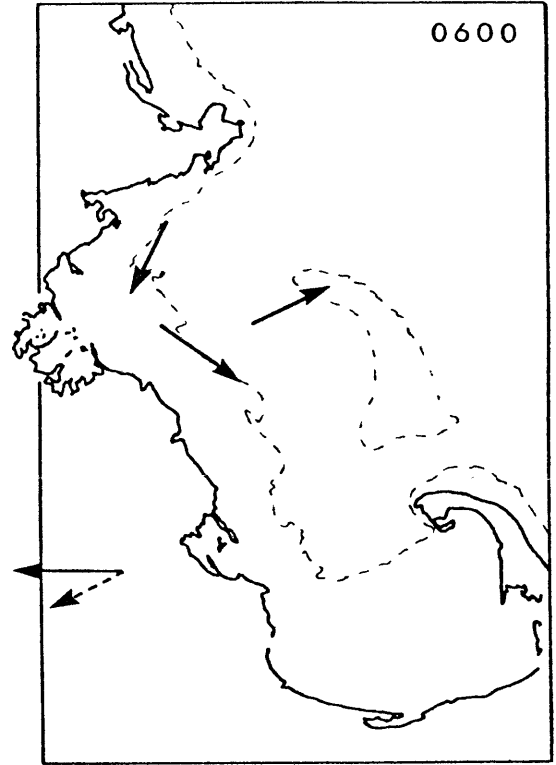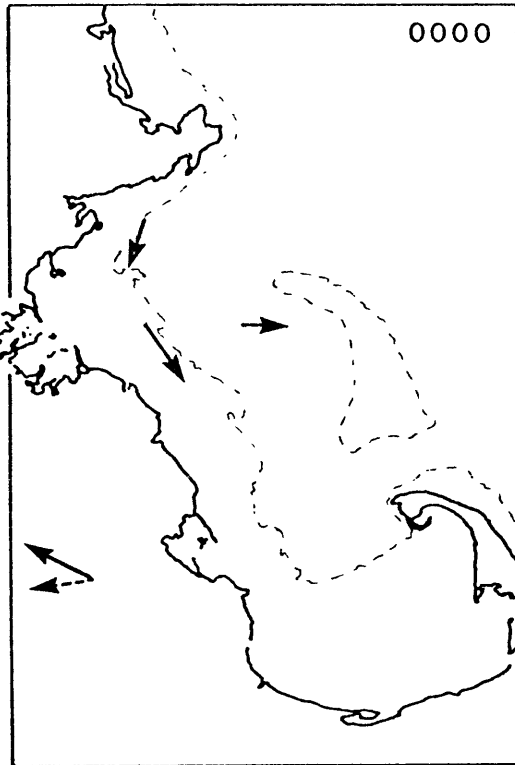
FEB. 20, 1972
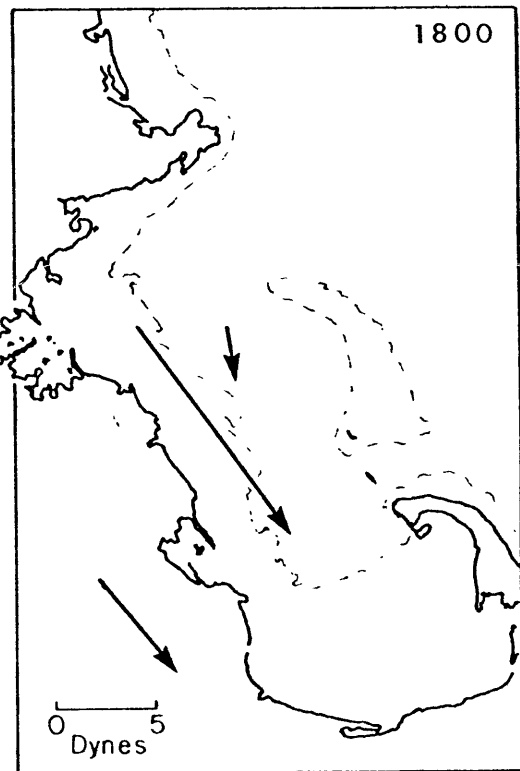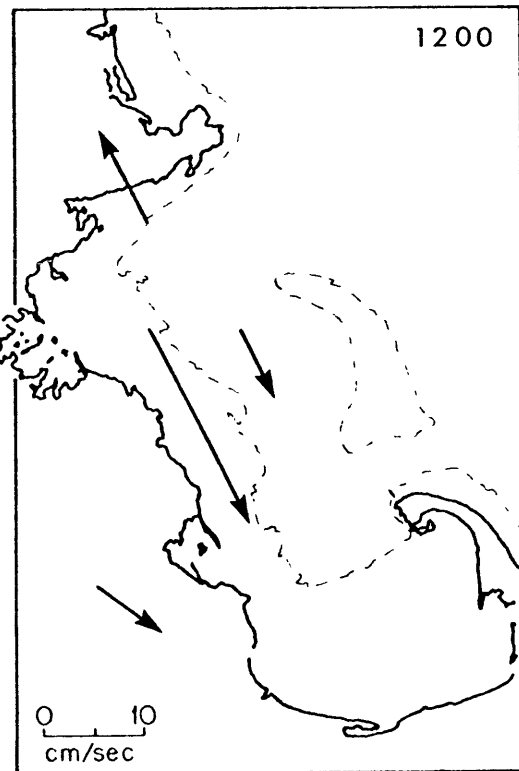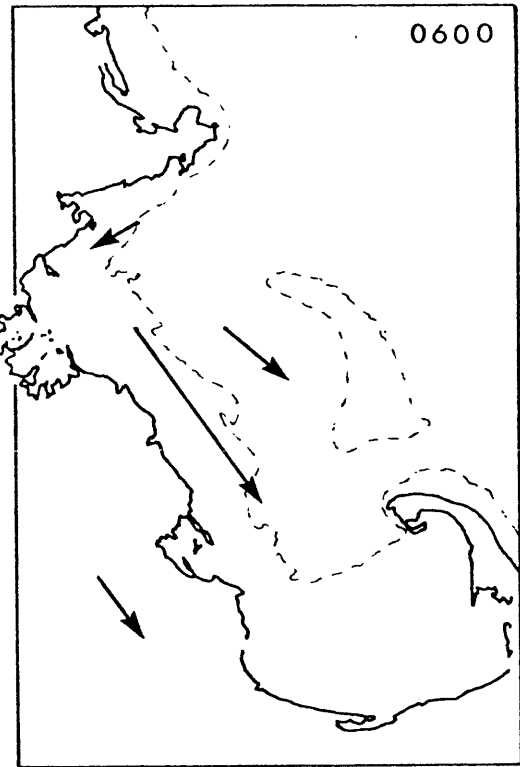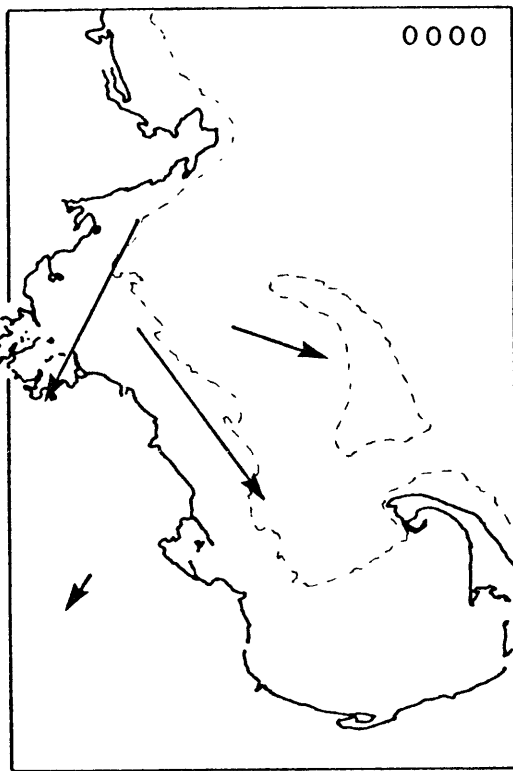
FEB. 21, 1972
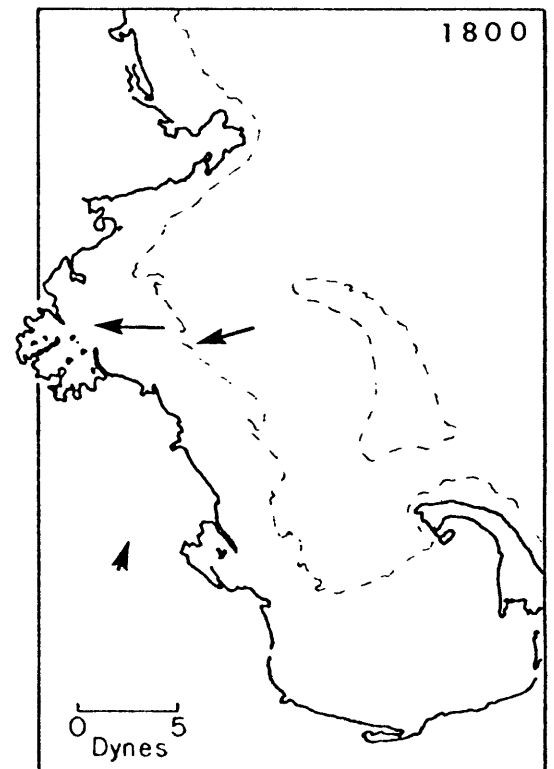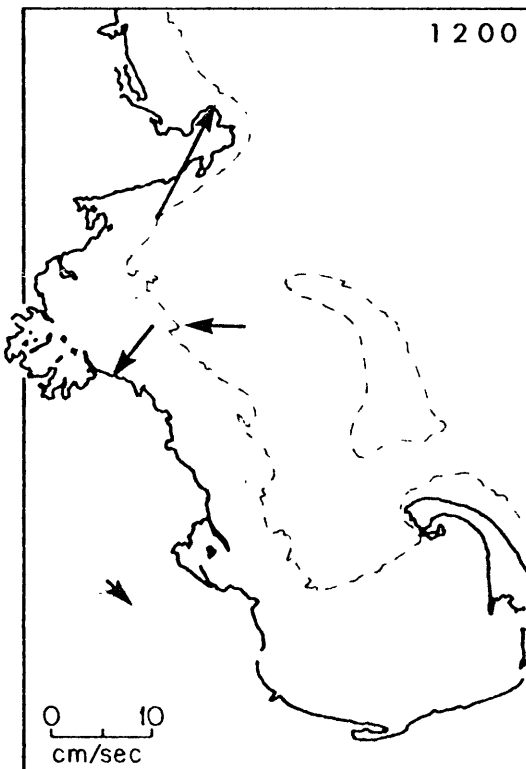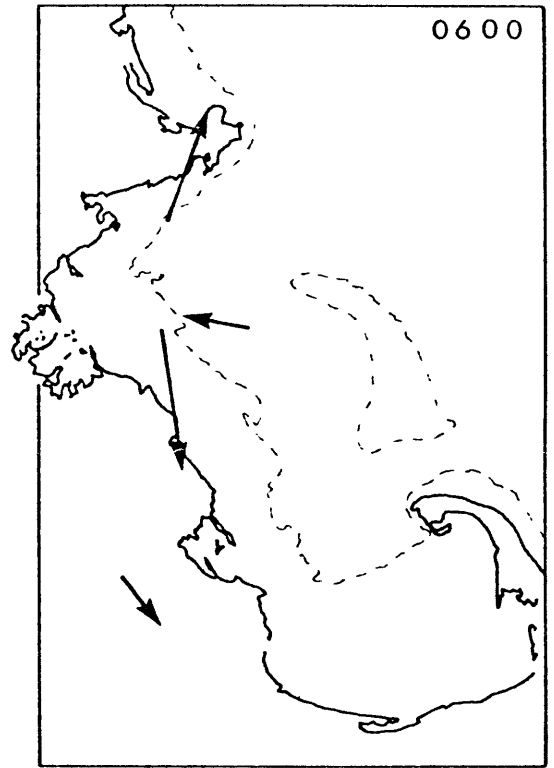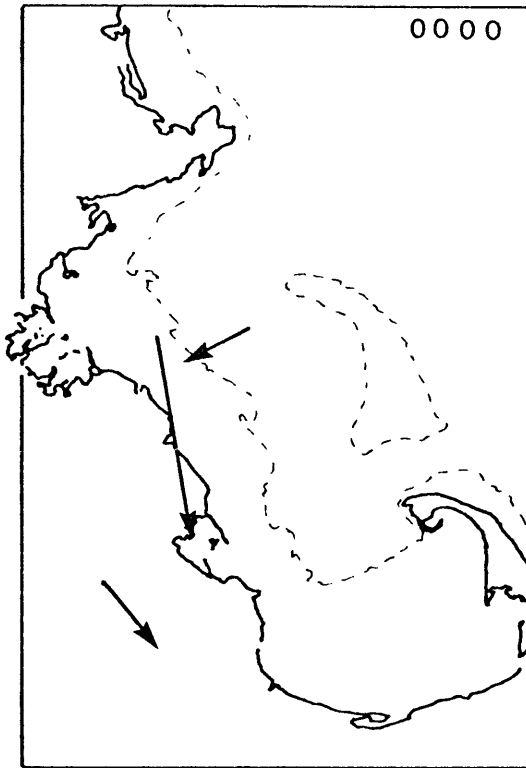
Figure 1.14   Generalized response of bottom currents to wind
              constructed from measurements made at different
              times but under similar wind conditions. Magnitude
              of the current is not indicated, although some
              relative magnitudes are suggested for wind stress
              on the order of 1 - 3 dynes. If no flow is indicated
              at a station, no measurement was made for that
              wind direction.

BASIN RESPONSE (BOTTOM)
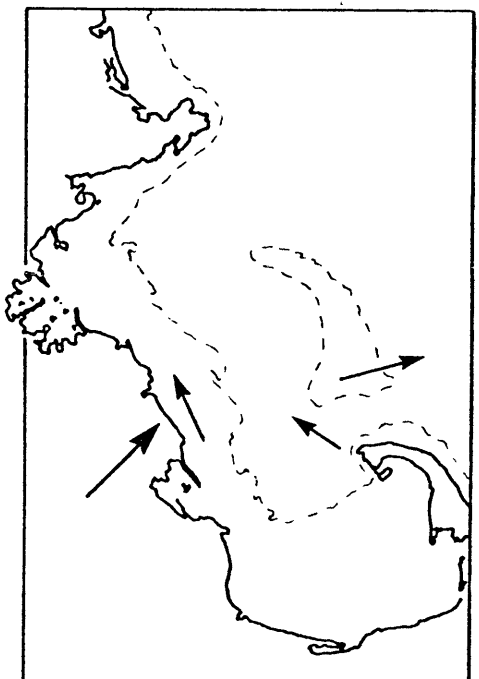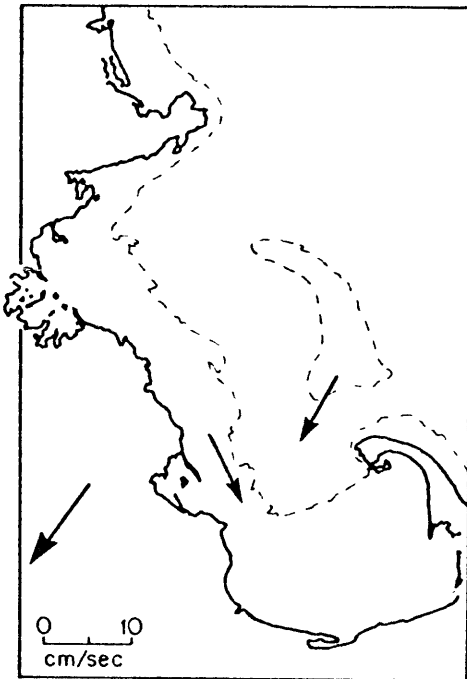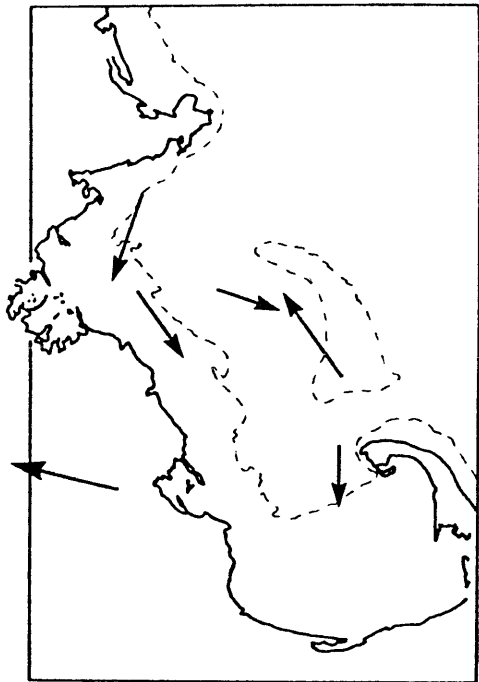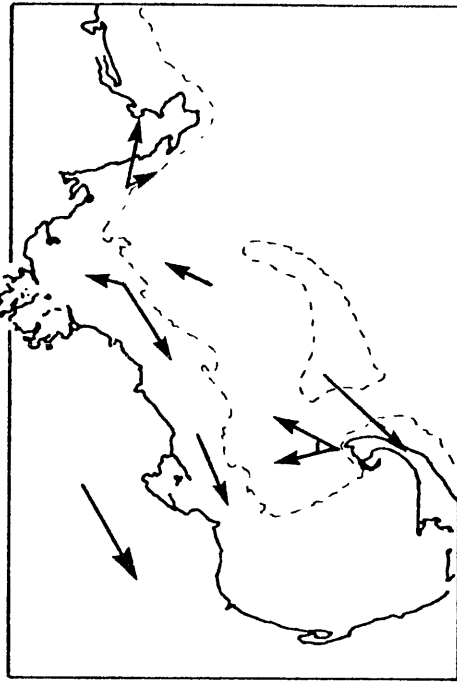
flow in Stellwagen Basin for a northwest or southeast wind is nearly opposite to the wind direction. The observed northwesterly flow at Boston Lightship with a northwest wind appears to accept the flow from the deep basin and feed the northeast flow at station B, or the southerly flow at station E. Similarly, the southerly flow at Boston Lightship associated with a southeast wind may feed the easterly flow in the central portion of the basin, and not continue down the coast.

In summary, the response of sea level and of the bottom currents in Massachusetts Bay in winter to strong wind stress is as follows:

(1) A sea surface setup in the direction of the wind. Superimposed on the setup are changes in the absoluted level of the Bay controlled primarily by the response of the Gulf of Maine. Local setup is established in less than 1 hr; absolute changes require 6 - 12 hours.

(2) The bottom current is coherent over basin scales during strong wind events, with flow in the direction of the wind in the shallow parts of the basin and opposite to the wind in the deep basin. Flow is more complicated near the ends and corners of the Bay where the current must adjust to the coast. On Stellwagen Bank, flow is in or out of the basin as sea level adjusts to the level of the Gulf of Maine.

(3) The local bottom wind driven current is established approximately 12 hours after the wind stress is applied and remains basically unchanged even if the wind stress lasts as long as 24 hr. In some cases, however, the time to establish the flow pattern is as long as 18 - 24 hours, particularly in the corners of the basin, and there is a slight modification of the flow pattern with time. (The rapid adjustment of winter wind driven currents is also observed on the New England continental shelf, and is investigated in Chapter 3.)

F. Summary and Conclusions

The bottom currents in Massachusetts Bay have been monitored over a one year period in areas of different sediment types, bottom roughness and depth. With the reservations about stress estimates, critical erosion stress and the effects of bioturbation, it appears that the bottom sediments are in equilibrium with the bottom currents: the observed currents are not sufficient to move existing material regularly, except possibly on Stellwagen Bank and in the shallow nearshore regions. The speed distribution is primarily determined by the strong tidal currents.

In the winter, the net near bottom current is dominated by strong wind events. Despite the limited nature of the data and the only partially closed geometry of the Bay, there is indication of a two gyre flow pattern, with flow in the direction of the wind in the shallow areas and opposite to the wind in the central basin. Sea level is controlled both by local wind in the Bay and by the response of the Gulf of Maine; inflow and outflow over the shallow bank at the mouth of the Bay is observed as sea level in Massachusetts Bay adjusts to the Gulf. The net bottom flow pattern could be important in redistributing fine material from the shallow bank and nearshore areas, where occasional incipient sediment motion occurs, into the deep basin.

CHAPTER II

THE SPRING RUNOFF IN MASSACHUSETTS BAY

A. Introduction

This chapter investigates the currents during the period of the spring runoff in Massachusetts Bay, and the relation of the current pattern to the observed density field. Recent investigations have shown the importance of wind, topography, and thermal structure in determining the circulation on the continental shelf, shallow seas, and the Great Lakes (for example, Bennett, 1974; Csanady, 1973a,b, 1974 , and others). A somewhat neglected aspect (with the notable exception of Stommel and Leetmaa (1972)), or assumed to be less important, has been the circulation driven by the discharge of fresh water at the coast by rivers. This study is concerned with river influenced currents in regions somewhat distant, on the order of 10-20 km from a river mouth, but not distant enough to consider the in-flow as in Stommel and Leetmaa's model. The major discharge of fresh water from rivers in temporate regions is from the spring runoff; typically fifty percent of the yearly streamflow occurs in March, April and May. Because of this major increase in river flow and the generally weak wind stress, density gradients associated with river discharge may have an important influence on the currents in nearshore areas in spring, even those distant from major rivers.

Studies of rivers as they discharge into the sea fall into two broad categories: studies of the surface plume of fresh water near the river mouth (the near field), [for example, studies by Wright and Coleman (1971) of the Mississippi River, and by Garvine (1974a) and Garvine and Monk (1974) of the Connecticut River], and studies of the large scale salinity

distribution associated with the river discharge far from the initial

mixing zone (the far field), [for example, studies by Barnes et al (1972)

of the Columbia River and by Gibbs (1970) and Ryther et al (1967) of the

Amazon River]. The studies show a major influence of river discharge on

the surrounding ocean. For example, freshening associated with the Amazon

and Columbia Rivers extends several hundred kilometers seaward in a large

plume. The shape and position of the plume may depend on the local cur-

rents, winds, and the river discharge; the position of a river plume

with respect to the river mouth may vary on short time scales, for example

due to tidal currents (Garvine, Connecticut River), or on a seasonal time

scale due to seasonal large scale ocean currents (Barnes, Columbia River).

The studies generally interpret the surface plume as passively advected

on the prevailing currents. Garvine (1974a)did measure currents in the

frontal zone of the plume, but none of these studies included direct cur-

rent measurements of the large scale currents directly associated with the

source of buoyancy.

Models of river discharge into the ocean have primarily been of the

near field, or of the small scale structure of the river plume (Garvine,

1974b;Takano, 1954; Wright and Coleman, 1971) and have generally ignored

the effects of rotation and the far field circulation, with two exceptions.

One model of the medium to far field circulation driven by river discharge

in a rotating system is of steady river flow distributed evenly along a

coastal boundary. The discharge will result in fresher water nearshore,with

the strength of the associated horizontal density gradients dependent

on the magnitude of the fresh water discharge and on the extent of the

vertical and horizontal mixing. Because of the thermal wind relation,

offshore horizontal gradients will tend to produce flow parallel to shore,

to the right (looking out from shore) in the northern hemisphere. Such

a model is presented by Stommel and Leetmaa (1972) for the U.S. east coast

continental shelf.

A second relevant model (Csanady, 1971) is of the inertial adjustment

of a column of light warm water nearshore and a column of heavier water

offshore. The two layer adjusted state is either a 'wedge-shaped' or a

'lens-shaped' thermocline with length scales of the internal Rossby radius.

For the wedge-shaped thermocline currents are to the right in the surface

layers and to the left in the bottom layer (looking offshore). In the

lens-shaped thermocline flow in upper and lower layers is in the same

sense, to the left on the inshore edge of the lens, looking offshore, and

to the right on the outer edge. The model was developed to explain the

thermally driven spring lake circulation, but the dynamics are similar if

applied to coastal freshening by river flow.

The effects of river discharge on the currents in Massachusetts Bay

will differ from these models in several ways: (1) the current pattern is

three dimensional and varies over length scales of 10-20 km in the along-

shore direction, (2) the major source of fresh water is not at the coast

but to the north of the basin, (3) the major fresh water flow occurs as

spring runoff and is thus not steady throughout the year, and (4) a

summer thermocline gradually develops during the runoff period.

B. Background

Studies in the Gulf of Maine show a general freshening of the near-

shore waters in the spring as a result of increased river runoff, and an

increased local freshening adjacent to the large river systems (Meade, 1971;

Graham, 1970; Colton, 1968; Bigelow, 1927). Associated with the nearshore

freshening is a southerly flow of about 10 cm sec^{-1} along the western coast

(Bumpus, 1973; Graham, 1970; Bumpus and Lauzier, 1965), the western side of the Gulf of Maine gyre. The strength of the gyre is strongest in spring suggesting the importance of runoff, but interpretation of the gyre as a wind driven flow can also be made (Csanady, 1974).

Massachusetts Bay is a semi-enclosed basin, located on the southwestern end of the Gulf of Maine, 'downstream' from all the major rivers which discharge into the Gulf (figure 2.1). There are two river systems which affect the salinity distribution. A small system of several rivers, of which the largest is the Charles River, discharges directly into the Bay through Boston Harbor. This group of rivers will be referred to as the Charles River system. The spring runoff typically begins in late February and continues through March (figure 2.2a), with a maximum spring flow of approximately 30 m^3 sec^{-1}. The second nearby source of fresh water is the Merrimack, a major river which discharges 30 km to the north of Massachusetts Bay. The peak spring runoff of approximately 500 m^3 sec^{-1} generally occurs in April, somewhat after the peak runoff from the Charles River system (figure 2.2b). The two fresh water sources are thus separated in time and space. On the average, the first inflow of fresh water to Massachusetts Bay is at the coast from the Charles River and is relatively small; the second source is much larger, dominated by the Merrimack, and is located to the north and east of the open side of Massachusetts Bay. In the spring of 1973, discharge was much larger than average and considerably more time dependent than the monthly average figures might suggest; the discharge over a five-day period may change by a factor of two during the peak runoff season.

During the period of the spring runoff a seasonal thermocline gradually develops in Massachusetts Bay. The water column in March and April is

Figure 2.1 Map of Massachusetts Bay showing study area (boxed),
location of major river systems, current meter moorings,
tide and meteorological stations. Smoothed 40 and 80 m
contours indicate major topographic features.
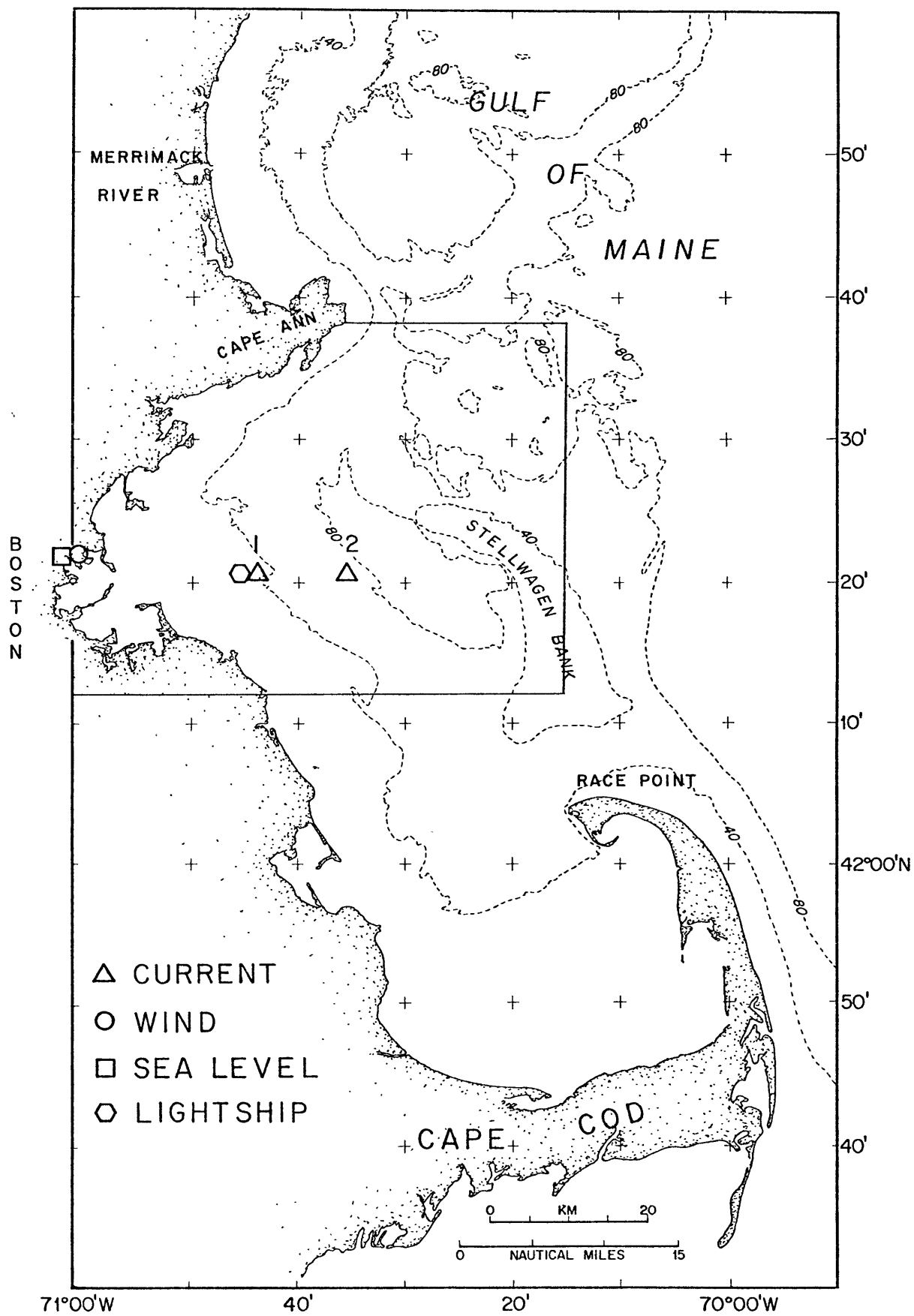
Figure 2.1

Figure 2.2   (a) Charles River streamflow at Waltham, Mass.; five
day average discharge January-June 1973 (dotted lines);
mean discharge and monthly mean discharge 1956-1973
(solid lines).

(b) Merrimack River streamflow at Lowell, Mass.; five
day average discharge January-June 1973 (dotted lines);
mean discharge and monthly mean discharge 1923-1965
(solid lines).

Data from U.S. Geological Survey and UNESCO (1969).

A

DISCHARGE OF CHARLES RIVER
MONTHLY AVERAGE (1965-1973)
JAN. - SEPT. 1973 (5 DAY AVERAGE)
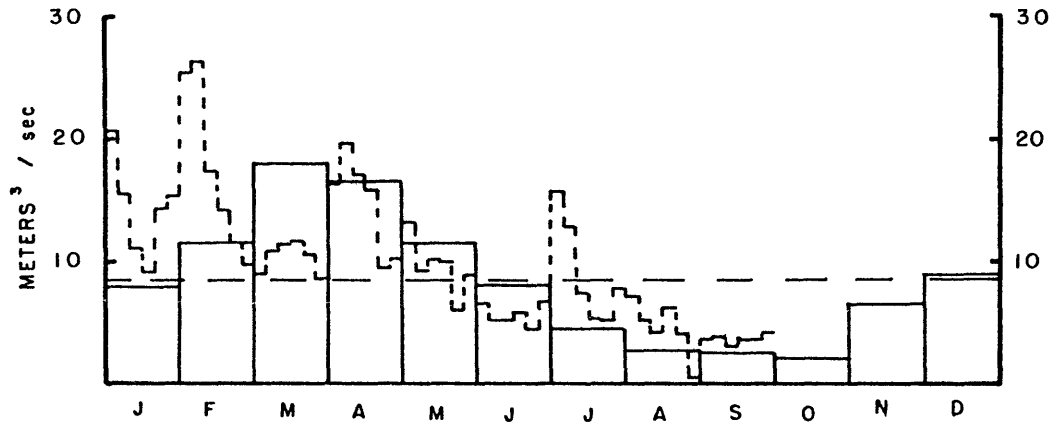
B

DISCHARGE OF MERRIMACK RIVER
MONTHLY AVERAGE (1923-1965)
JAN. - SEPT. 1973 (5 DAY AVERAGE)
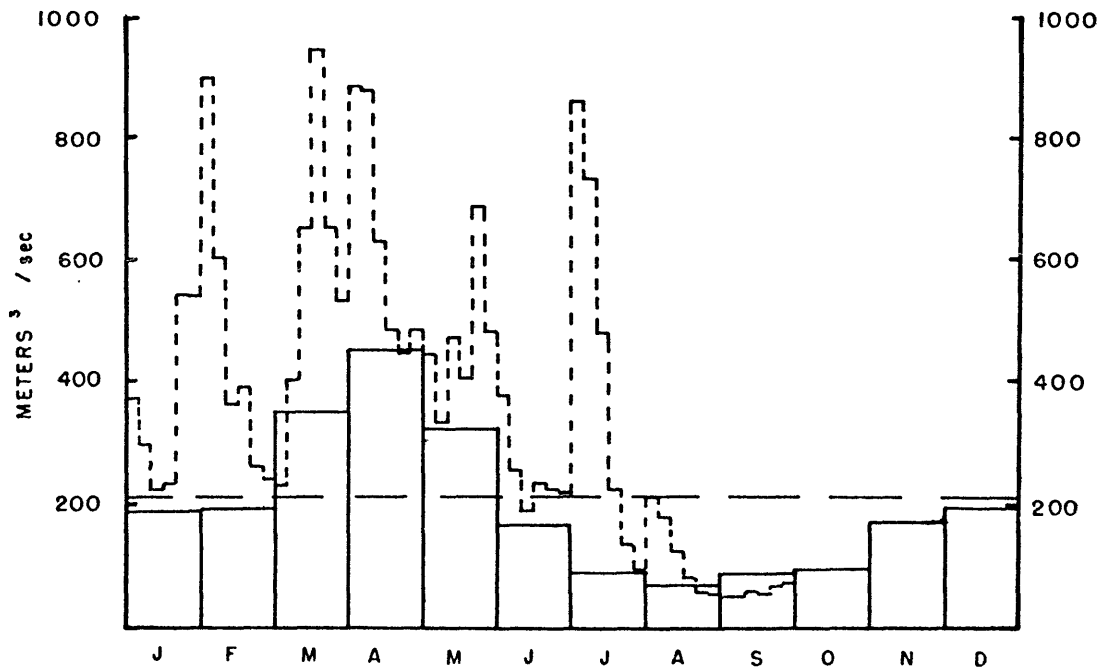
Figure 2.2

isothermal, but by late May and early June the difference between surface and bottom temperature is 5-10°C (Bumpus, 1974). The early river discharge is into an unstratified water column, while the later discharge is into a more stable water column, both due to the surface heating and surface freshening. In addition, wind stress during the spring months is not large. Because of the increased stratification, downward mixing of the fresh water discharge may be significantly reduced as the spring progresses.

C. The Field Program

Hydrographic observations and moored current meter measurements were made during the spring runoff period of March-May, 1973. The objectives of the field program were to:

(1) describe the spatial and temporal variation of the salinity and density fields during the runoff period in the northern part of Massachusetts Bay (north of 42°10'),

(2) describe the major (subsurface) current patterns associated with the density field, particularly the competing influence of the local discharge of the Charles, and the expected freshening from the north and east.

1. The Current Measurements

Three Savonius rotor Richardson current meters were deployed in Massachusetts Bay from March 4 - June 3, 1973 (figure 2.1). Two instruments were located near the Boston Lightship at 20 and 30 m in water 35 m deep (station 1). A third current meter was located 15 km due west at a depth of 35 m in water 65 m deep (station 2).

Several considerations heavily influenced placement of the three available current meters. Current measurements at the Boston Lightship (figure 2.1) made in the spring of 1972 indicated strong currents

Figure 2.3   Progressive vector diagram of current at Boston Light-
ship 10 m from the bottom, spring 1972   (see figure 2.1
for location). The surface salinity dropped approximately
$1^{\circ}/_{oo}$ on April 25 and May 5, coincident with the major
change in current flow. The bottom salinity did not
change significantly, although the data is sparse
(salinity from U.S. Coast Guard).

KILOMETERS

BOSTON LIGHTSHIP

72 – IV – 04 TO 72 – V – 16

Figure 2.3

(10-20 cm sec^{-1}) aligned northwest-southeast parallel to the coast with

periods of 5-10 days; abrupt changes of flow direction, occurring in less

than one day, were often associated with a major change in the surface

salinity (figure 2.3). The long time scale of the flow, the associated

surface salinity changes, and lack of obvious wind dependence strongly

suggested that the flow was density driven. Currents measured during

this period were the largest sustained flows observed throughout the year

at the lightship station. It was of interest to investigate this aspect

of the spring flow further. Four questions were of particular interest,

and the three available instruments were deployed with these in mind:

(1) Is the pattern associated with the local fresh water flow,

or due primarily to the influence of the Merrimack?

(2) What is the spatial scale of the current?

(3) What causes the reversing nature of the flow?

(4) Is the flow barotropic or sheared (as in Csanady, 1971)?

To minimize wave influence, instruments were deployed on subsurface

moorings with the flotation 20 m from the surface.

2. The Hydrographic Observations

Detailed surveys of the density field were made on a two-week

basis while the current meters were deployed. Four surveys were conducted

by Mr. Veshpati Manohar-Maharaj (March 29-30, April 14-15, 21-22, May 5-6,

and June 2-3) and an additional survey was made on May 15-16. Approximately

30 stations 7-9 km apart were occupied on each cruise in a period of 24

hours. The cruise of April 14-15, 21-22 was broken into two parts due

to bad weather. Unfortunately, due to equipment problems, the first hydro-

graphic cruise was not made until late March.

An M.I.T. built C.T.D. was used to obtain vertical profiles of conductivity and temperature. Salinity was computed from conductivity and temperature. The C.T.D. was not well calibrated; a temperature dependent correction was made on the basis of surface C.T.D. readings and bottle samples (See Maharaj and Beardsley (1974) for details). Estimated relative errors in temperature, salinity, and sigma-t are T $\pm$ .1°C, S $\pm$ .1°/$_{oo}$, sigma-t $\pm$ .1 . The relatively poor accuracy of the instrument will not affect the conclusions of this study.

D. Results

In this work, the main concern will be the spatial distribution of density, the changes of the distribution during the spring, and the relationship of the currents to the observed density field. Throughout the spring period the density is primarily controlled by the salt distribution, although temperature becomes an important factor later in the spring.

The salinity observations, with the exception of the cruise of May 15-16, are presented in Maharaj and Beardsley (1974) but they do not discuss the density or temperature distribution. A volumetric analysis of the amount of fresh water in the basin as a function of time compared favorably with the amount discharged by the Charles River system and Merrimack River, with suitable corrections for time lag and mixing. Maharaj and Beardsley conclude that the major freshening of the bay is due to fresh water which enters from the north (inferred from a distinct surface plume), and that within experimental error, all of the fresh water runoff of the Merrimack and Charles River systems can be accounted for in the freshening of Massachusetts Bay north of 42°25'N and west of 70°20'W. The volumetric aspects of the salt distribution will not be discussed further.

The current observations must be discussed in the context of the entire spring runoff period. Thus, although Maharaj and Beardsley (1974) have previously described the salt distribution, a brief review which emphasizes the changes in the spatial distribution of salinity and density is appropriate. The previously unreported observations of May 15-16, 1973 as well as a discussion of the changes in temperature and sigma-t is included. With the exception of the surface salinity distribution, the observations have been recontoured. With this hydrographic background, the current measurements will be presented and the two hydrographic cruises made while the current meters were deployed will be discussed in detail.

1. The Hydrographic Observations

a. The surface salinity distribution

The surface salinity distribution clearly shows the effect of the spring runoff (figure 2.4,a-e). The major features are summarized below:

March 29-30, 1973

The central portion of the basin is occupied by water with salinity greater than 31‰. The surface water nearshore, offshore (east of approximately 70°30'), and north of 42°30'N is slightly fresher, between 30-31‰. A salty core occupies the central basin with fresher water to the west, north, and east. The nearshore freshening is attributed to local runoff and the offshore freshening to the general freshening of the Gulf of Maine.

April 15-16, 21-22, 1973

The surface salinity over the surveyed area is between 30.2‰ and 30.8‰. The major accumulation of fresh water in the Bay occurred between March 29-30, and April 21-22.

Figure 2.4 Surface salinity distribution in northern part of
            Massachusetts Bay and east-west salinity distribution
            along 42°20'N, spring, 1973. Surface distribution in
            a,b,c,e drawn from continuous sampling along indicated
            track (redrafted from Maharaj and Beardsley, 1974);
            distribution in d drawn from surface samples at indi-
            cated stations. East-west section contoured from CTD
            stations at indicated locations , usually starting
            between 1 - 3 m. Slight discrepancies between east-
            west and surface contours result from the different
            data sources (CTD casts starting at approximately 2 m
            vs. continuous surface sampling) used to draw the
            contours.
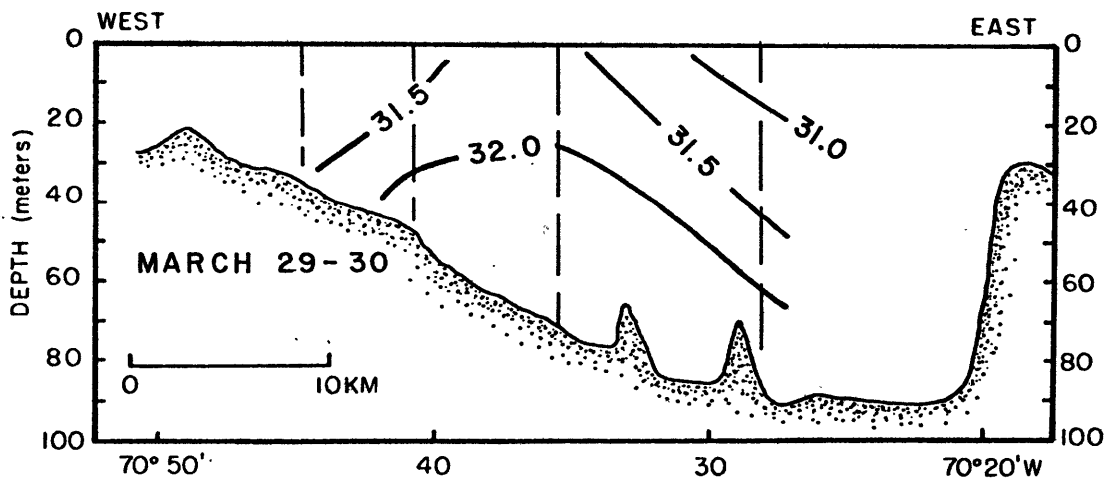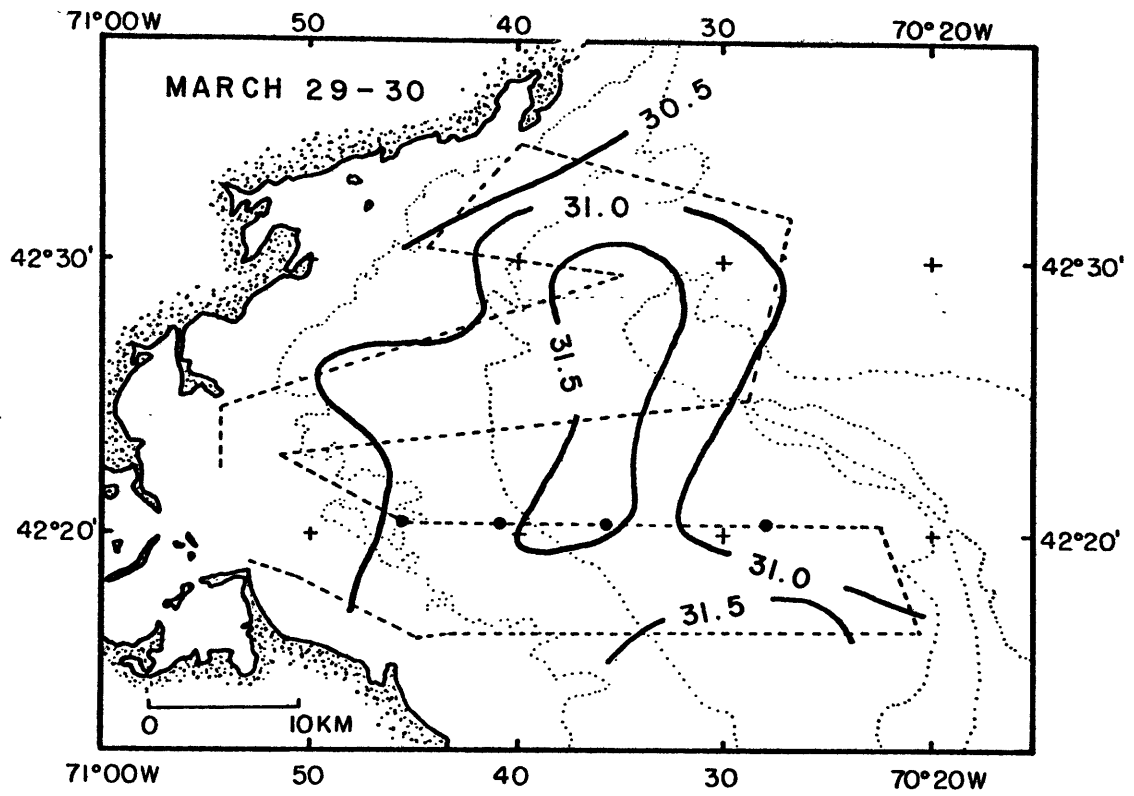
Figure 2.4a
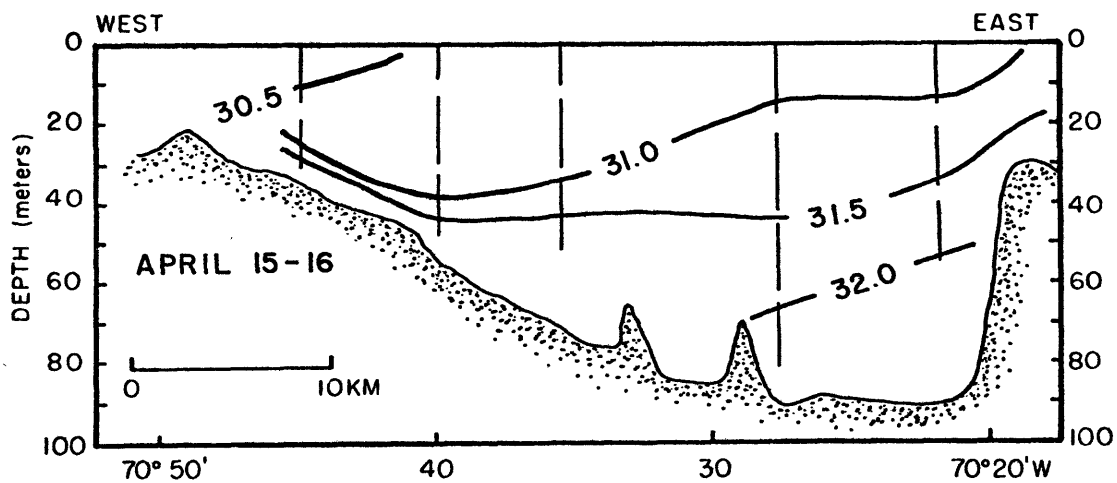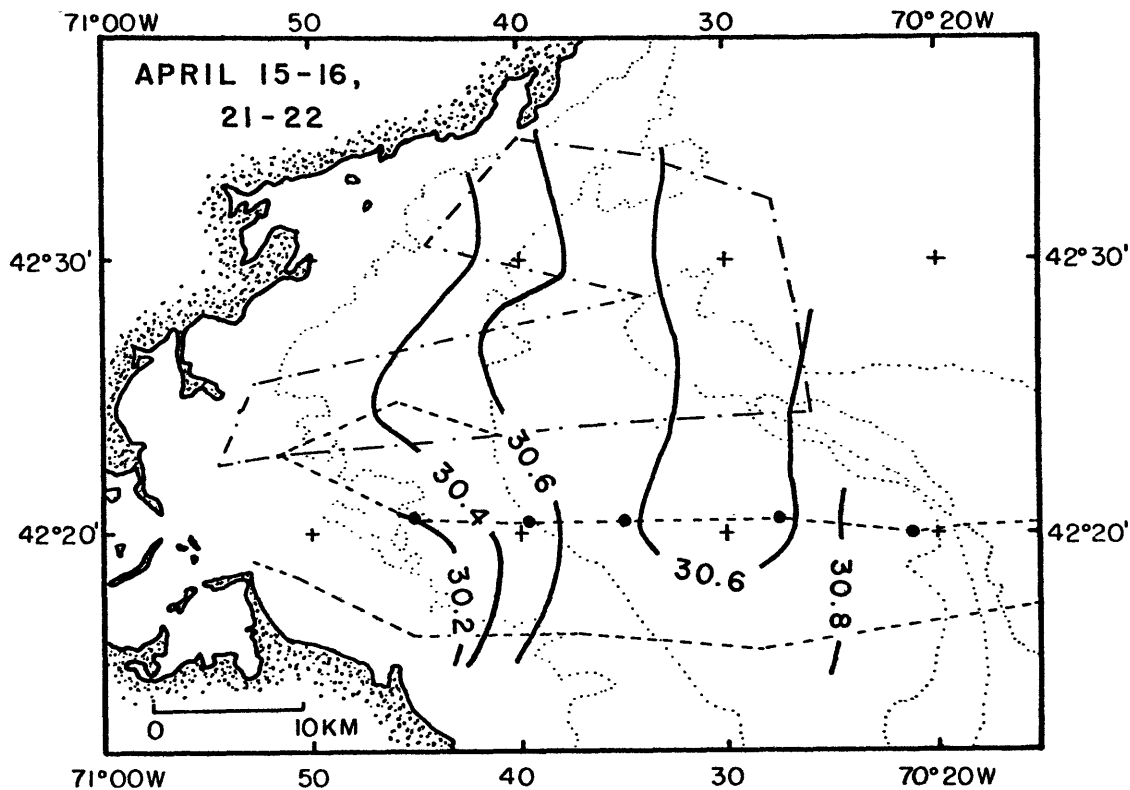
Figure 2.4b
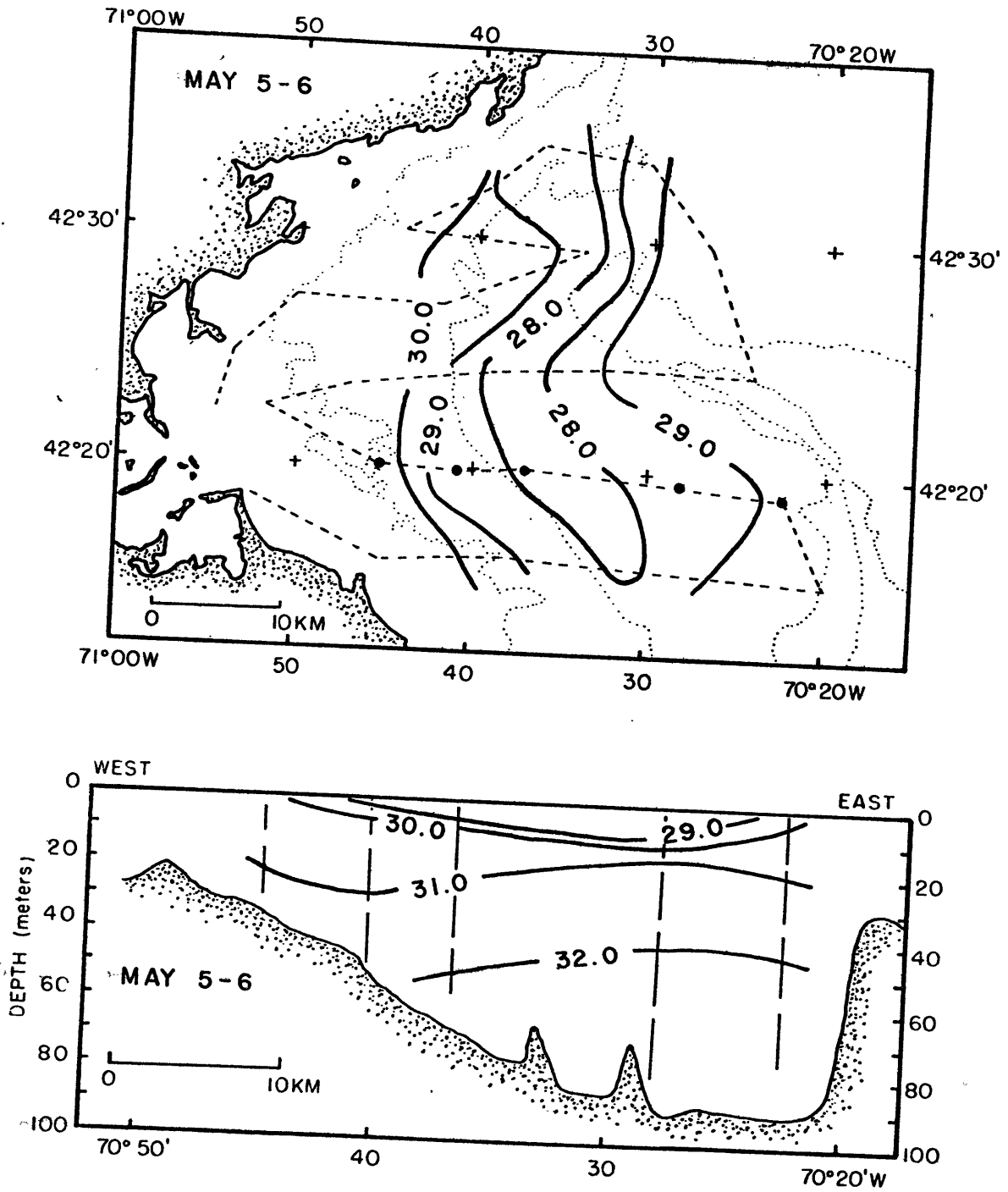
MAY 5-6
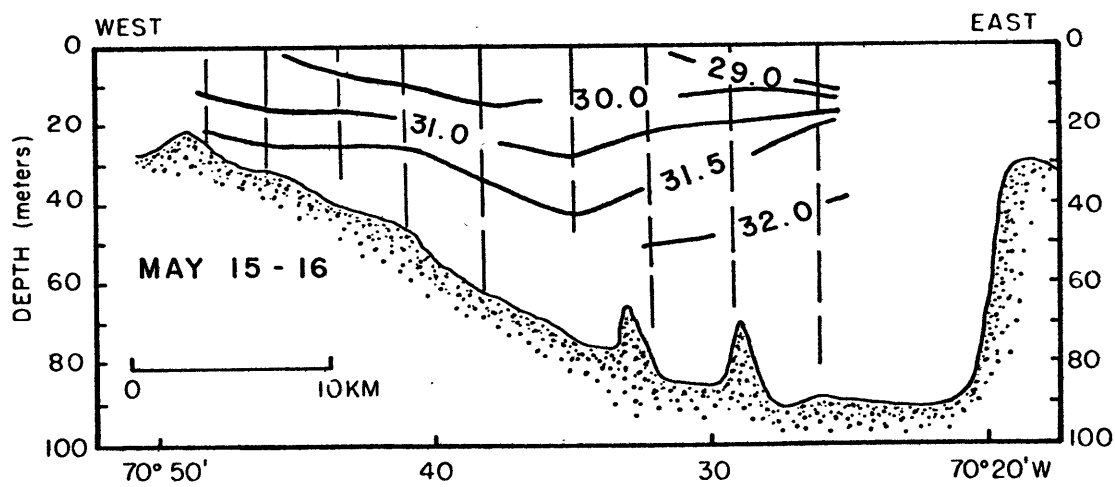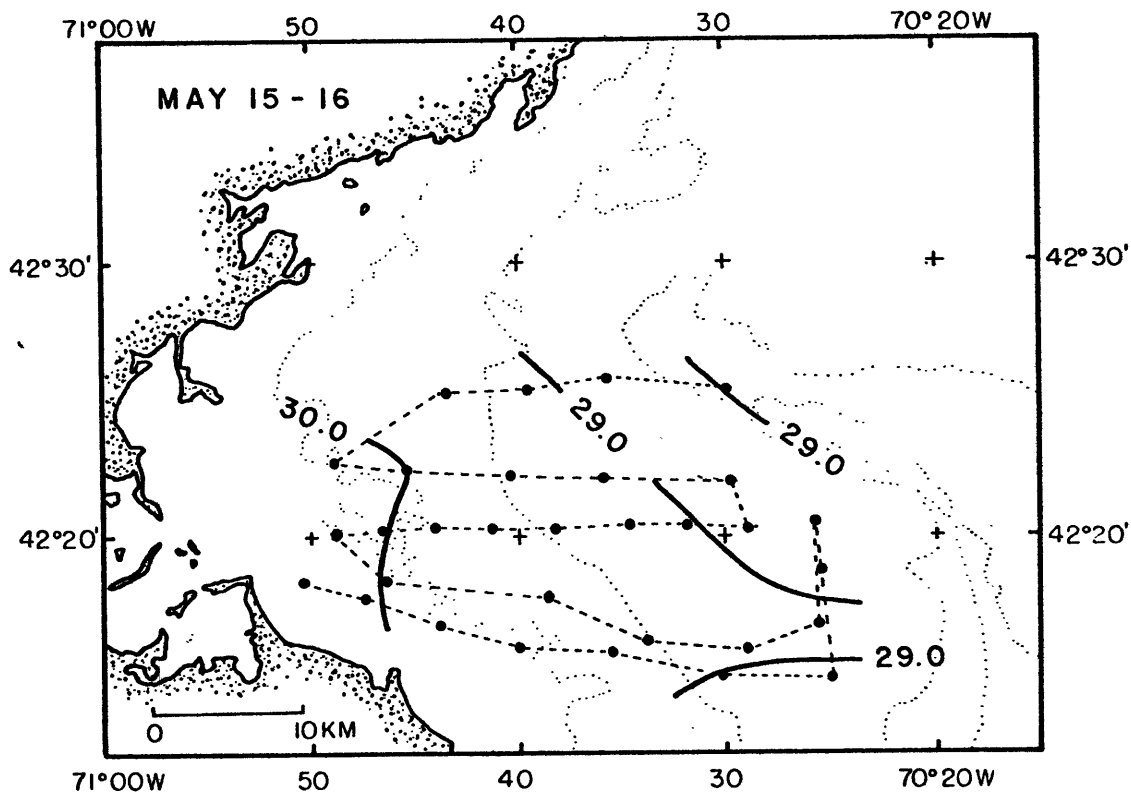
MAY 5-6

Figure 2.4c

Figure 2.4d
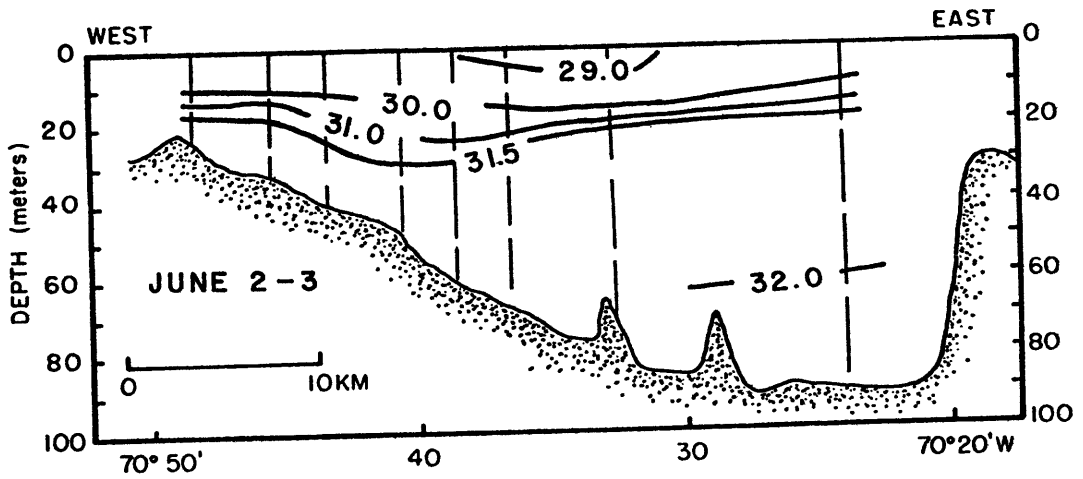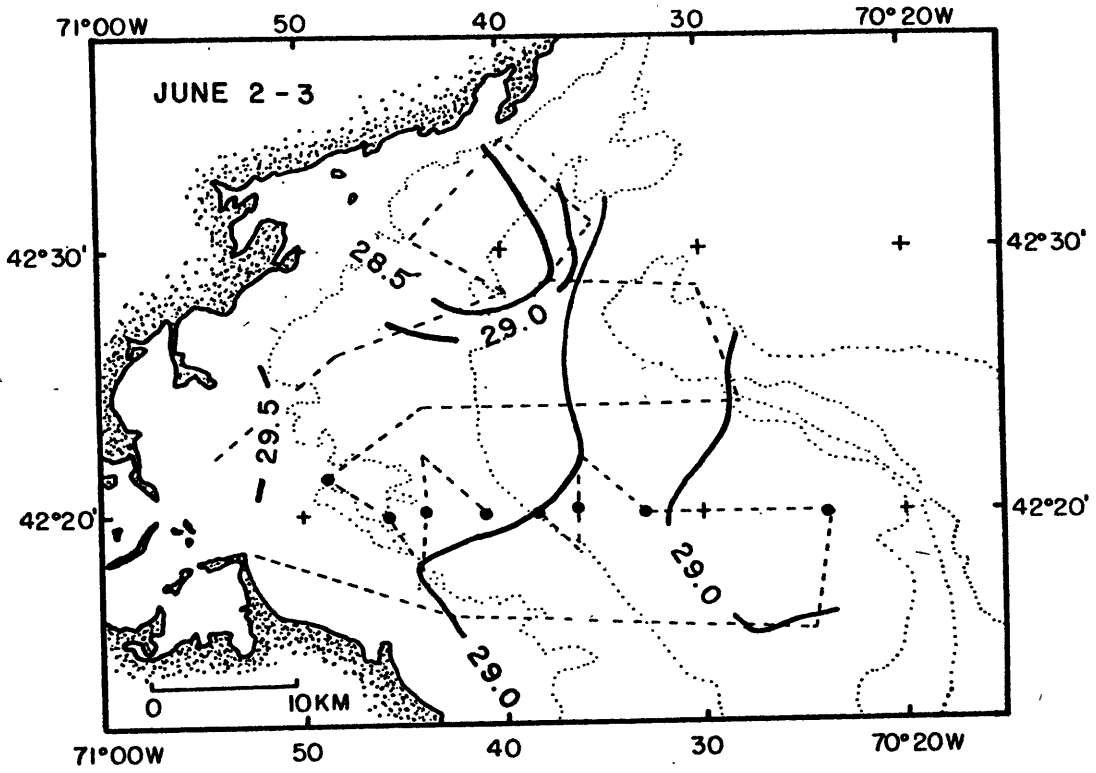
Figure 2.4e

May 5-6, 1973

A clearly discernible plume with salinity less than 29°/$_{oo}$ occupies the center of the basin with saltier water to the west and east. The plume only occurs in the upper layers and does not contribute a major volume of fresh water to the basin.

May 15-16, 1973

The surface plume, indicated by the 29°/$_{oo}$ isohaline, has moved approximately 10 km to the east and is compressed from the previous section. The 30°/$_{oo}$ isohaline remains near the Boston Lightship. (It should be noted that the survey is of smaller north-south extent than the others, but with closer station spacing).

June 2-3, 1973

The surface plume has moved back to the west toward the center of the basin and is somewhat narrower. There is no 30°/$_{oo}$ water left on the surface; an intrusion or pool of fresher water appears in the northwest.

b. The horizontal salinity distribution

Two features dominate the east-west salinity distribution (figure 4a-e) during the spring period which are not adequately resolved by the surface distribution. The major freshening of the basin occurs as a relatively deep lens of water located on the western side of the basin with salinity less than 31°/$_{oo}$. The lens does not occur on the first section of 29 March; at that time fresher water to the east and west surrounds a central salty core, as discussed in the surface distribution. The fresh lens is well established on April 15 however (figure 4b), and is most clearly marked by the 31°/$_{oo}$ isohaline. During the spring the lens gradually becomes more salty and less distinct, and moves 5-10 km in an east-west direction. Cruises were not frequent enough to determine

if the lens was a continuous feature which remained in the Bay throughout the spring or was a series of low salinity patches which advected through the basin.

The second major feature of the east west salinity distribution is the well defined lens of fresh water which appears near the surface during the later stages of the spring. The freshest water occurs in this lens (marked by the $29°/_{oo}$ isohaline in figure 4); the lens occurs in mid basin, but there is horizontal movement. In particular, both the surface and deep lens are displaced significantly to the east on the 15th of May.

c. The vertical structure at mid basin

As the spring progresses there are four major changes in the vertical structure of the water column: a decrease in the salinity of the water column in early spring primarily in a deep well mixed surface layer, a gradual increase of salinity at depth and further freshening at the surface, a warming of the water column, and the establishment of a pycnocline between 10 m and 30 m. These changes are illustrated for a typical mid basin station in figure 2.5a-c (near station 2, figure 2.1).

The sequence of vertical profiles are a result of vertical mixing, horizontal advection, and changes in the river flow. The surface layer changes can be explained in the following way. The major runoff occurs before the development of a seasonal thermocline, and the large volume of fresh water mixes deeply (a fresh mixed layer extends to 35 m on April 15-16). During the later part of the spring season, although there is smaller volume of runoff, the fresh water does not mix as deeply and thus the surface layers continue to freshen. The decreased vertical mixing is attributed to the establishment of a spring thermocline and to the generally weak wind stress in May (figure 2.7). The depth to which the

Figure 2.5   Progression of (a) temperature,   (b) salinity and
(c) signa-t at mid-basin (42°20'N, 70°35'W, near
station 2, figure 2.1).
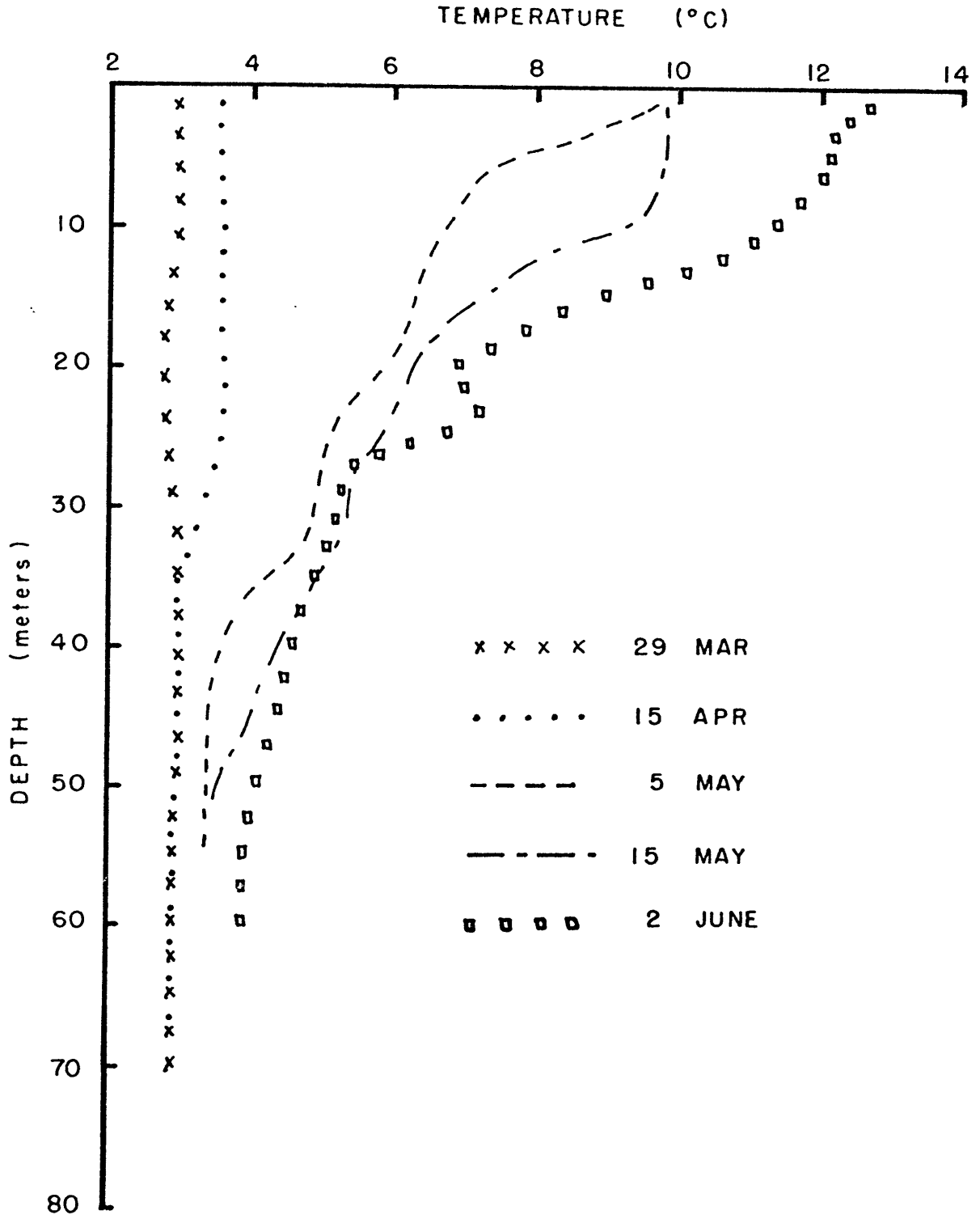
Figure 2.5a
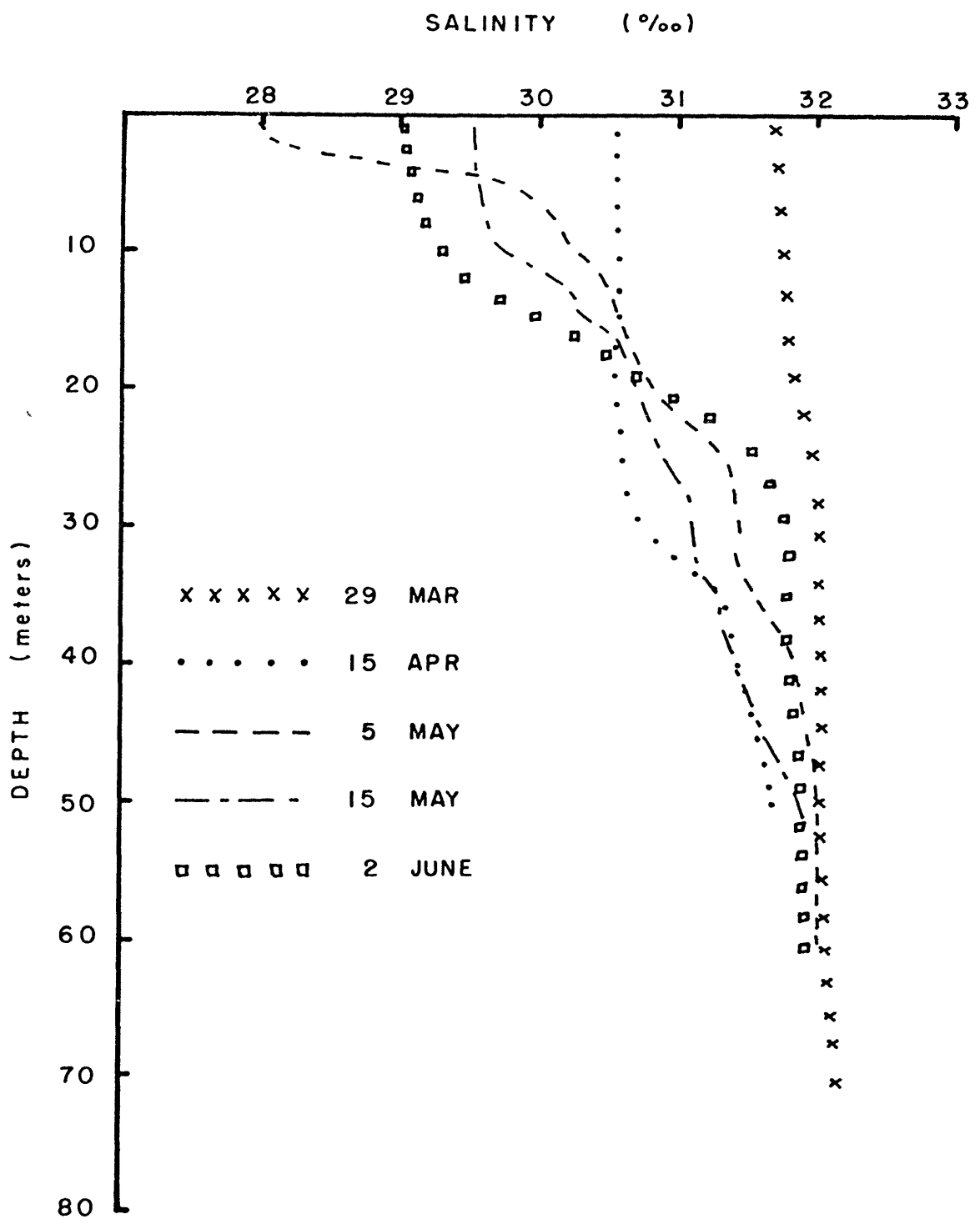
Figure 2.5b
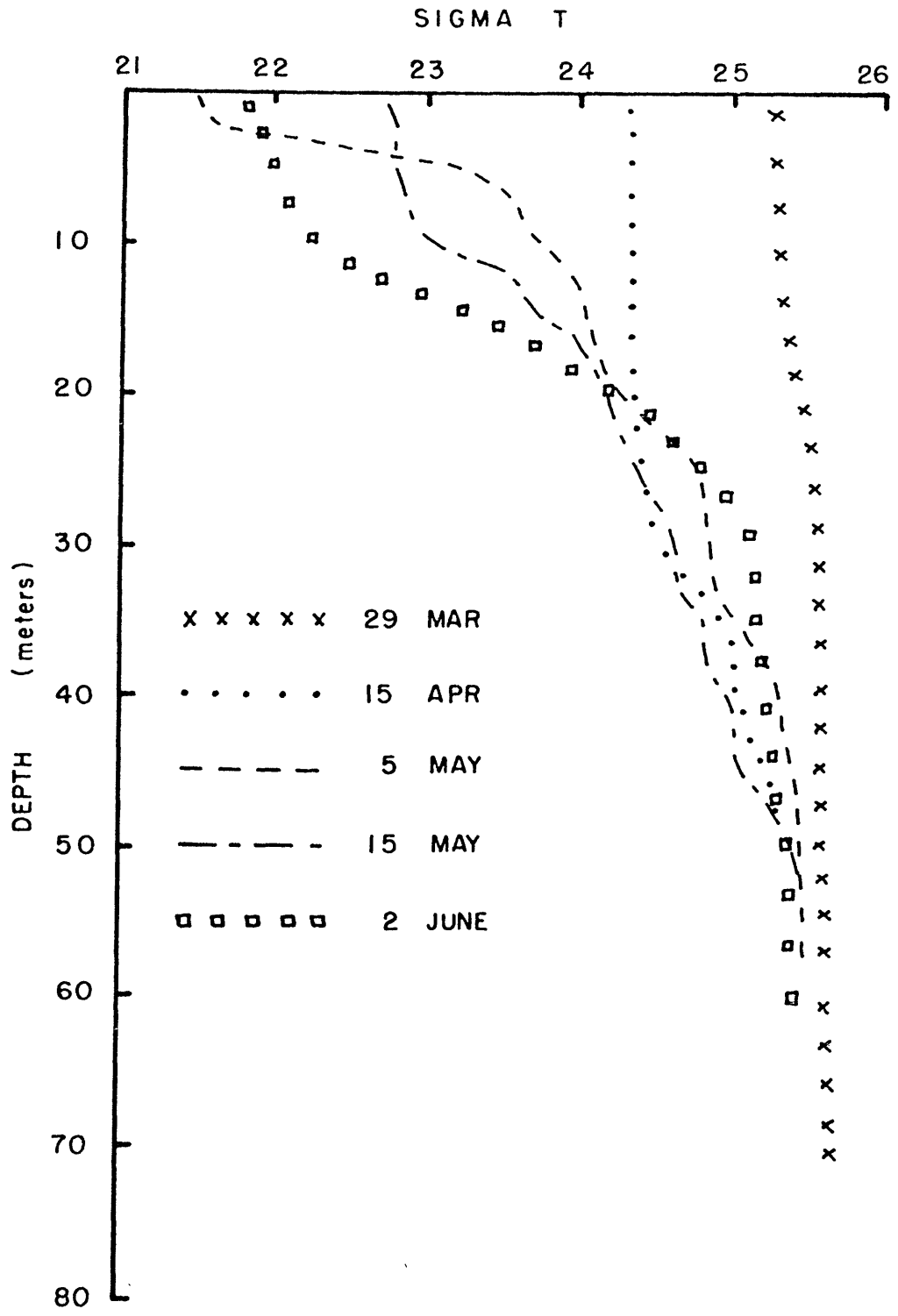
Figure 2.5c

runoff mixes may also be a function of local conditions at the river mouth during various stages of river flow. Changes in the position and strength of the near surface plume also affect the distributions in the surface layer.

The change with time of salt and heat in the deep layers is somewhat more difficult to interpret. The gradual warming of the deep water must occur by the downward mixing of heat. The surface waters are low salinity however, and thus downward mixing cannot be accompanied by an increase in the salinity, as is observed. The changes in the deep water thus must be advective, which implies that the basin flushing rate during the spring is less than two weeks. This rate is consistent with the net drift of Bumpus (1973, 1965) for the western Gulf of Maine in spring.

d. Summary: Stages of the spring runoff

In summary, there are four stages of the spring runoff which can be identified by the hydrographic measurements:

| Stage	River Flow	Hydrography
Early Spring	moderate	Freshening of the eastern and western edges of the basin, central salty core, well mixed water column
Mid Spring	maximum	Major decrease in salt throughout the basin, small horizontal variations, deep well mixed surface layer
Mid Spring	moderate	Well defined surface plume in basin with lateral movement, gradual heating
Late Spring	moderate, decreasing	Decrease in size and integrity of plume, gradual salting of deep layers and continued warming

2. The Current and Simultaneous Density Observations

The low passed current records from the upper instruments at stations 1 and 2 are characterized by relatively strong currents (5-20 cm sec^{-1}) which persist for 5-10 days (figure 2.6). The record obtained at station 1 is very similar to the one obtained in the spring of 1972 (figure 2.3). The magnitude of the current at least suggests that displacements on the order of basin scales occur in a few days during the spring period. Both northerly and southerly current is observed at station 1, but only southerly flow at station 2. The major flow axis is north-south. The current 5 m from the bottom at station 1 is similar to the current 15 m from the bottom, but much reduced in magnitude; the low passed current at the lower instrument does not exceed 5 cm sec^{-1} during the experiment.

The wind stress is relatively weak throughout the measurement period, except for one event on the 26th and 27th of April where the stress reaches one dyne (using a drag coefficient of 1.1×10^{-3}). In response, the current at station 1 accelerates parallel to shore and the flow at station 2 is offshore, opposite to the wind, as discussed in Chapter I. Otherwise the low passed wind stress (as measured at Logan Airport) is less than .5 dynes cm^{-2} . Sea level at Boston, shown in Chapter I to be a good indicator of wind driven currents, also shows little change during the experiment except for 26-27 April and May 17-18.

The slow change of the currents with time and the lack of strong winds suggests that the observed flows are density driven. Any model of the currents during the spring runoff period must satisfactorily explain the following characteristics:

Figure 2.6 Low passed current, wind and sea level, April 26 –
June 2, 1973. Arrows indicate period of hydro-
graphic observations.

a) Current at station 2, 35 m.

b) Current at station 1, 20 m.

c) Current at station 1, 30 m.

d) Wind stress at Logan Airport
(computed using $\tau = \rho \, C_D \, u^2$, $C_D = 1.1 \times 10^{-3}$).

e) Sea level at Boston.

All series have been filtered with a Gaussian filter
($\frac{1}{2}$ power at 56 hours) to suppress tidal and inertial
oscillations. The current meter records have been
subsampled every three hours and plotted as vectors
(north at top of page). A time base malfunction on
the lower current meter at station 1 has been graphic-
ally corrected (see Beardsley and Butman, 1974b).
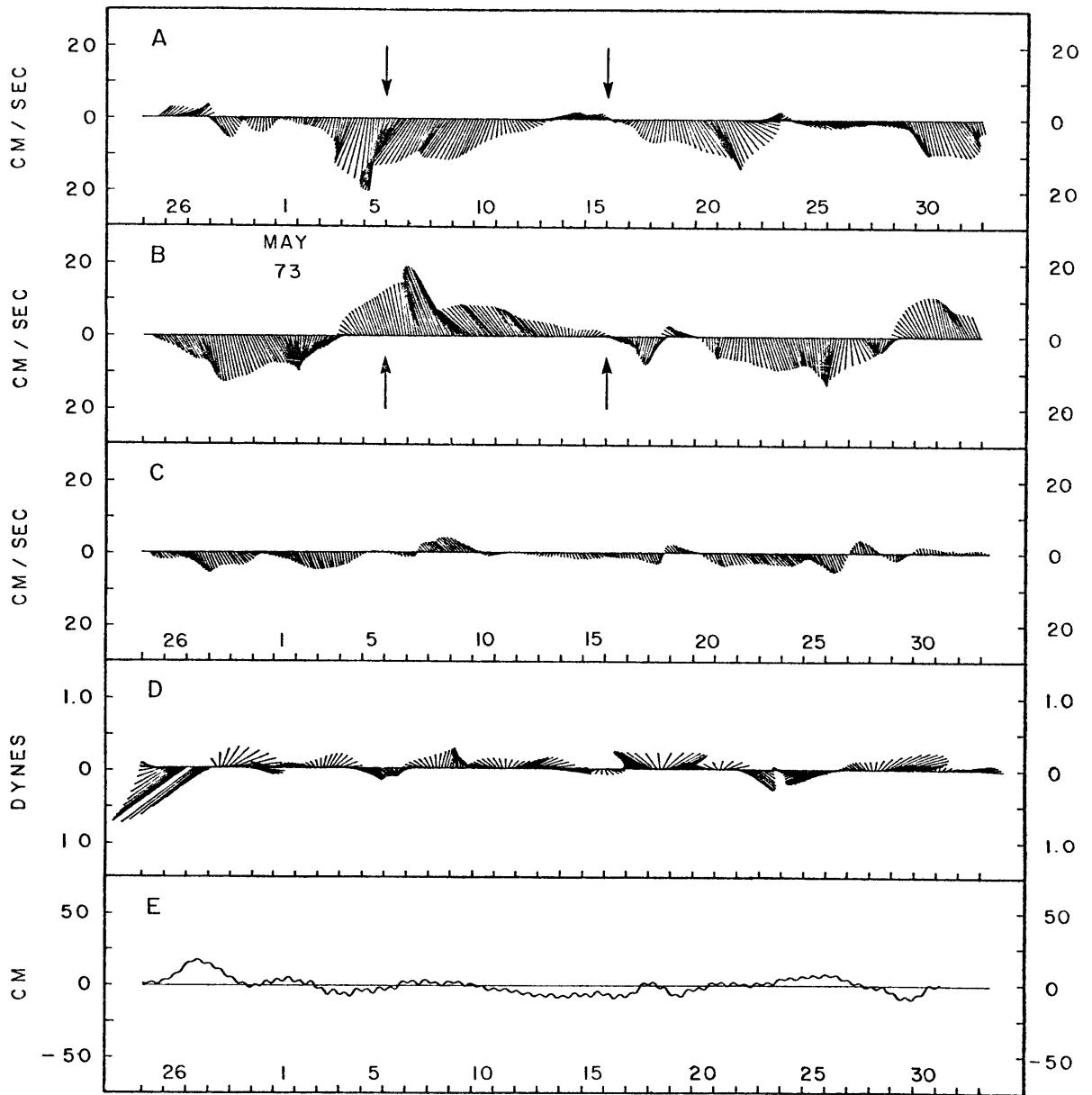
Figure 2.6

(1) large current velocities (5-20 cm sec^{-1}) which persist for

5-10 days,

(2) rapid reversals in direction of flow,

(3) large horizontal shear,

(4) large vertical shear with low velocities near the bottom.

To begin, the observed current and density distribution on May 5-6, 1973

and May 15-16, 1973 are presented in detail.

a. Observations of May 5-6, 1973

On May 5-6 the surface density distribution is dominated by

a shallow plume of fresh water (figure 2.4c and figure 2.7a) which enters

the basin from the north. Denser water is found to the east and west.

At 20 m (figure 2.7b) the plume is displaced to the west. At 30 m (figure

2.7c) an isolated lens of lighter water (sigma-t less than 24.6) is found

on the western edge of the basin, offset from the center of the surface

plume. Denser water occurs to the north, east, and south, and the lens

appears to intersect the bottom on the western side of the bay. An east-

west density section clearly shows the surface plume and the deep lens

(figure 2.7e).

The hydrographic cruise was conducted during a major current event

(figure 2.6); the low passed current was to the northwest at station 1 and

to the southwest at station 2 for approximately eight days from May 4-12.

The direction of the low passed current is parallel to the sigma-t con-

tours (figure 2.7b,d) to within the accuracy with which the contours can

be drawn. It should be noted that at the 30 m surface the 24.80 sigma-t

contour in the southwest corner of the basin has been closed. It would

be consistent with the data however to have both the inshore and offshore

24.8 contour continue to the south, without closing. At 35 m (figure 2.7d)

Figure 2.7   Density distribution and observed low passed current,
             May 5-6, 1973.

a)   Sigma-t, surface .

b)   Sigma-t at 20 m and observed current.

c)   Sigma-t at 30 m and observed current at 35 m.

d)   Sigma-t at 35 m and observed current .

e)   East-west section of sigma-t along 42°20'N, observed
     north-south current and geostrophic shear relative
     to indicated level. Northerly flow is shown to the
     right, southerly flow to the left.

SIGMA-T SURFACE
MAY 5-6, 1973

Figure 2.7a

SIGMA-T and CURRENT
20 m.
MAY 5-6, 1973

CURRENT (cm/sec)

0   10

71°00 W   50   40   30   70°20 W

42° 30   42° 30

42°20   BOSTON   42° 20

0   K M   10

71°00 W   50   40   30   70°20 W

Figure 2.7c

SIGMA-T and CURRRENT
35 m.
MAY 5-6, 1973
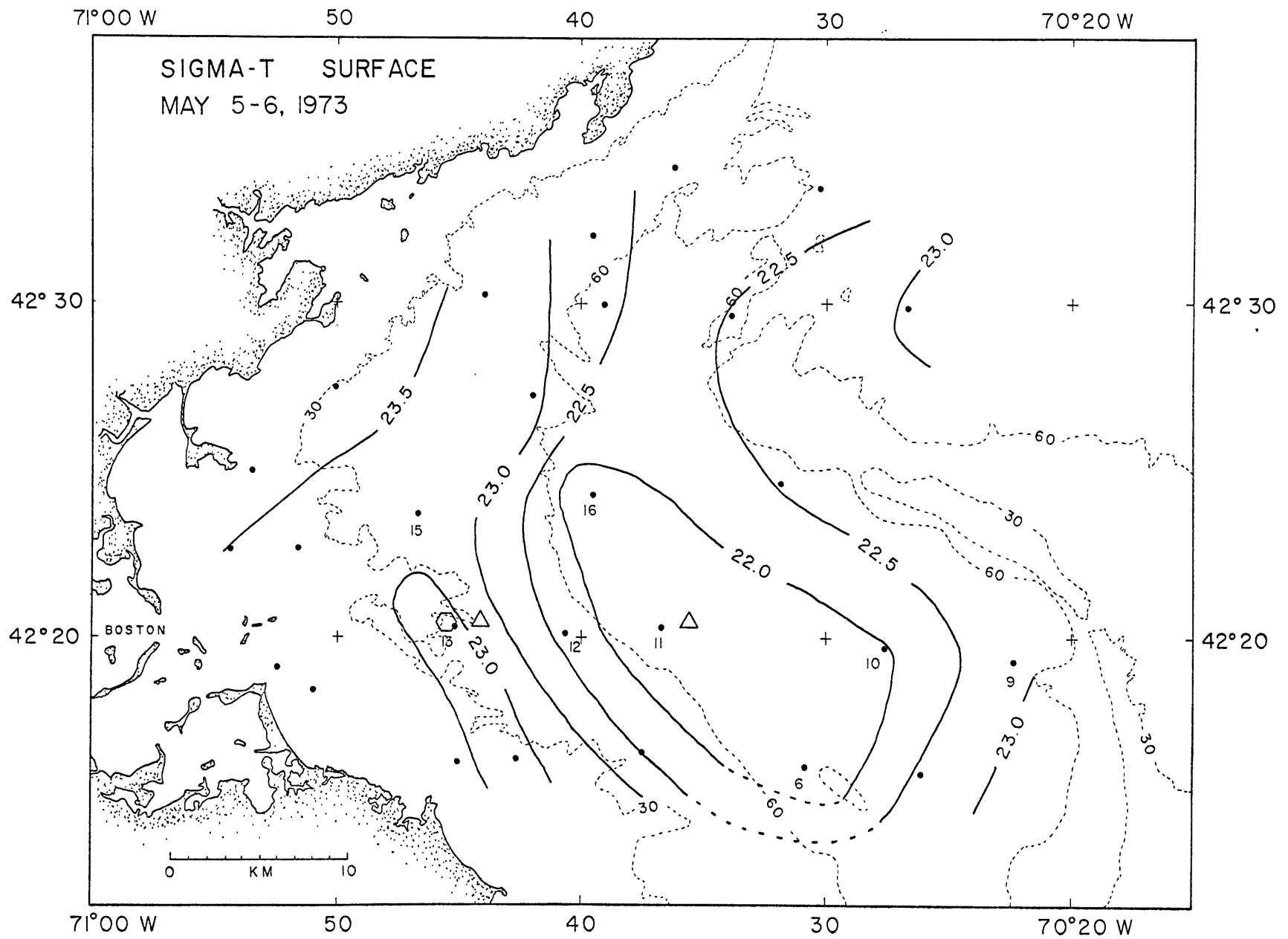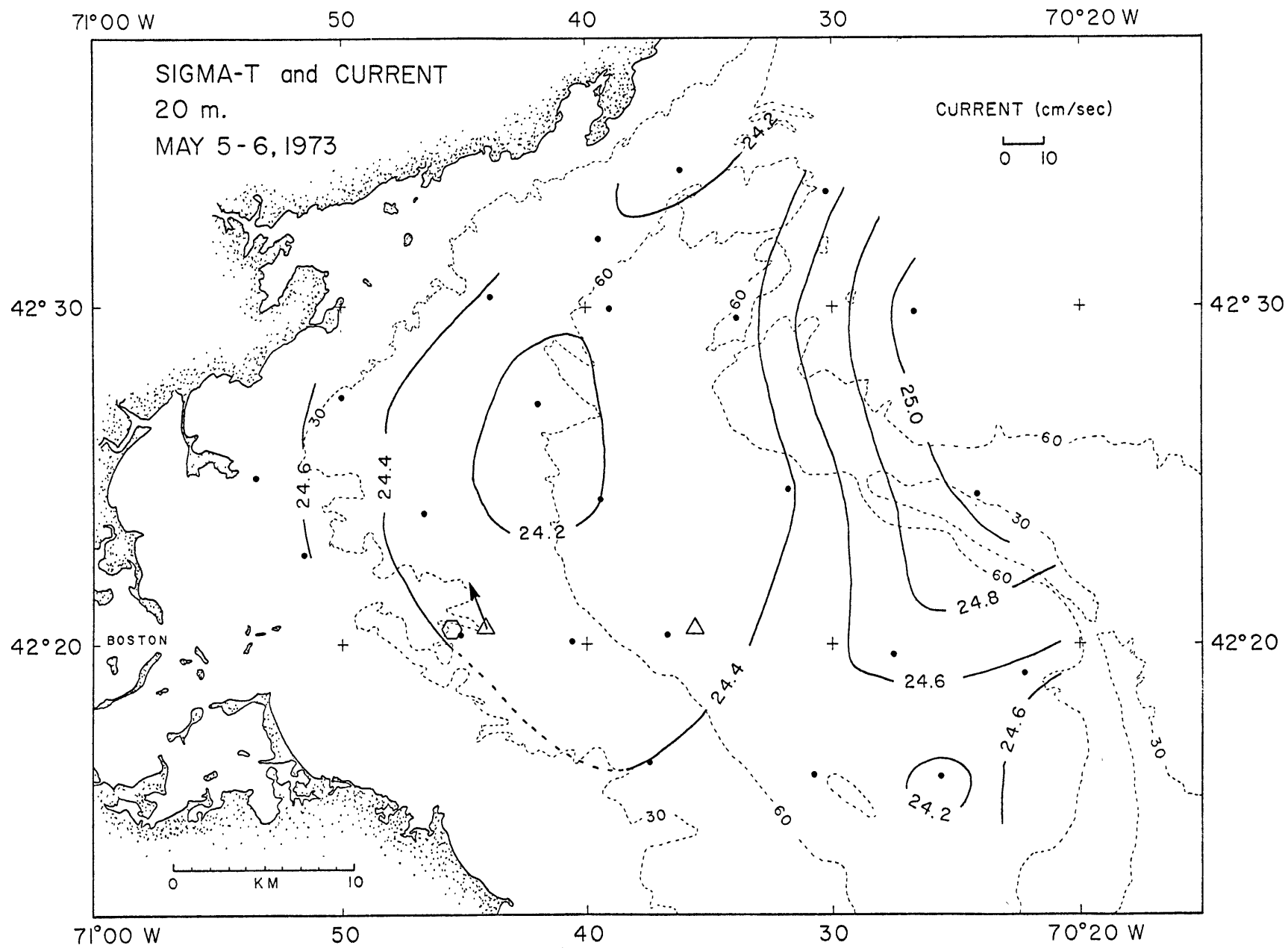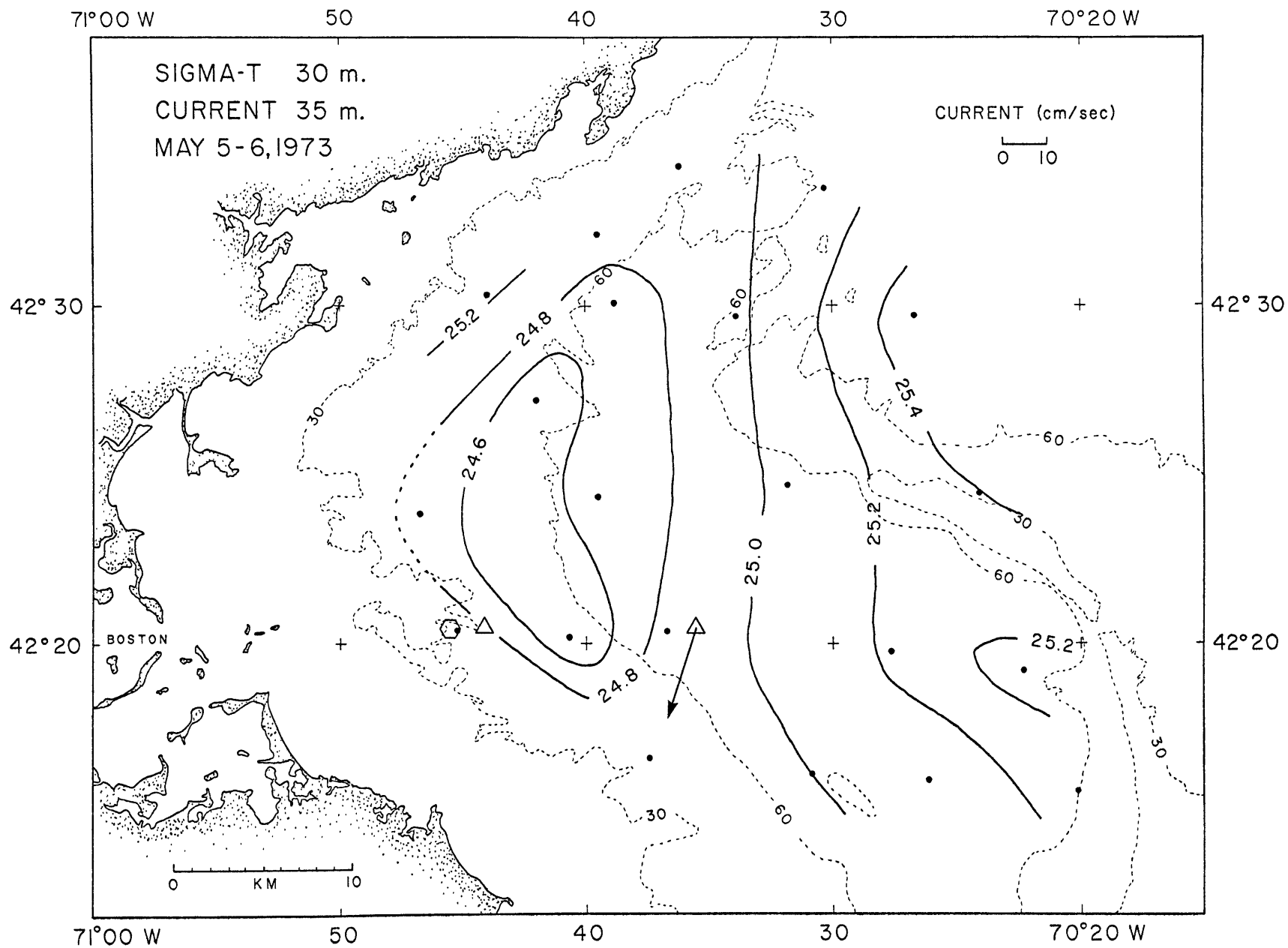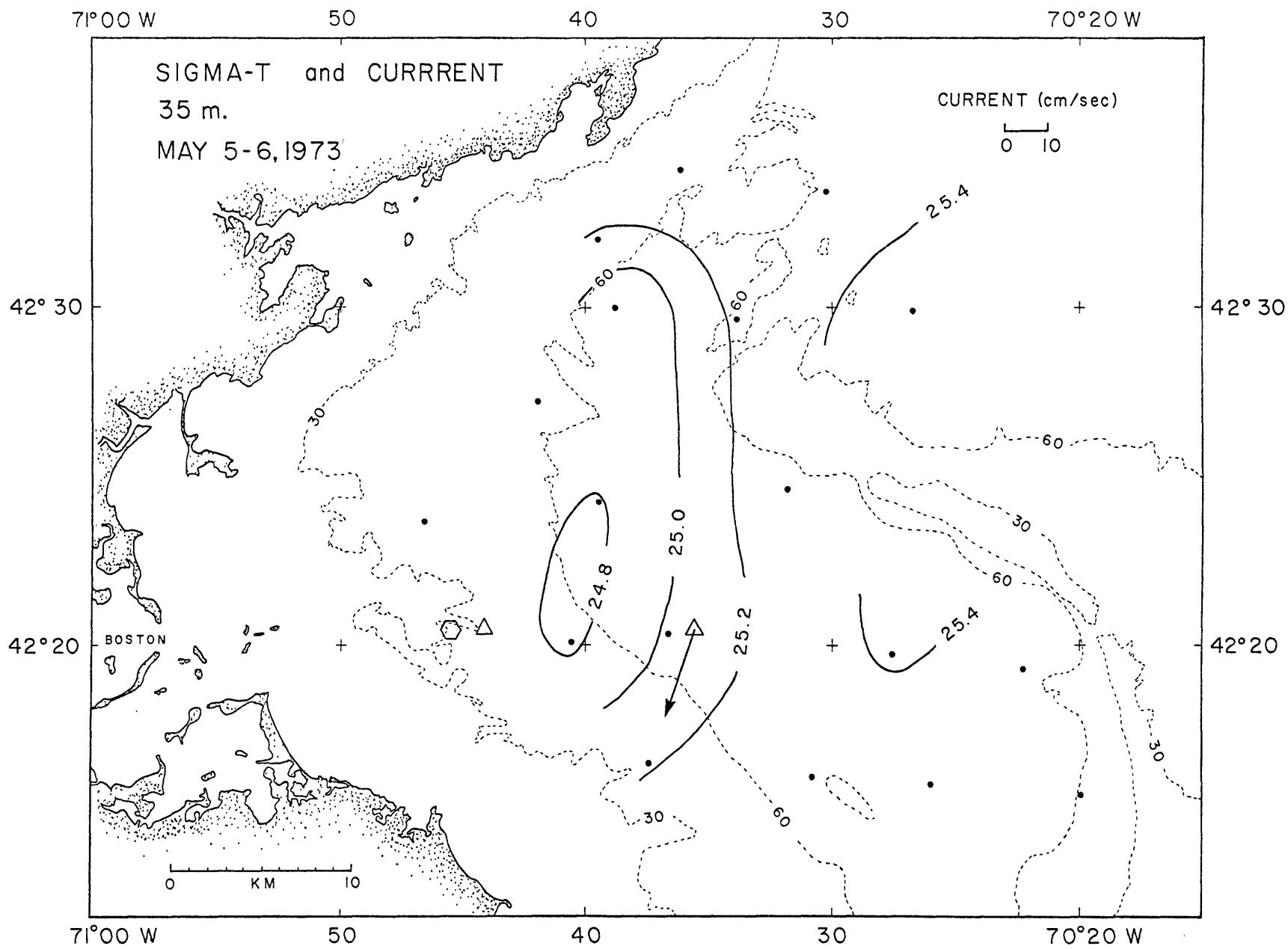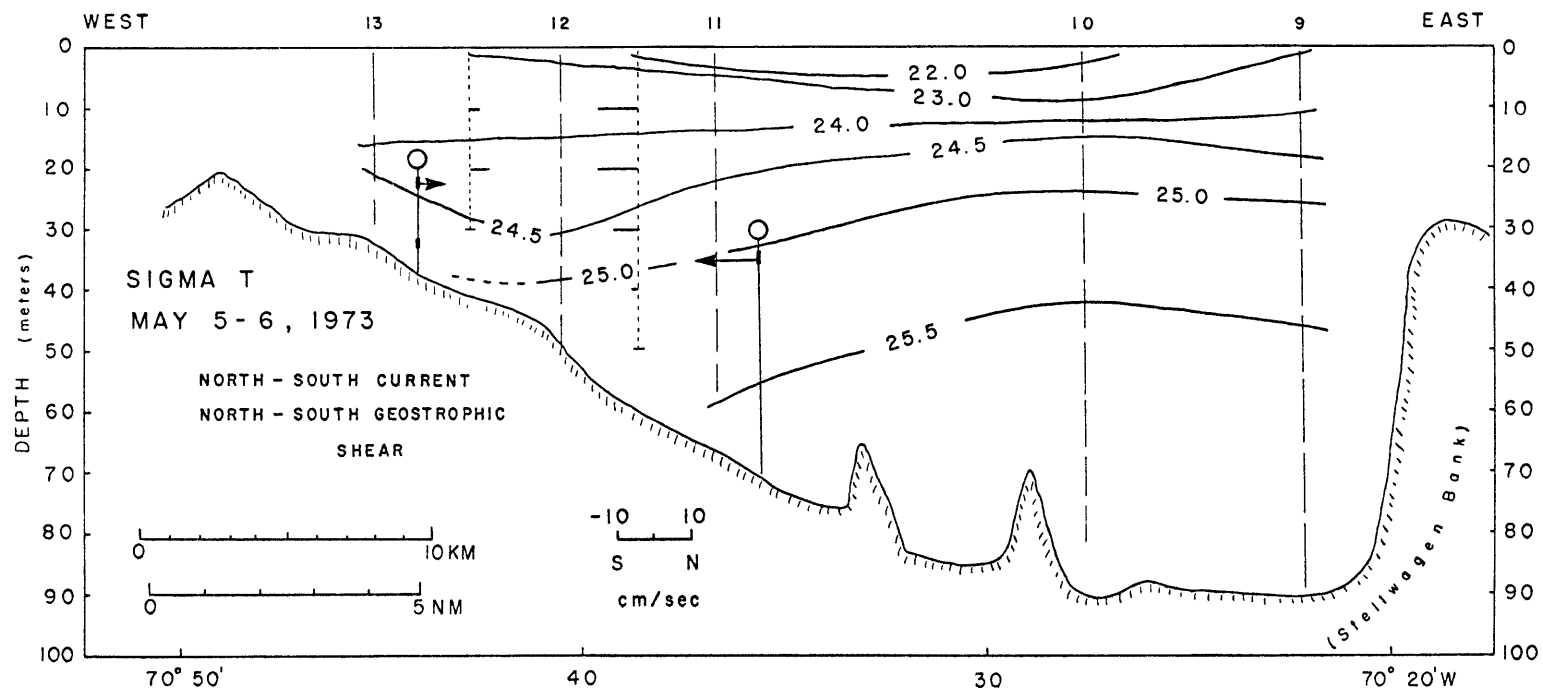
Figure 2.7d

Figure 2.7e

the sigma-t contours appear to run normal to the coast; the station
spacing is not close enough to accurately map the adjustment of the
fresh lens to the boundary.

The geostrophic shear computed from the thermal wind relation
accounts for all of the observed east-west shear and 60% of the north-
south shear at station 1 (figure 2.7e and Table 2.1). At station two,
the computed shear relative to 50 m (the deepest observed depth) accounts
for about 40% of the observed current and is in the correct sense. The
estimates of shear are judged to be accurate to ±10% on the basis of
station position errors alone. It should also be noted that only one
station defines the fresh water lens (station 12, figure 2.7e), and thus
the observed density differences could reasonably be distributed over a
smaller distance. Finally, the low passed currents are compared to an
instantaneous measurement of the density field.

Despite these reservations, several conclusions can be made from
the section of 5-6 May and the observed currents.

   (1) The major current event of May 4-12 is associated with a
       subsurface fresh water lens, not directly with the well
       defined surface plume.

   (2) The observed shear at station 1 is approximately geostrophic
       and the shear at station 2 is in the correct sense if we
       assume zero flow near the bottom.

   b. Observations of May 15-16, 1973

In contrast to the strong currents and large horizontal
shear observed on May 5-6, the low passed current on May 15-16 was almost
zero at both stations. The sigma-t distribution shows clearly that the
surface plume has moved to the east at the surface (figure 2.8a), and that

TABLE 2.1

GEOSTROPHIC SHEAR AND OBSERVED CURRENT

May 5-6, 1973

BOSTON LIGHTSHIP

Hydrographic[1] Stations	Computed Shear (cm/sec)			Observed Current (cm/sec)				
	Depth(m)	E-W	N-S	Sta.Depth (m)	Depth Obs. (m)		E-W	N-S
12-13	29-20	–	6	35	30		∿ 0	∿ 0
	29-10	–	3		20		– 3	+10
	29- 1	–	5					
15-13	29-20	-4	–					
	29-10	-6	–					
	29- 1	-7	–					

STELLWAGEN BASIN

11-12	50-40	–	-5	65	35		– 6	-20
	50-30	–	-8					
	50-20	–	-12					
	50-10	–	-12					
	50- 1	–	– 4					
6-16	64-50	0	–					
	64-40	-2	–					
	64-30	-4	–					
	64-20	-5	–					
	64-10	-6	–					
	64- 1	-1	–					

[1]See figure 2.7 a,e for station location.

Figure 2.8 Density distribution and computed shear, May 15-16, 1973.

a) Sigma-t surface.

b) Sigma-t at 30 m.

c) East-west section of sigma-t along 42°20'N, and north-south geostrophic shear relative to indicated level. Northerly flow is to the right, southerly to the left. Observed low passed current at stations 1 and 2 approximately zero.

SIGMA-T SURFACE
MAY 15-16, 1973

Figure 2.8a

SIGMA-T   30 m.
MAY 15-16, 1973
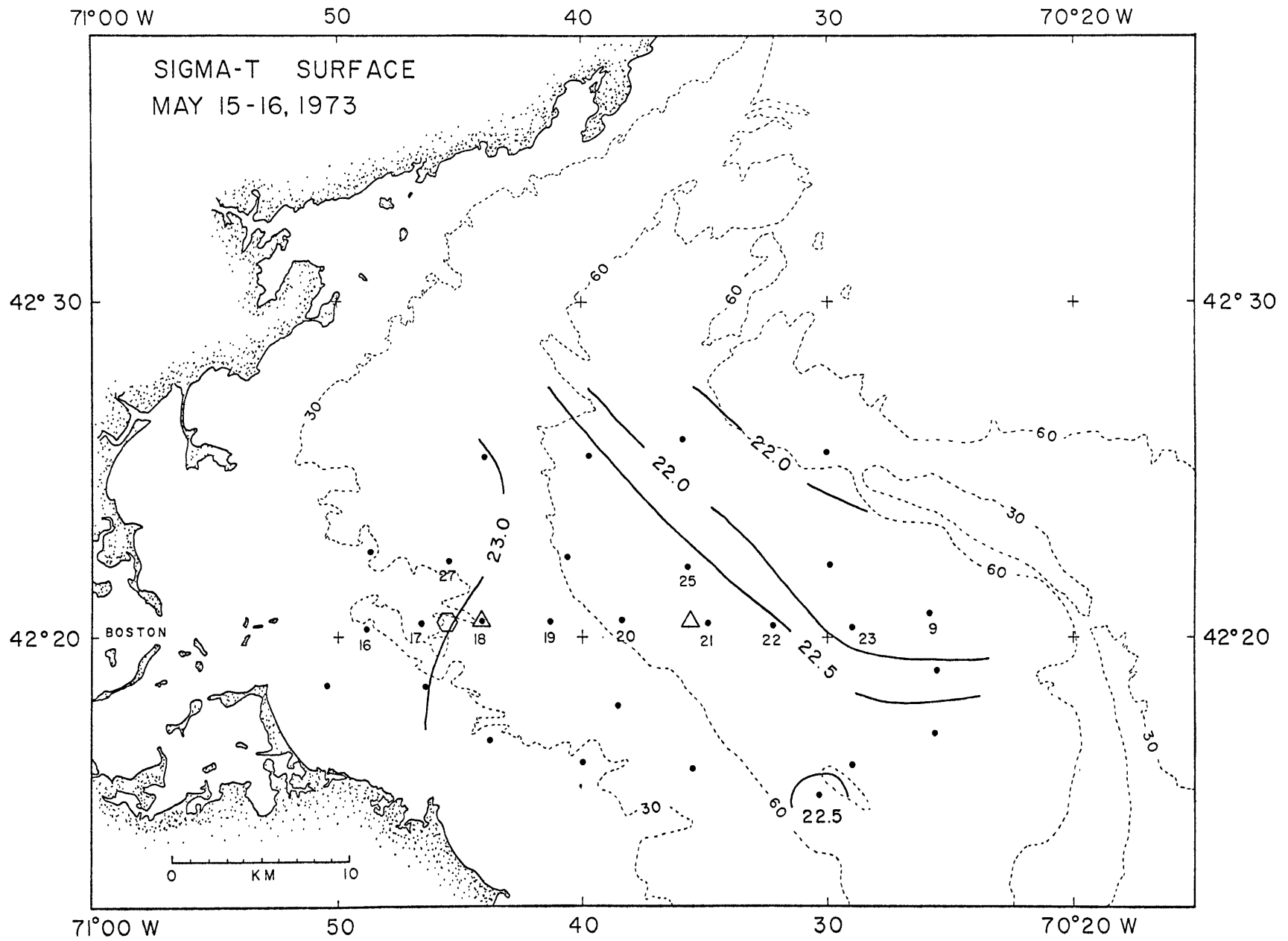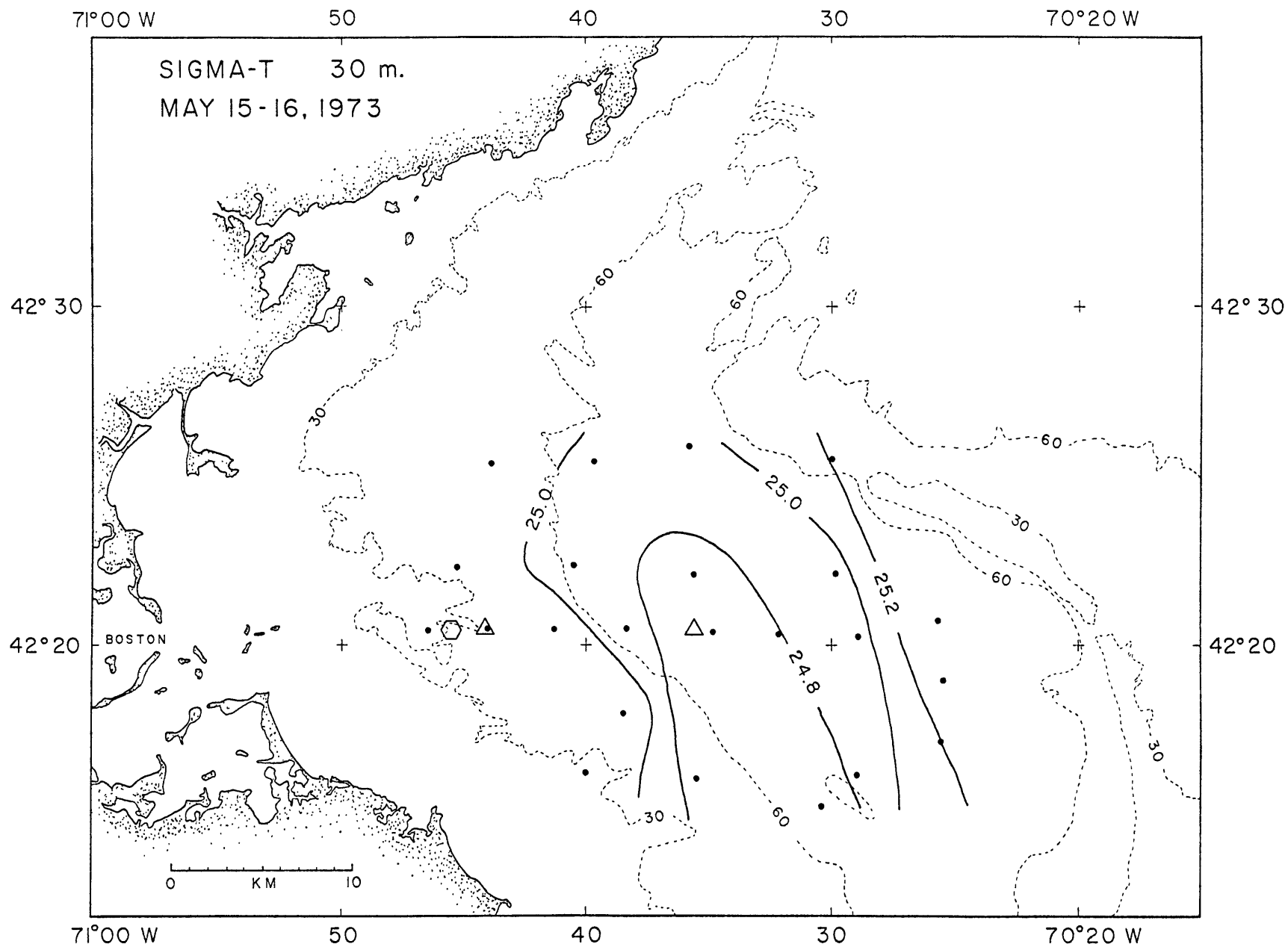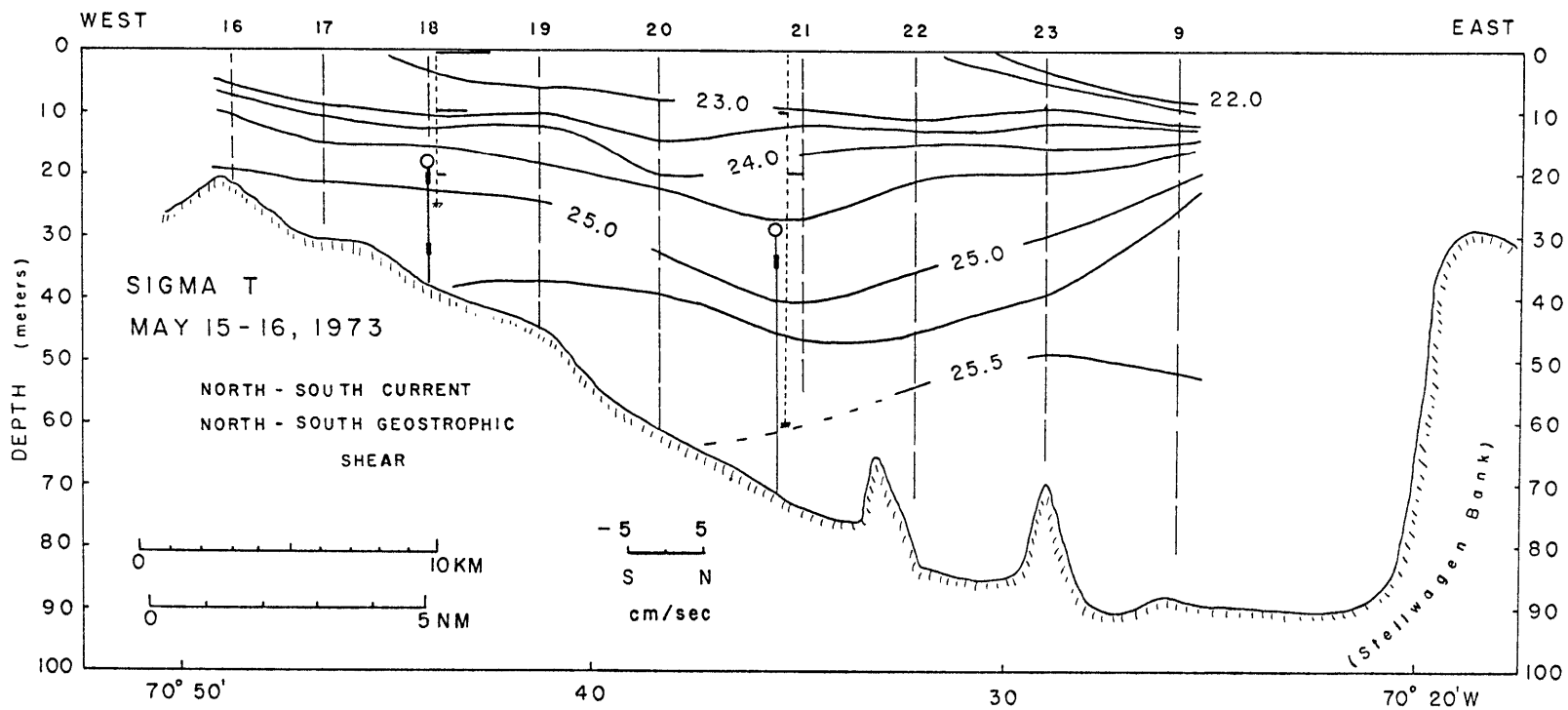
Figure 2.8c

TABLE 2.2

GEOSTROPHIC SHEAR AND OBSERVED CURRENT

May 15-16, 1973

BOSTON LIGHTSHIP

Hydrographic [1] Stations	Computed Shear (cm/sec) Depth (m)	E-W	N-S	Observed Current (cm/sec) Sta.Depth (m)	Depth Obs. (m)	E-W	N-S
17-19	25-20	−	1	35	30	+ 1	− 1
	25-10	−	4				
	25- 1	−	7		20	3	− 1
18-27	30-20	1	1				
	30-10	1	0				

STELLWAGEN BASIN

	Computed Shear (cm/sec) Depth (m)	E-W	N-S	Observed Current (cm/sec) Sta.Depth (m)	Depth Obs. (m)	E-W	N-S
20-22	60-50	−	-1	65	35	1	0
	60-40	−	+1				
	60-30	−	+1				
	60-20	−	2				
	60-10	−	-1				
	60- 1	−	1				

[1]See figure 2.8 a,c for station locations.

the deep lens has also moved to the east (figure 2.8b,c). The current meter at the nearshore station is removed from the region of large horizontal gradients, while the offshore instrument is located in the center of the lens.

The geostrophic shear (Table 2.2, figure 2.8a,c) is much reduced at station 2. Unfortunately, at station 1 the hydrographic observations did not extend deep enough to compute the north-south shear between the two levels.

E. Discussion and Conclusions

The simultaneous current and hydrographic observations show that the density distribution associated with the spring river runoff dominates the low frequency currents observed during the spring period in Massachusetts Bay. The major observed flow for a period of eight days was due to clockwise flow around a lens of light water; in this case much of the flow can be accounted for using the thermal wind relation and assuming zero flow near the bottom. The northerly flow at station 1 is a result of freshening offshore, not to local discharge and a vertically sheared current, as in Csanady (1971). The similarity between the spring records at station 1 in 1972 and 1973 suggests that the decreasing surface density offshore and the associated nearshore northerly flow is a yearly occurrence.

Although the observed flow during the period 4-12 May and 15-16 May can qualitatively be explained, it remains to explain other similar low frequency events in the current record. As an academic exercise, one can speculate about the density distribution required to produce the flow patterns but such speculation does not really serve a useful purpose; two comments are appropriate however. If the currents are a result of similar light lenses as observed on 5-6 May, the axis of these features must be

to the west (inshore) of station 2 since only weak or southerly flow is observed at that station, while both north and south flow is observed at station 1. The internal radius of deformation is on the order of 10 km in the spring period (radius = $\sqrt{g'H}/f$ where $g' = g\,\Delta\rho/\rho$, $\Delta\rho$ = density difference between top and bottom layers, H = layer depth, g = gravity, f = Coriolis parameter). Density features will be on this scale as is observed in the deep lens and surface plume, and current may not be highly correlated over larger distances.

A central question unanswered by the observations is whether the observed lens of light water is established during the period of maximum runoff and remains throughout the spring season, gradually modified, or whether the changes in the deep hydrography are advective, as in the surface layers. It is difficult to explain the deep changes in salt and temperature without advection, and the hydrographic section of 15-16 May suggests that the lens of 5-6 May is slowly moving to the south. In addition, the river discharge is hardly constant but consists of short bursts of flow which would tend to create an uneven, patchy salt distribution. On the other hand, the horizontal structure across the basin is similar throughout the season (figure 4). These inferences and questions can only be tested by further observations with denser hydrographic sampling both in time and space. An appropriate sampling interval for the hydrographic sections would be 5 days.

In conclusion, the low frequency currents in Massachusetts Bay in spring are primarily controlled by the density distribution established by the spring runoff; wind stress is not important. The major influence is due to freshening from the outer side of the basin, not from local discharge and is attributed to the Merrimack River.

CHAPTER III

CURRENTS ON THE NEW ENGLAND CONTINENTAL SHELF IN WINTER: AN ESTIMATE
OF THE VERTICAL EDDY VISCOSITY AND THE BOTTOM DRAG COEFFICIENT

A. Introduction

This chapter is concerned with the currents on the broad conti-
nental shelf of the east coast of North America under winter conditions.
Of primary interest is the role of the vertical turbulent eddy viscosity
or mixing (broadly defined) on the currents, and the parametrization
of the mixing.

Wind stress and the discharge of fresh water at the coast due to
river runoff will be two fundamental driving forces of the currents.
Csanady (1974) has discussed the idealized transient wind circulation,
while Stommel and Leetmaa (1972) have addressed the steady wind and
density driven flow problem, both with simplified topography. Using
basically linear dynamics, Csanady studied the forced integrated flow
pattern associated with short intense wind events and showed that the
flow in the shallow parts of the shelf will reach a frictionally
controlled state in a period of order 10^4 seconds. The work suggests
that barotropic transient frictionally limited currents associated with
major wind events may dominate the currents on a shallow shelf. Recent
observations on the New England continental shelf (Beardsley and Butman,
1974) show that short intense wind events do drive strong alongshore
currents.

Stommel and Leetmaa (1972) investigate the steady flow pattern
associated with wind stress and river discharge. The basic mechanism
for transport of salt across the shelf is offshore surface wind driven

transport of fresh water, with return flow of saline water at the bottom. The cross shelf transport is short circuited by vertical mixing which gives an effective horizontal eddy viscosity of $A_x = (T_x/\rho f)^2/3A_v$ where A_v is the vertical eddy viscosity, ρ is density, and T_x is the along shelf wind stress. The observed salt distribution gives $A_x = 2.3 \times 10^6$ cm^2 sec^{-1} and a vertical eddy coefficient of 30 cm^2 sec^{-1}. Stommel and Leetmaa note the strong dependence of the effective horizontal eddy viscosity on the wind stress.

The extent of the vertical mixing, in essence the value of the vertical eddy viscosity, is a critical parameter in both of these models. Stommel and Leetmaa calculate a relatively small vertical turbulent eddy viscosity consistent with their model of the salt balance and the mean wind field, while a well mixed water column requires a larger vertical turbulent eddy viscosity at least during the wind events.

Several other aspects of the winter shelf circulation also depend on the value of the vertical eddy viscosity and the change in viscosity during wind events. Beardsley and Butman (1974a) observed no large amplitude inertial oscillations on the shelf in winter (less than 5 cm sec^{-1} at mid depth) in contrast with observations of the mixed layer at open ocean sites (Pollard and Millard, 1970). The oscillations may be frictionally damped, confined to a small surface layer, or the wind energy may occur in free modes not possible in the open ocean, for instance surface setup. Finally, the mixing of momentum downward in the water column in response to strong winds is of interest. Several mechanisms for the downward transport of momentum on a shallow shelf are conceivable; direct mixing is one possible mechanism but requires a large eddy viscosity on the order of 500 cm^2 sec^{-1} (Ekman depth of 30 m).

Acceleration of alongshore current at depth by a cross shelf surface pressure gradient or by cross shelf transport are other possibilities.

It is of interest then to estimate from field observations the magnitude of the turbulent vertical eddy viscosity and the bottom drag coefficient and the changes of these parameters during winter storms. The basic nature of the density driven circulation and of the wind driven currents, in addition to the mixing of momentum, depend on the magnitude of the vertical eddy viscosity and bottom drag: the bottom drag coefficient is a measure of the damping associated with a particular current speed and thus of the adjustment or decay time for integrated motions, while the vertical eddy viscosity determines the distribution of the stress in the vertical. Although use of an eddy viscosity in dynamic models is a crude parametrization of nonlinear effects and leaves much to be desired, estimates should qualitatively assist in our understanding of the continental shelf circulation. In this chapter, observations of the vertical structure of the tidal current in the bottom Ekman layer are used to estimate the vertical eddy viscosity and the bottom drag coefficient during non-storm conditions, while coastal tide guage observations are used to estimate changes in an average shelf wide bottom drag coefficient during storms. The spirit throughout is to use relatively simple dynamical models.

B. The Vertical Structure of a Tidal Current

    1. The Model

        To investigate the vertical structure of a tidal current in a rotating system with viscosity, consider the following linear equations in a horizontally infinite constant depth ocean:

$$\frac{\partial u}{\partial t} - fv = A \frac{\partial u}{\partial z^2} + B_1 \cos\omega t + B_2 \sin\omega t,$$

$$\frac{\partial v}{\partial t} + fu = A \frac{\partial v}{\partial z^2} + B_3 \cos\omega t + B_4 \sin\omega t,$$

(1)

where

u,v = horizontal velocity components,

z = vertical coordinate, $z = 0$ at the bottom,

f = Coriolis parameter,

B_1-B_4 = arbitrary constants,

ω = frequency of tidal forcing,

A = constant vertical eddy viscosity,

H = total depth.

The boundary conditions are:

a)   surface $(z = H)$,

$$\frac{\partial u}{\partial z} = \frac{\partial v}{\partial z} = 0 \qquad \text{(no stress)},$$

(2)

b)   bottom $(z = 0)$,

$$u = v = 0 \qquad \text{(no slip)}, \quad \text{or}$$

(3a)

$$\left. \begin{array}{l} A \dfrac{\partial u}{\partial z} = ku \\[2mm] A \dfrac{\partial v}{\partial z} = kv \end{array} \right\} \qquad \text{(slip)}.$$

(3b)

For the bottom condition 3b, the bottom drag coefficient k is

$C_D \overline{|\underset{\sim}{U}|}$ (overbar designates time average) which approximates the non-

linear bottom boundary condition (as best as possible in a linear system)

$$\tau_{bottom} = \rho \ C_D |\underset{\sim}{U}| \underset{\sim}{U} \ , \tag{4}$$

where

$\underset{\sim}{\tau}$ = vector bottom stress , $\underset{\sim}{U}$ = vector velocity ,

C_D = drag coefficient , ρ = water density.

This constant viscosity model with various bottom boundary conditions is the simplest system which incorporates the effects of viscosity on a tidal current with the surface tide modeled as a presecribed body force at a point (B_1 - B_4 are arbitrary constants). The objective is not to model the complete tidal current pattern over the continental shelf, but to use a very local model of the bottom Ekman layer in a tidal current to estimate the vertical eddy viscosity.

A scale analysis of the full equations of motion for shelf dimensions shows that the nonlinear and frictional terms are small (about 1%) compared to the time dependent, forcing and Coriolis term (for example, see Welander, 1951). The ratio of the inertial to the vertical viscous term is

$$\varepsilon = \frac{u \ H^2}{A_v \ L} \cong \frac{50}{A_v} \ , \tag{5}$$

where

A_v = vertical eddy viscosity ($cm^2 sec^{-1}$) ,

L = shelf width (5×10^6 cm) ,

H = depth (5×10^3 cm) ,

u = typical tidal velocity (10 cm sec^{-1}) .

For A_v = 50 , the vertical viscous term and nonlinear term are equal.

For $\varepsilon < .1$ the depth of the frictional layer is $2.2 \times 10^2 \ (A_v)^{\frac{1}{2}}$ or about 15 m $(A_v = 50 \ cm^2 \ sec^{-1})$ and frictional effects will be observable only in a relatively thin bottom layer. The horizontal viscous terms may be safely neglected with respect to the vertical viscous terms as long as $A_H/A_v < 10^5$.

The solution of (1-3) is:

$$u = \frac{1}{L} \ (M \cos\omega t + N \sin\omega t),$$

$$v = \frac{1}{L} \ (P \cos\omega t + Q \sin\omega t),$$

(6)

where

$$L = (\omega^2 - f^2) \ ,$$

$$M = -\lambda_1 B_1 + \lambda_3 B_2 + \lambda_2 B_3 + \lambda_4 B_4 \ ,$$

$$N = -\lambda_3 B_1 - \lambda_1 B_2 - \lambda_4 B_3 + \lambda_2 B_4 \ ,$$

$$P = -\lambda_2 B_1 - \lambda_4 B_2 - \lambda_1 B_3 + \lambda_3 B_4 \ ,$$

$$Q = \lambda_4 B_1 - \lambda_2 B_2 - \lambda_3 B_3 - \lambda_1 B_4 \ ,$$

and

$$\lambda_1 = \omega(b_1 + b_2) + f(b_2 - b_1) \ ,$$

$$\lambda_2 = \omega(a_2 - a_1) + f(a_1 + a_2 - 1) \ ,$$

$$\lambda_3 = \omega(a_1 + a_2 - 1) + f(a_2 - a_1) \ ,$$

$$\lambda_4 = \omega(b_2 - b_1) + f(b_1 + b_2) \ .$$

For the no slip bottom condition (3a)

$$a_i = \frac{\cosh\beta_i z \ \cos\beta_i (z - 2H) + \cosh\beta_i (z - 2H) \ \cos\beta_i z}{2(\cosh2\beta_i H + \cos2\beta_i H)} \ ,$$

$$b_i = \frac{\sinh\beta_i z \ \sin\beta_i (z - 2H) + \sinh\beta_i (z - 2H) \ \sin\beta_i z}{2(\cosh2\beta_i H + \cos2\beta_i H)} \ .$$

For the slip bottom boundary condition (3b)

$$a_i = \frac{R_i}{D_i} \quad , \qquad b_i = \frac{I_i}{D_i} \quad ,$$

$$R_i = \beta_i k [\sinh\beta_i z \, \cos\beta_i (z-2H) + \cosh\beta_i z \, \sin\beta_i (z-2H)$$

$$-\sinh\beta_i (z-2H) \, \cos\beta_i z - \cosh\beta_i (z-2H) \, \sin\beta_i z]$$

$$+k^2 [\cosh\beta_i z \, \cos\beta_i (z-2H) + \cosh\beta_i (z-2H) \, \cos\beta_i z] \quad ,$$

$$I_i = \beta_i k [\cosh\beta_i z \, \sin\beta_i (z-2H) - \sinh\beta_i z \, \cos\beta_i (z-2H)$$

$$+\sinh\beta_i (z-2H) \, \cos\beta_i z - \cosh\beta_i (z-2H) \, \sin\beta_i z)]$$

$$+k^2 [\sinh\beta_i z \, \sin\beta_i (z-2H) + \sinh\beta_i (z-2H) \, \sin\beta_i z] \quad ,$$

$$D_i = 4\beta_i^2 (\cosh 2\beta_i H - \cos 2\beta_i H)$$

$$+4\beta_i k (\sinh 2\beta_i H - \sin 2\beta_i H)$$

$$+2k^2 (\cosh 2\beta_i H + \cos 2\beta_i H) ,$$

$$\beta_1 = \left(\frac{\omega+f}{2A}\right)^{\frac{1}{2}} \qquad \qquad \beta_2 = \left(\frac{\omega-f}{2A}\right)^{\frac{1}{2}} \quad .$$

For $\quad \omega < f \quad , \quad \beta_2 = \left(\frac{|\omega-f|}{2A}\right)^{\frac{1}{2}}$

and $b_2 = -b_2$.

For moderate values of the viscosity (length scales of viscous effects $\beta_1^{-1}, \beta_2^{-1}$ small) the solution approaches the inviscid solution far from the bottom (figure 3.1). For $\omega < f$ the major axis is aligned with the body force and lags by 90 degrees; the ellipse rotates clockwise. For $\omega > f$, the current is more geostrophic with the tidal ellipse in phase with the body force and oriented 90 degrees to the right. Near the bottom frictional effects become important. For $\omega < f$,

Figure 3.1 Tidal ellipse for $B_1 = 1$, $B_2 = B_3 = B_4 = 0$,
$A_v = 100$ cm^{2}sec^{-1} f = 10^{-4}sec^{-1} , slip and no slip
bottom boundary condition (equation 6). Ampli-
tude of major and minor axis (scale by $10^4|B_1|$),
phase lag with respect to body force, and ellipse
orientation (clockwise from x-axis).

Top) $\omega = 1.4 \times 10^{-4}$ (>f).

Bottom) $\omega = .73 \times 10^{-4}$ (<f).

See Appendix C for ellipse reprentation.

AMPLITUDE   PHASE   ORIEN

DEPTH (M)

VISC = 100
BI = 1
F = 10^{-4}
W = 1.4×10^{-4}
PERIOD = 12.42 HR

NO SLIP ——
K = .05 ·······

W = $.73 \times 10^{-4}$
PERIOD = 24 HR
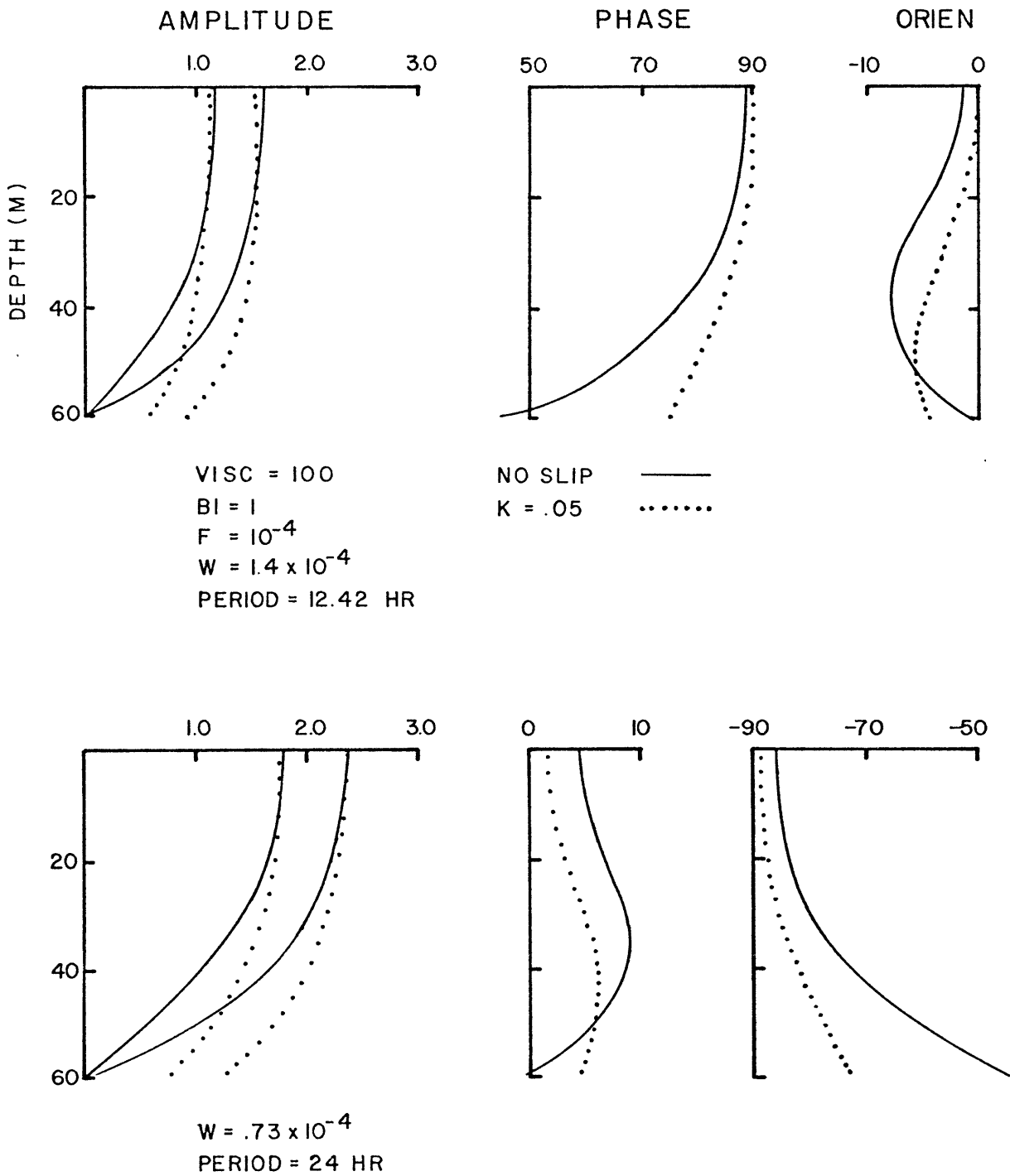
Figure 3.1

the near bottom current is more in phase with the body force and thus leads the interior flow and the ellipse is rotated slightly to the right of the body force. For $\omega>f$, the ellipse orientation is more closely aligned with the body force than the interior flow. With the slip bottom condition, the viscous effects are reduced and the solution approaches the interior flow closer to the bottom, as if the bottom layer is cut away. For smaller values of the viscosity or frequencies further from the inertial, the viscous effects are confined in a smaller boundary layer. Similar solutions are obtained by Sverdrup (1927) and Fjelstad (1929).

In general the phase and amplitude of the flow at any depth is a relatively complicated function of the viscosity, the bottom drag coefficient, and the body forces B_1-B_4 , which are not known. However, there are four properties of the tidal current at two depths which are only a function of the vertical eddy viscosity and the bottom drag coefficient. Using current observations at two points in the water column, the vertical viscosity and the bottom drag coefficient can be estimated without explicit knowledge of the body forces. If the current at two depths is represented as a tidal ellipse, with a clockwise and counterclockwise rotating component (see Appendix C for ellipse notation), the following quantities depend only on the vertical eddy viscosity, the bottom drag coefficient, and the depth.

a. $\dfrac{\text{Counterclockwise component at depth 1}}{\text{Counterclockwise component at depth 2}} = \dfrac{U_+(z_1)}{U_+(z_2)} = \left[\dfrac{\delta(z_1)}{\delta(z_2)}\right]^{\frac{1}{2}}$,

$$\delta(z) = \lambda_1{}^2 + \lambda_2{}^2 + \lambda_3{}^2 + \lambda_4{}^2$$

$$- 2(\lambda_1\lambda_4 + \lambda_2\lambda_3) .$$

(7)

b. $\dfrac{\text{Clockwise component at depth 1}}{\text{Clockwise component at depth 2}} = \dfrac{u_-(z_1)}{u_-(z_2)} = \left[\dfrac{\gamma(z_1)}{\gamma(z_2)}\right]^{\frac{1}{2}}$,

$$\gamma(z) = \lambda_1{}^2 + \lambda_2{}^2 + \lambda_3{}^2 + \lambda_4{}^2$$
$$+ 2(\lambda_1\lambda_4 + \lambda_2\lambda_3) \ .$$

c. Rotation of major axis with depth

$$\tan 2[\theta(z_1) - \theta(z_2)] = \frac{2[\xi(z_1)\epsilon(z_2) - \xi(z_2)\epsilon(z_1)]}{\epsilon(z_1)\epsilon(z_2) + 4\xi(z_1)\xi(z_2)} \ ,$$

$$\epsilon = \lambda_1{}^2 + \lambda_3{}^2 - \lambda_2{}^2 - \lambda_4{}^2 \ ,$$

$$\xi = \lambda_1\lambda_2 - \lambda_3\lambda_4 \ .$$

d. Phase difference in flow along major axis

$$\tan 2[\tau(z_1) - \tau(z_2)] = \frac{2[\alpha(z_1)\beta(z_2) - \alpha(z_2)\beta(z_1)]}{\beta(z_1)\beta(z_2) + 4\alpha(z_1)\alpha(z_2)} \ ,$$

$$\alpha = \lambda_1\lambda_3 - \lambda_2\lambda_4 \ ,$$

$$\beta = \lambda_1{}^2 + \lambda_2{}^2 - \lambda_3{}^2 - \lambda_4{}^2 \ .$$

The derivation is straightforward using the ellipse parameters
(Appendix C) and the solutions for the velocity. Observations of the
tidal current at two depths thus give four independent estimates of
pairs of the vertical eddy viscosity and the bottom drag coefficient
at a particular frequency.

2. Observations and Data Analysis

Current observations at two depths within approximately 15 m
of the bottom in a well mixed water column during steady state tidal condi-
tions are required to match to the model of the bottom Ekman layer.

Three current moorings were deployed on the New England continental shelf from Feb. 27 - Apr. 3, 1974 as part of the MIT Shelf Dynamics Program (Fig. 3.1). At mooring one (40°55.8'N 71°6.9'W), Richardson current meters (Table 3.2) were located 1.2, 15 and 30 m from the bottom in 58.5 m of water. Because of the expected size of the bottom boundary layer, analysis is concentrated on the bottom instruments; a time base error occurred five days after deployment in these instruments, however, and thus only the first part of the records are used. Data obtained at moorings 2 and 3 is not used because the bottom instrument at mooring 2 has a serious time base malfunction, while the shelf slope-water interface may complicate the vertical structure at station 3.

The model of the bottom Ekman layer is valid for body forces at any frequency and can be applied to the semidiurnal and the diurnal tide to estimate the vertical eddy viscosity and the bottom drag coefficient. However, estimates of the tidal ellipse at the diurnal frequency were noisy and only the semidiurnal estimates are presented. The semidiurnal tidal ellipse at each depth was computed from the current records in the following way; the record was broken into overlapping segments two tidal cycles long (24.84 hours) and a sine and cosine at the tidal period of interest (12.42 hours) was fit by least squares to the data. The semidiurnal tidal ellipse and the four independent parameters (7a-d) were computed for each data segment, giving eight estimates over the first four days of record (Table 3.2). The standard error was computed to estimate the range of confidence for the parameters.

Figure 3.2   Map of the New England continental shelf showing location
of current meter moorings and tide guage stations.
Smoothed 40 m, 100 m and 1000 m depth contours indicated
(after Uchupi, 1968).   Nantucket (N). Montauk Pt. (M).
Sandy Hook (SH), Atlantic City (AC), Cape May (CM),
Nantucket Lightship (NLS), Current meter moorings (1,2,3).
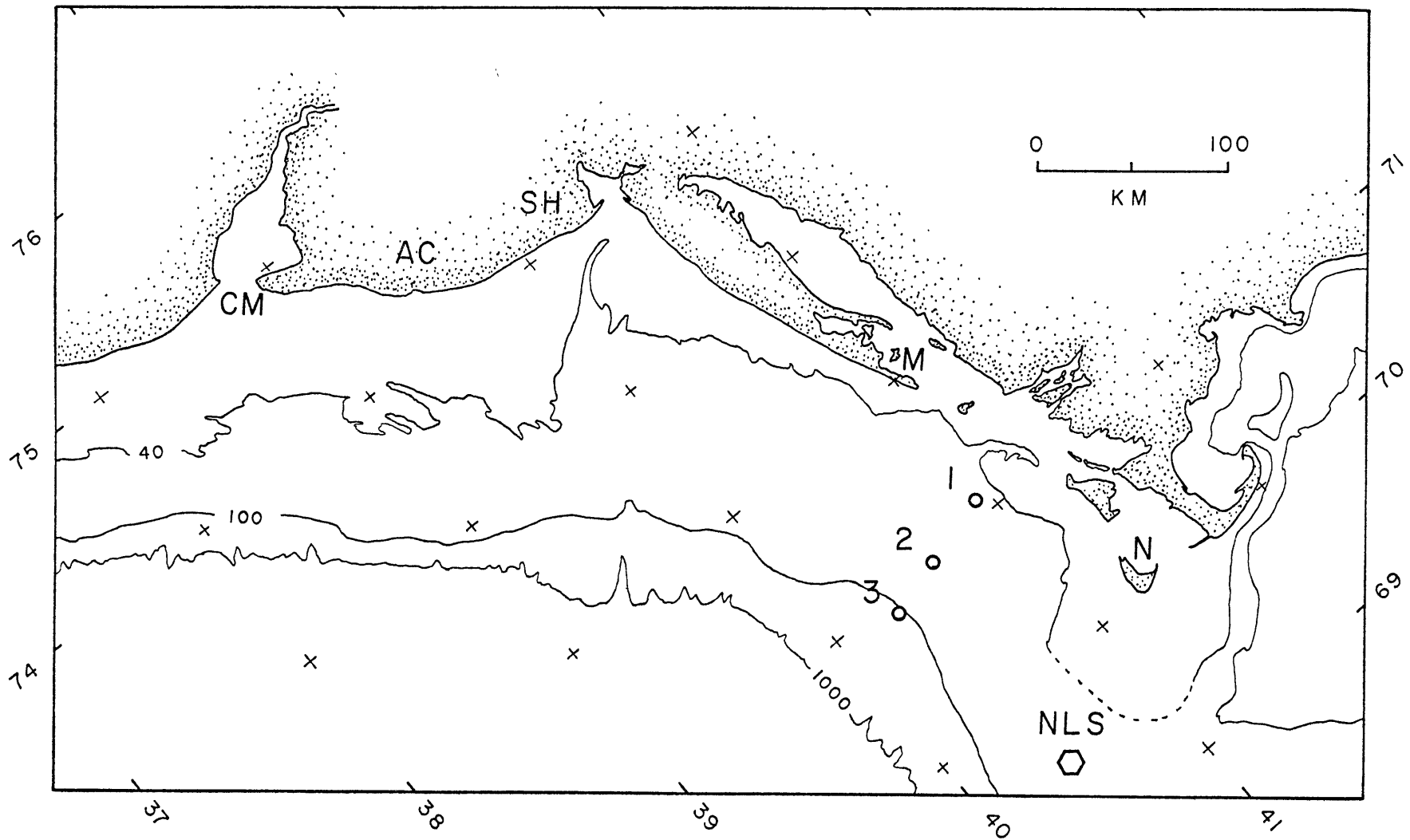
Figure 3.2

TABLE   3.1

INSTRUMENT DEPLOYMENT ON MOORING ONE

(40° 55.8' N   71° 6.9' W   Depth = 58.5 M)

INST.	DEPTH (M)	DEPTH FROM BOTTOM (M)	INST. TYPE	SAMPLING INTERVAL
11	28.5	30.0	VACM[1]	continuous
12	43.5	15.0	101[2]	30 min
13	57.3	1.2	102[2]	5 min

[1]Vector averaging current meter. Data stored every 7.5 minutes.

[2]Film recording EG&G current meter. Instruments burst sampled [12 samples

at 5 second intervals each sampling interval].

TABLE 3.2

ESTIMATES OF THE SEMI-DIURNAL TIDAL ELLIPSE

AT STATION 1, FEB. 28 - MARCH 4, 1974

INST[1]	U_+	SE[2]	U_-	SE	ORIEN[3]	SE	PHASE[4]	SE	$\overline{\|U\|}$[5]
11	.75	.15	8.59	.28	-152	16	60	14	
12	.73	.12	6.59	.21	-169	16	29	16	9
13	.84	.17	3.89	.18	-156	20	24	22	6

INDEP[6] PARAM	U_+/U_+ [a]		U_-/U_- [b]		$\Delta\theta$ [c]		$\Delta\phi$ [d]	
a	1.15		.59		- 13		5	
b	1.20	.25	.60	.03	- 13	4°	3	4°

NOTES

1 11 - 30 m from bottom ;

   12 - 15 m from bottom ;

   13 - 1.2 m from bottom .

2 SE = standard error = standard deviation/$\sqrt{N}$,

     N = number of observations = 8 .

3 orientation measured counterclockwise from east.

4 phase lag, relative to 74 II 27, 2200 GMT .

5 average speed .

6 a. computed from average ellipse parameters .

   b. computed piecewise for each data segment .

a U_+/U_+ = counterclockwise (13)/counterclockwise (12) .

b U_-/U_- = clockwise (13)/clockwise (12) .

c $\Delta\theta$ = orientation (12) - orientation (13) ;

      >0 top to left of bottom ,

      <0 top to right of bottom .

d $\Delta\phi$ = phase lag (12) - phase lag (13) ;

      >0 top lags bottom ,

      <0 top leads bottom .

The accuracy of the ellipse estimates is of considerable importance, with error due to instrument calibration and to noise in the record. Absolute direction is assumed to be good to ±5 degrees. This is typical of VACM instruments (Harry Bryden, personal communication), but may be optimistic for the film instruments. Errors in speed are difficult to estimate. Ratios of speed are used in the model so that percentage errors (due to rotor pumping, or from calibration) will not be as important, but offsets will be.

The semidiurnal tide dominates the current spectrum and is almost completely clockwise. The energy continuum beneath the tidal peak is $.05 - .10$ cm^2sec^{-1}, which corresponds to errors in a sine or cosine coefficient of approximately $±.5$ cm sec^{-1}. Because the tidal ellipse is nearly circular (counterclockwise component = 0), small errors in the coefficients give large errors in the ellipse orientation and phase. The random phase and orientation errors become smaller if the ellipse is flatter or if a number of estimates are averaged, and thus longer records would be desirable to reduce noise and to obtain better frequency resolution.

The accuracy of the time base of the current meters is important. The time base on the film current meters (12 and 13) is established by marking the record at known times before and after deployment of the instrument, with elapsed time computed from the number of samples recorded from the start. The relative accuracy of the time base established by this method is at worst one sampling interval, assuming no instrument malfunction occurs. A crystal clock is used in the VACM and the time of each sample is recorded as part of the data record;

time base errors with the VACM are negligible. The relative time base error for instrument 13 (5 minutes $\cong$ 2.5° for the semidiurnal tide) is small compared to the expected signal. The error for instrument 12 is significant (30 minutes $\cong$ 15° for the semidiurnal tide) and a serious ambiguity arises. With several assumptions however, the time marks specify the time base to within 15 minutes (7.5° for the semidiurnal tide) and thus the maximum time base difference between 12 and 13 is ±20 minutes (10°).

As a test of the steadiness of the body force assumed in the model the amplitude and phase of the semidiurnal tide at the coast as a function of time was estimated from sea level records at Woods Hole, Mass., Sandy Hook, N.J., and Atlantic City, N.J. by a similar least squares procedure. The period Feb. 28 - Mar. 5 is during the neap tide, and the amplitude of the semidiurnal tide was quite constant. However, the tidal signal in the current meter records is weaker than during the spring tide.

3. An Estimate of the Vertical Eddy Viscosity and Bottom Drag Coefficient

The expected value of the four parameters (7a-d) as a function of the bottom drag coefficient and vertical eddy viscosity are shown in Figure 3.3 for a water depth of 58 m and observations 1.2 and 15 m from the bottom. It is clear from the ratio of clockwise components that the slip bottom condition is superior to the no slip condition. As expected, the near bottom flow does lead the interior flow, with the amount uncertain due to the time base errors. Further support for the near bottom flow leading the interior flow is found by comparing instruments 11 and 13 which have accurate time bases. Although phase changes

Figure 3.3   Ellipse parameters as a function of viscosity and
             bottom drag coefficient for observations 1.2 m
             (instrument 13) and 15 m (instrument 12) from the
             bottom, and observed values with error bars
             1.9 x standard error (see equation 7 and Table 3.2)
             plus estimated instrument error.

        a)   Ratio of counterclockwise components (13/12).

        b)   Ratio of clockwise components (13/12).

        c)   Change in ellipse phase lag (Phase (12) - Phase (13))
               (>0, top lags bottom) Time base uncertainty ± 10°.

        d)   Change in ellipse orientation (Orien (12) - Orien (13))
               (<0, top to left of bottom) Estimated instrument error ± 10°.
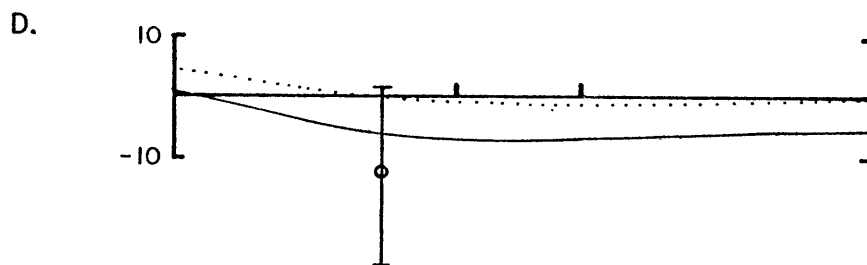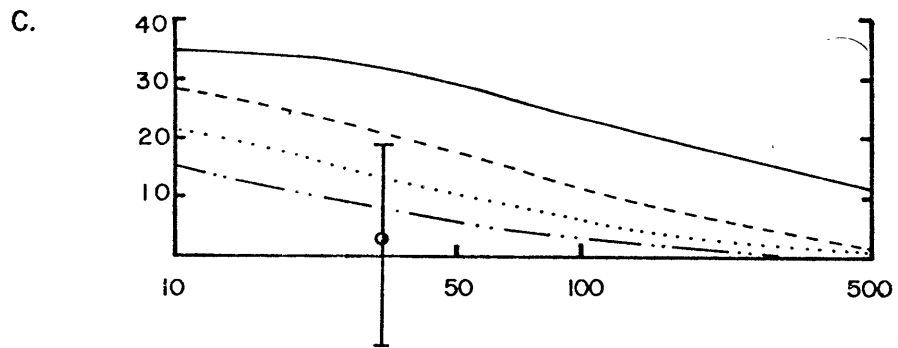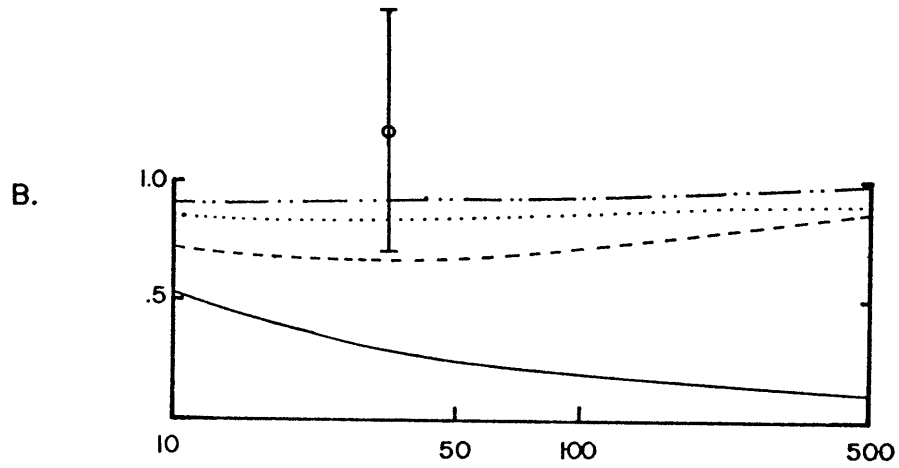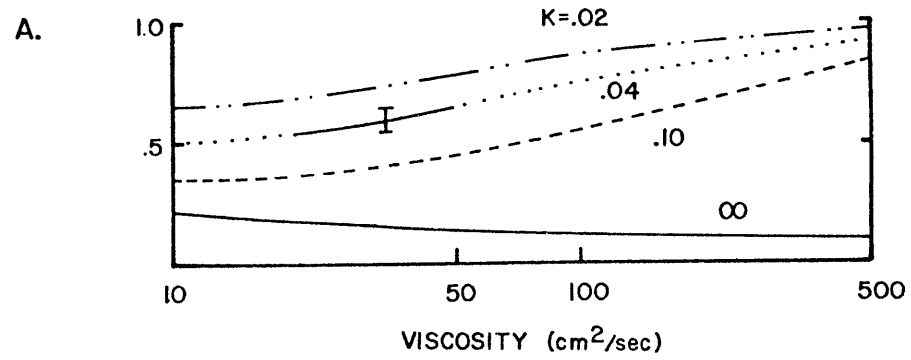
Figure 3.3

cannot be entirely attributed to frictional effects, the ellipse 30 m from the bottom does lag the ellipse 1 m from the bottom by 30 degrees. The ratio of clockwise components is in large part noise, and should be disregarded. The orientation estimates fall within the instrument error and would agree more favorably if an absolute 10° correction were applied to direction of 12.

It is difficult to choose an eddy viscosity and bottom drag pair because of the noise in the estimates and the relative sensitivity of the curves; the ratio of the clockwise components has the smallest error. From physical considerations, the bottom drag coefficient should be in the range .01 - .05 cm sec^{-1} (k $\cong$ $c_D \overline{|U|}$, $\overline{|U|}$ $\cong$ 5 - 10 cm sec^{-1}). The observed ratio of clockwise components suggests that k > .02 cm sec^{-1}. For k = .04 cm sec^{-1} the ratio of clockwise components gives A_v = 20 - .50 cm^{2}sec^{-1} . More accurate estimates should be possible with longer records and instruments placed more closely in the bottom layer.

This estimate of the vertical eddy viscosity is in agreement with scaling arguments and with measurements in the near surface layer of the Great Lakes (Csanady, 1972a), which suggest that the vertical eddy viscosity should be a function of the friction velocity (u* = $(\tau/\rho)^{\frac{1}{2}}$ cm sec^{-1}), depth (H) , and the Coriolis parameter (f) . Specifically,

$$A_v \simeq f(u^*,f,H) ,$$

$$\simeq \frac{u^*H}{20} \quad \text{for} \quad H < \text{Ekman depth,} \tag{8}$$

$$\simeq \frac{1}{200} \frac{u^{*2}}{f} \quad \text{for} \quad H > \text{Ekman depth.}$$

From this scaling,

$u_{bottom} \backsim 5\text{-}10$ cm sec^{-1}; u^{*2}= k u_b = .2-.4 cm^{2}sec^{-2}; $A_v \backsim 10\text{-}20$ cm^{2}sec^{-1}. The estimate is similar to the value found by Stommel and Leetmaa (1972)

of $30 \text{ cm}^2 \text{sec}^{-1}$, but is somewhat higher than estimates of Carter and

Okubu (1965) of $2 - 20 \text{ cm}^2 \text{sec}^{-1}$. The Carter and Okubu estimates were

under summer conditions however. Estimates of the vertical eddy viscosity

under storm conditions using the scaling arguments give

$$A_v = 100 - 200 \text{ cm}^2 \text{sec}^{-1} (u_*^2 \cong 2 - 4 \text{ cm}^2 \text{sec}^{-2}).$$

C. Response of the Tide to a Change in Bottom Drag

The adjustment of currents during storms is of particular interest

because storm generated currents appear to dominate the flow on the

shallow shelf in winter. It is expected that the vertical eddy viscosity

will increase with increased surface or bottom stress, and that the

bottom drag coefficient $(k \simeq C_D \overline{|\underset{\sim}{U}|})$ may increase due to a larger mean

current or to waves. In this section the change in bottom drag coefficient

during storm conditions is estimated from coastal tide observations. The

typical storm duration is one or two days and the adjustment time of the

bottom boundary layer to a changing eddy viscosity or bottom drag coeffi-

cient is f^{-1} ; the steady state assumption of the previous model is thus

not satisfied and the method is not appropriate. However, the bottom

drag coefficient apparently increases significantly during storms so that

an integrated tidal model can be considered in steady state.

1. The Model

As in the previous section the simplest model which incorporates

the desired effects of friction on the shelf tides is developed. Consider

the following model of the tide on the continental shelf forced by the

deep ocean tide:
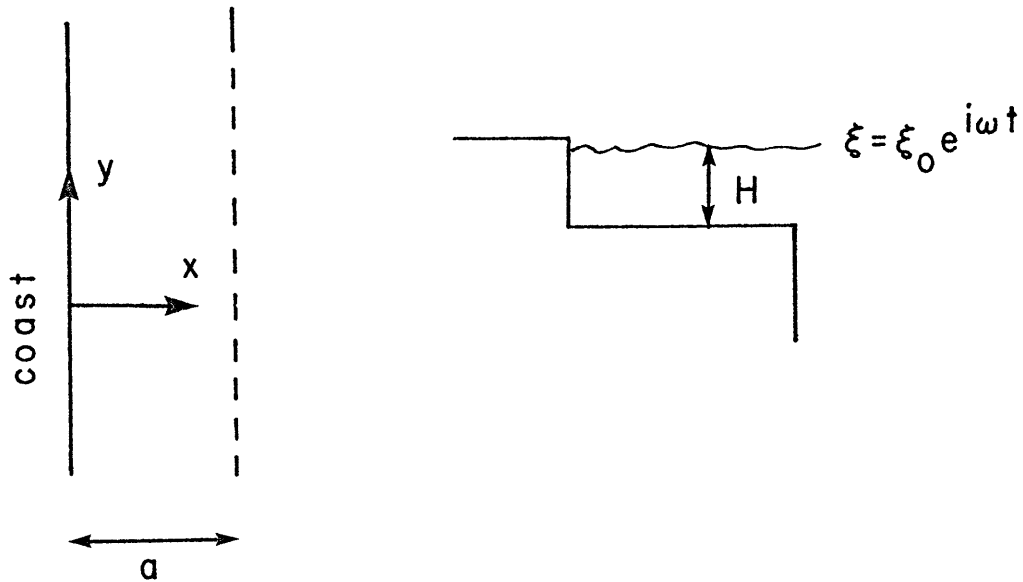
The integrated linear equations of motion are:

$$\frac{\partial u}{\partial t} - fv = -g \frac{\partial \xi}{\partial x} - Ru \, ,$$

$$\frac{\partial v}{\partial t} + fu = -g \frac{\partial \xi}{\partial y} - Rv \, ,$$

(9)

$$\frac{\partial u}{\partial x} + \frac{\partial v}{\partial y} = - \frac{1}{H} \frac{\partial \xi}{\partial t} \, ,$$

where u,v = depth averaged velocities,

f = Coriolis parameter,

ξ = surface elevation above equilibrium,

R = bottom drag coefficient,

g = gravity,

H = depth.

Here the bottom stress is modeled as a bottom drag proportional to the velocity $(R \cong C_D |\underline{U}|/H \cong k/H$; R has units sec^{-1} and is assumed constant across the shelf). The surface stress is assumed to be zero. The boundary conditions are

$$\text{at the coast} \quad (x = 0) , \quad u = 0 ,$$
$$\text{at the shelf edge} \quad (x = a) , \quad \xi = \xi_o \cos\omega t . \tag{10}$$

Assuming that there is no along shelf variation $(\frac{\partial}{\partial y} = 0)$, the complex solution for the velocity and surface elevation is:

$$u = \frac{-i\omega\xi_0}{H\alpha} \frac{\sinh \alpha x}{\sinh \alpha a} e^{i\omega t} ,$$

$$v = \frac{\omega\xi_0}{H\alpha} \frac{f}{(\omega^2+R^2)} (\omega+iR) \frac{\sinh \alpha x}{\sinh \alpha a} e^{i\omega t} , \tag{11}$$

$$\xi = \xi_o \frac{\cosh \alpha x}{\cosh \alpha a} e^{i\omega t} ,$$

where

$$gH\alpha^2 = \omega^2 \left[\frac{f^2}{\omega^2+R^2} - 1\right] + i\omega R \left[\frac{f}{\omega^2+R^2} + 1\right] ,$$

$$\frac{v}{u} = \frac{f}{(\omega^2+R^2)^{1/2}} e^{i(\phi-\pi/2)} ,$$

$$\tan \phi = R/\omega .$$

For $R = 0$ the solution is a trivial one of a wave travelling in the $\pm$ x direction with phase speed

$$\frac{\omega}{k} = \sqrt{gH} \frac{1}{[1-(f/\omega)^2]^{1/2}} . \tag{12}$$

The ratio of the along shelf to cross shelf velocity is

$$\frac{v}{u} = -\frac{f}{\omega} e^{-i\pi/2} .$$

The velocity vector rotates clockwise and the amplitude ratio of the velocity components is independent of the cross shelf position. For $R \ll f$ the solution is not frictionally affected while for $R > \omega$ there is a phase lag in the current and surface elevation with respect to the forcing at the shelf edge (figure 3.4). For R between 10^{-4}-$10^{-2} \sec^{-1}$ the amplitude of the cross shelf velocity and the elevation remain approximately constant but the along shelf velocity is significantly damped.

Although the model is oversimplified to fit in detail to current or sea level observations to estimate the damping coefficient R, especially because of the idealized topography, changes in phase of the tide at the coast might indicate approximate changes in the damping coefficient during storm conditions. Assuming that the forcing at the edge of the shelf remains constant during storms, an increase in the damping coefficient R will be reflected in a phase lag of the surface tide at the coast with respect to normal conditions. From the previous calculations, the damping coefficient R is estimated to be approximately $10^{-5} \sec^{-1}$ ($R \sim C_D \overline{|\underset{\sim}{u}|}/H \cong k/H = .05/5 \times 10^3 \sec^{-1}$) under non-storm conditions. The phase and amplitude of the tide at the coast relative to the forcing at the shelf edge is shown in figure 3.5 at three east coast tide stations and for the range of expected R . A 10 degree phase lag from normal conditions at these tide stations would suggest an increase in R by a factor of 4 to 5 . The slope of the phase

Figure 3.4

    a)   Amplitude of tide height and tidal current at mid-shelf as a function of damping coefficient for a shelf 40 m deep and 120 km wide (equation 11).

    b)   Phase of tide height and tidal current at mid-shelf.
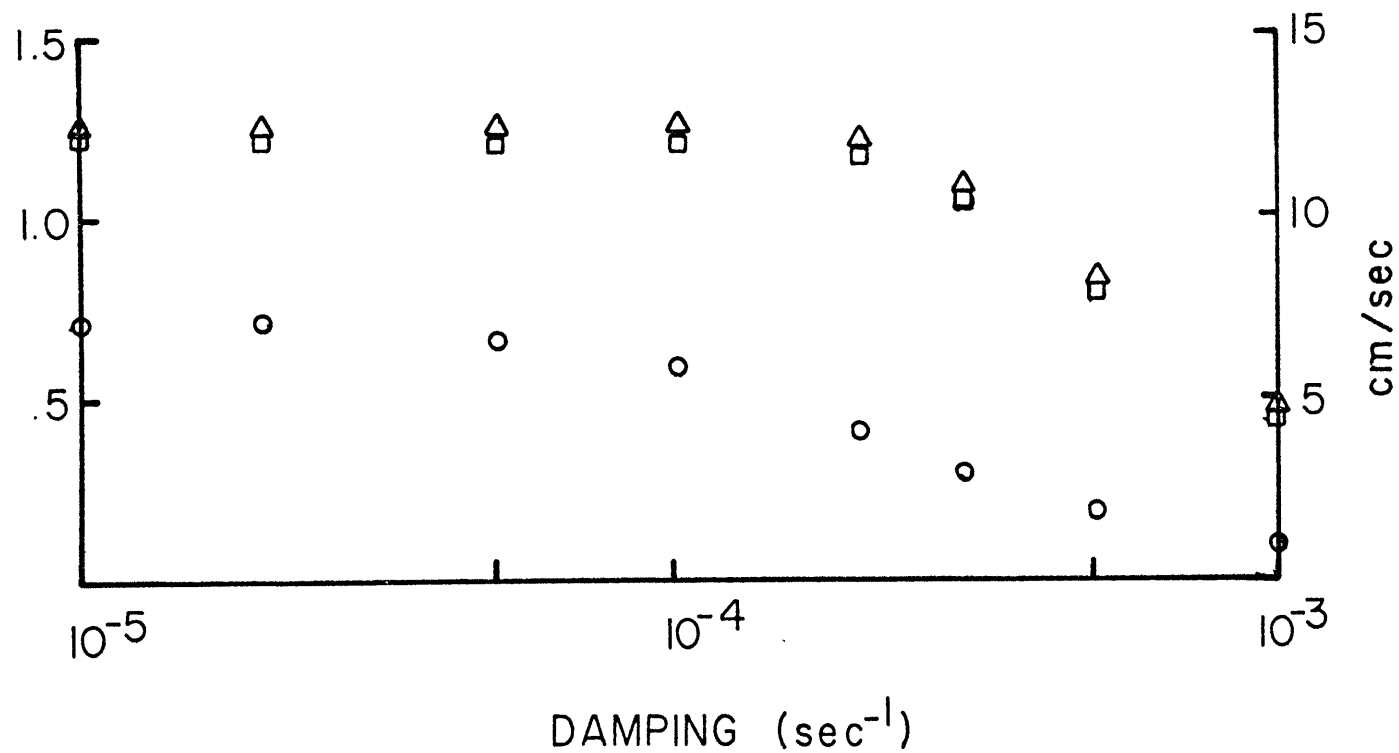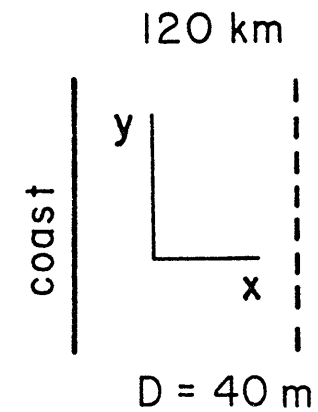
Figure 3.4a

PHASE

Z(coast) △

U(60 km) □

V(60 km) ○

DAMPING (sec^{-1})
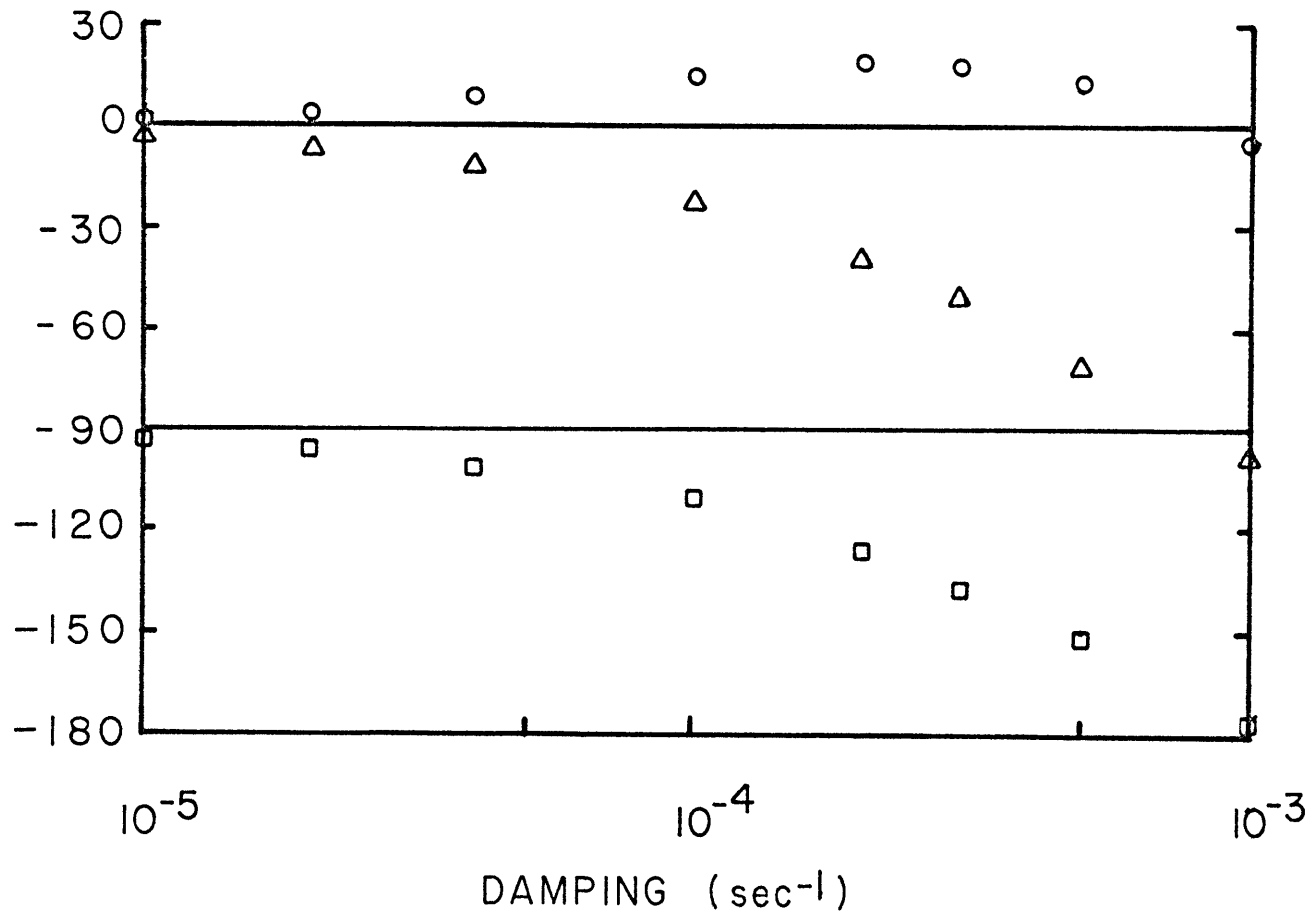
Figure 3.5   Phase (with respect to tide at shelf edge) and
              amplitude ratio (coast to shelf edge) as a function
              of damping coefficient for shelf dimensions which
              approximate New England shelf at Montauk (110 km,
              65 m), Sandy Hook (160 km, 50 m), Atlantic City and
              Cape May (120 km, 40 m). See figure 3.2 for locations.
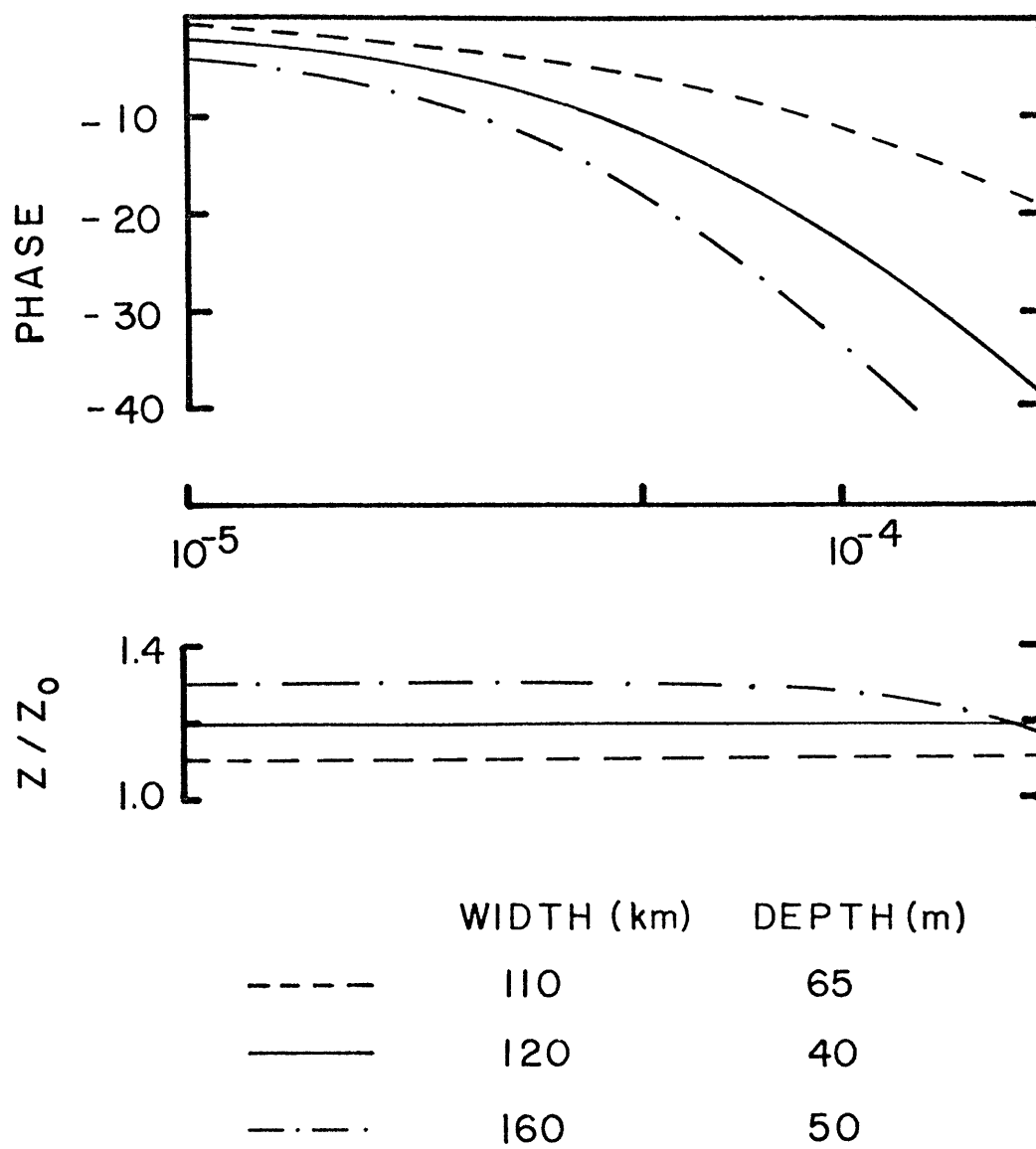
Figure 3.5

change is greater as R increases and thus for a given phase change the
associated change in R will be greater the smaller the non-storm value.
Note that if the non-storm value of R is unknown an observed shift of
phase can be used to estimate at least a lower bound on the value of R
under storm conditions by assuming R = 0 initially. Also note that for
these shelf dimensions the amplitude of the tide is insensitive to damping
in the range 10^{-5} to 10^{-4} sec^{-1}. Finally, the predicted ratio of the ampli-
tude of the semi-diurnal tide at Atlantic City to Sandy Hook is .92, in agree-
ment with the observed value of .89 (Redfield, 1958; Hicks and others, 1965).

2. Observations of Tidal Phase During Storms

Beardsley and Butman (1974a) described the response of sea level
and currents on the New England continental shelf to three winter storms
in March of 1973. The first storm occurred on March 18 and 19 with strong
winds from the west which produced little alongshore flow and a sea surface
setup in the direction of the wind. The second and third storms (March 22-23,
March 27-28) were northeasters and winds produced alongshore flow and a
rise of sea level at the coast, but little setup. The asymmetric response
of the currents and sea level was attributed to differences in the large
scale wind pattern arising from different storm tracks. We will investigate
the change in the semidiurnal tide at the coast during these three storms.

Estimates of the phase and amplitude of the semidiurnal tide at
Sandy Hook, Atlantic City, and Cape May as a function of time were obtained
by fitting by least squares a cosine and sine with a period of 12.42 hours
to sea level data over 24.84 hour overlapping segments. The sea level
records were first high pass filtered by subtracting a low passed version
(Gaussian filter, one half power at 43.6 hours) from the original series.
This left the semidiurnal signal essentially unchanged, reduced the diurnal

tidal signal by 30% and removed the lower frequency sea level fluctuation due to the storms. A reference tidal signal was generated from harmonic constants supplied by the National Ocean Survey using constituents with amplitudes greater than 3 cm and periods shorter than 30 hours. The following tidal lines were used:

Sandy Hook M_2, S_2, N_2, K_2, ν_2, K_1, O_1

Atlantic City M_2, S_2, N_2, K_2, K_1, O_1, P_1

Cape May M_2, S_2, N_2, K_2, K_1, O_1, P_1

The generated records were high pass filtered and the amplitude and phase of the semidiurnal tide as a function of time computed in an identical manner to that used for observed sea level. The unfiltered sea level record, filtered record, and generated record at Sandy Hook are shown in figure 3.6.

The difference in phase lag of the semidiurnal tide between the observed signal and the generated signal (figure 3.7) clearly shows a delay in the tide at the coast during each storm by about 5 - 10 degrees (10-20 minutes), with the increased phase lag most pronounced during the second and most intense storm. The ratio of observed amplitude to generated amplitude at the semidiurnal frequency (figure 3.7b) shows no consistent change in amplitude during the storms. The tide at Montauk shows similar results while the signal at Nantucket is less consistent, perhaps due to local conditions and the adjacent Gulf of Maine. Using the curves in figure 3.5 and a non-storm R at $10^{-5} \sec^{-1}$, a change in tidal phase of 5-10° gives an estimate for R of $3 - 5 \times 10^{-5} \sec^{-1}$ during storms and an adjustment time (R^{-1}) of 6 hours, justifying application of the integrated steady state model under storm conditions.

Figure 3.6 Sea level at Sandy Hook New York, March, 1973 .

    a)   Raw unfiltered sea level record .

    b)   High passed record, corrected for atmospheric pressure .

    c)   High passed generated record .

A   TIDE HEIGHT AT SANDY HOOK

B   OBSERVED SEA LEVEL. HIGH PASSED

C   TIDE HEIGHT GENERATED FROM HARMONIC CONSTANTS
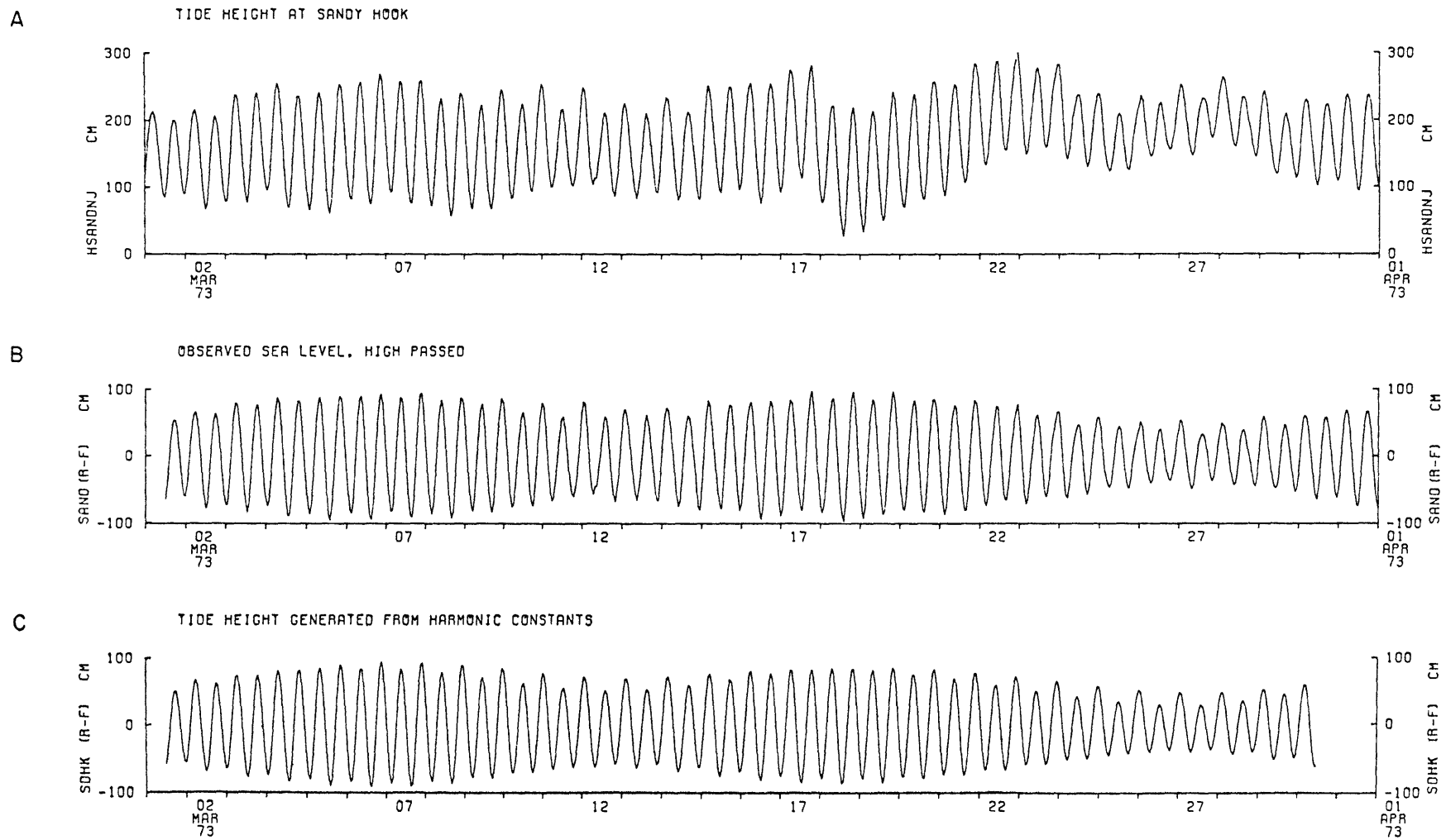
Figure 3.6

Figure 3.7

a) Difference between observed semidiurnal tidal phase
    lag and semidiurnal phase lag of generated signal
    (with respect to 73-III-10, 1200 EST) at Sandy Hook,
    Atlantic City and Cape May as a function of time .

b) Ratio of observed semidiurnal tidal amplitude to
    semidiurnal amplitude of generated signal as a
    function of time.

OBSERVED – GENERATED PHASE LAG

CAPE MAY

SANDY HOOK

ATLANTIC CITY

10°

STORM   1   2   3

OBSERVED / GENERATED AMP.

CAPE MAY

SANDY HOOK

ATLANTIC CITY

.2
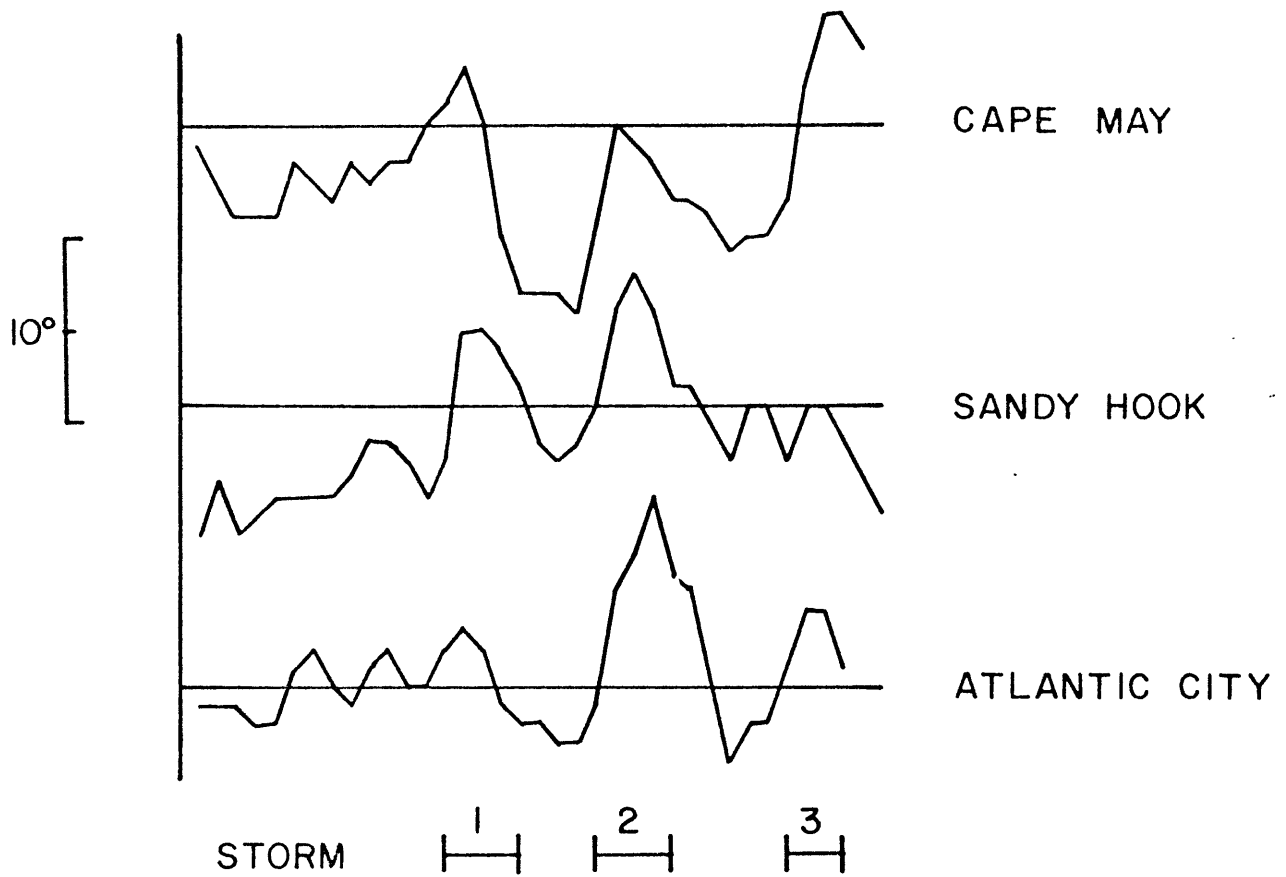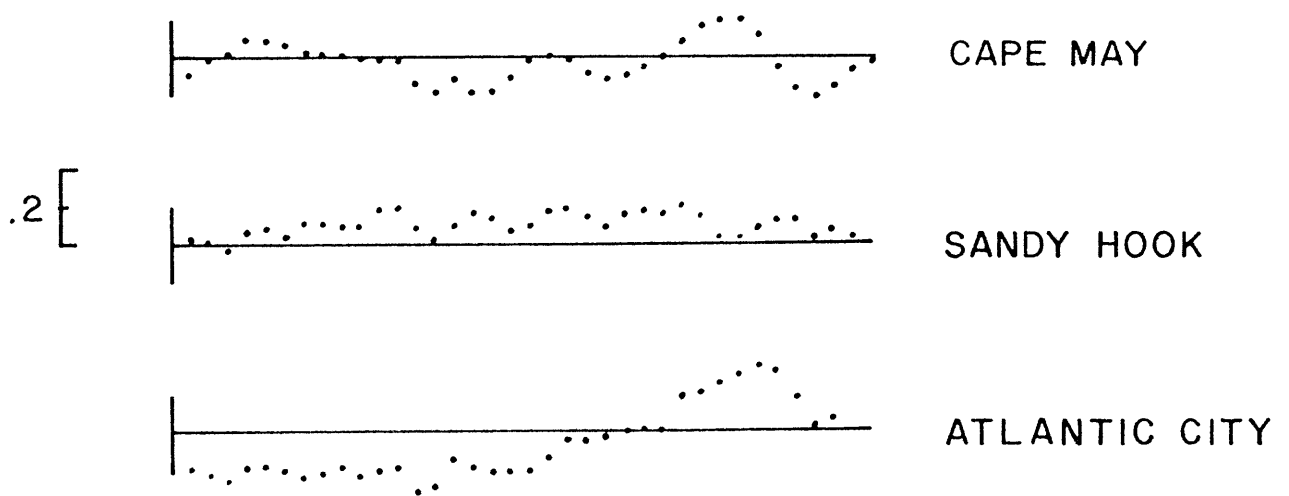
Figure 3.7

The increase in the damping coefficient $(R \sim C_D \overline{|U|}/H)$ must be attributed to an increased near bottom mean current or to waves, if the bottom drag coefficient C_D is assumed to be a fixed property of the bed. An increase in the mean flow was observed 20 m from the bottom during storms two and three, but it is unclear how much of the increase might be due to pumping of the current meter rotor by waves. There was not a significant mean current associated with the first storm, yet a change in tidal phase is observed.

Bottom velocities expected from waves were calculated using wave height and period reported by ships and observed at the Nantucket Light-ship during the three storms (Table 3.3). The bottom velocities are significant especially during the second storm, and are large enough to account for at least a doubling of the bottom drag assuming non-storm bottom velocities of 5-10 cm sec^{-1}. It should be noted that waves gen-erated by offshore winds will decrease toward shore, and should be less effective in increasing bottom drag than waves generated by onshore winds. Also, the increase in the damping coefficient (and thus a larger phase lag) will be larger for a shallow shelf where the wave induced bottom velocities are stronger and the bottom stress is distributed over a smaller depth. Neglect of topography, cross shelf and along shelf variations in damping and in the tide, and local effects may account for some of the variability in the phase and amplitude estimates.

D. Discussion and Summary

Two simple dynamical models of the semidiurnal tide on the continental shelf have been used to estimate the vertical eddy viscosity and the bottom drag coefficient at one location, and the change in an average shelf wide damping

TABLE   3.3

WAVE HEIGHT, PERIOD AND BOTTOM VELOCITY FOR THREE STORMS,
MARCH, 1973[1]

STORM	DATE	WAVE HEIGHT (Ft)	WAVE PERIOD (Sec)	DIRECTION[2]	AVG. BOTTOM[3] Speed (cm/sec)
1	18-19 Mar	15 (max 20)	5 - 10	26 - 30	11
2	22-23 Mar	20 (max 40)	5 - 10	03 - 04	15
3	27-28 Mar	5 - 15	5 - 10	05 - 07	7

[1]Source, Nantucket Lightship and ship reports .

[2]Direction in tens at degrees from true north .

[3]Average bottom speed estimated from

$$\overline{|u|} \cong \frac{2}{3} u_{max} = 2/3 \ a\sigma \ \frac{\cosh kz}{\sinh kh} \ ,$$

H = total depth = 50 m ,

k = 2π/L ,

L = wavelength $\cong$ 100 m
$\left[\text{from dispersion relation} \quad k = \frac{\sigma^2}{g} \frac{1}{\tanh kH} \right]$,

2a = waveheight ,

σ = frequency = 2π/T ,

T = wave period $\cong$ 7.5 sec .

TABLE 3.4

ESTIMATES OF BOTTOM DRAG AND EDDY VISCOSITY[1]

	K (cm/sec)	R (sec^{-1})	T DECAY (integrated)	A_V (cm^2/sec)	EKMAN D (m)
Quiet[2]	.04 $\longrightarrow$	10^{-5} $\longrightarrow$	28 hr.	20 - 50 $\longrightarrow$	10
Storm[3]	.25 $\longleftarrow$	$5x10^{-5}$ $\longrightarrow$	6 hr.		

[1]Estimates from data are underlined, arrows indicate input to derived quantities.

[2]Drag coefficient and viscosity are consistent with tidal observations at one station.

[3]The damping coefficient should be considered as averaged over the shelf.

coefficient during storms (Table 3.4). The available observations of tidal currents in the bottom Ekman layer are consistent with a bottom drag coefficient of .04 cm sec^{-1} and a vertical eddy viscosity of 20 - 50 cm^{2}sec^{-1}. In theory, two independent estimates of the bottom drag and viscosity are possible with current observations at two levels in the bottom boundary layer, but in practice the instrumental and estimation errors are large and only one parameter can be estimated with the other specified.

The value of the vertical viscosity is similar to the estimates of Stommel and Leetmaa (1972) and is consistent with scaling estimates (Csanady, 1972a). The Ekman depth is on the order of 10 m, which suggests that most wind generated flow under non-storm conditions will be confined to within 30 m of the surface although extrapolation of the viscosity to the surface layer is perhaps questionable.

During strong storms the surface semidiurnal tide arrives at the coast later (by about 10 degrees, 20 minutes) than under non-storm conditions. This phase lag is attributed to an increased bottom drag coefficient caused by increased bottom speeds due to waves and/or from a mean current generated by winds. The increase in bottom drag implies an adjustment time for integrated motions during storms of 6 - 9 hours, which is consistent with the observed rapid adjustment of sea level and currents during storms (Beardsley and Butman, 1974a). The large damping also implies that inertial energy during storms should not be observed at least in the depth averaged currents. Finally, the increased bottom drag coefficient suggests a significant average bottom stress over the shelf during major wind events.

REFERENCES

Allen, J.R.L. (1965) A review of the origin and characteristics of recent alluvial sediments. Sedimentology, 5, 19-191.

Bagnold, R.A. (1962) Mechanics of marine sedimentation. In Hill, M.N. (ed.), The Sea, V.3, Interscience Publ., John Wiley and Sons, New York.

Barnes, C.A., A.C. Duxbury, and B. Morse (1972) Circulation and selected properties of the Columbia River effluent at sea. In Prater, A.J. (ed.), The Columbia River Estuary and Adjacent Ocean Waters, Univ. of Washington Press, 868 pp.

Beardsley, R.C. and B. Butman (1974a) Circulation on the New England Continental Shelf: Response to strong winter storms. Geophys. Res. Letters, 1(4), 181-184.

Beardsley, R.C. and B. Butman (1974b) New England continental shelf dynamics pilot experiment. Mass. Institute of Technology GFD Lab Report 74-2, 60 pp.

Bennett, J.R. (1974) On the dynamics of wind driven lake currents. J. Phys. Oceanog., 4(3), 400-414.

Bigelow, H.B. (1927) Physical oceanography of the Gulf of Maine. Bull. U.S. Bur. Fish., 40(2), 511-1027.

Blanton, J.O. (1974) Some characteristics of nearshore currents along the north shore of Lake Ontario. J. Phys. Oceanog., 4(3), 415-424.

Bracewell, R. (1965) The Fourier Transform and Its Applications. McGraw Hill, Inc., New York, 381 pp.

Bumpus, D.F. (1973) A description of the circulation on the continental shelf of the east coast of the United States. Progress in Oceanography, 6, Pergamon Press, New York, 111-156.

Bumpus, D.F. (1974) Review of the physical oceanography of Massachusetts Bay. Woods Hole Oceanographic Institution unpublished manuscript, 74-8, 157 pp.

Bumpus, D.F. and L.M. Lauzier (1965) Surface circulation on the continental shelf off eastern North America between Newfoundland and Florida. Am. Geograph. Soc. Serial Atlas of the Marine Environment, Folio 7, 4 pp.

Carter, H.H. and A. Okubo (1965) A study of the physical processes of movement and dispersion in the Cape Kennedy area. Chesapeake Bay Inst., The Johns Hopkins Univ. Ref. 65-2, 150 pp.

Colton, J.B. Jr. (1968) Physical, chemical and biological observations on the continental shelf, Nova Scotia to Long Island 1964-1968. Bureau of Commercial Fisheries, Woods Hole, Mass., 189 pp.

Csanady, G.T. (1971) On the equilibrium shape of the thermocline in a shore zone. J. Phys. Oceanog., 1, 263-270.

Csanady, G.T. (1972a) Frictional currents in the mixed layer at the sea surface. J. Phys. Oceanog., 2(3), 498-508.

Csanady, G.T. (1972b) Geostrophic drag, heat and mass transfer coefficients for the diabatic Ekman layer. J. Atm. Sci., 29(3), 488-496.

Csanady, G.T. (1973a) Wind-induced baroclinic motions on the edge of the continental shelf. J. Phys. Oceanog., 3(3), 274-279.

Csanady, G.T. (1973b) Wind-induced barotropic motions in long lakes. J. Phys. Oceanog., 3(4), 429-438.

Csanady, G.T. (1974) Barotropic currents over the continental shelf. J. Phys. Oceanog., 4(3), 357-371.

Csanady, G.T. and J.R. Scott (1974) Baroclinic coastal jets in Lake Ontario during IFYGL. J. Phys. Oceanog., 4(4), 524-541.

Fjeldstad, J.E. (1929) Contribution to the dynamics of free progressive tidal waves. In The Norwegian North Polar Expedition with the Maud, 1918-1925, Scientific Results, IV, 3. Geofysik Institute, Bergen, 81 pp.

Garvine, R.W. (1974a) Physical features of the Connecticut River outflow during high discharge. J. Geophys. Res., 79(6), 831-846.

Garvine, R.W. (1974b) Dynamics of small scale oceanic fronts. J. Phys. Oceanog., 4(4), 557-569.

Garvine, R.W. and J.D. Monk (1974) Frontal structure of a river plume. J. Geophys. Res., 79(15), 2251-2259.

Gibbs, R.J. (1970) Circulation in the Amazon River estuary and adjacent Atlantic Ocean. J. Mar. Res., 28(2), 113-123.

Godin, G. (1972) The Analysis of Tides. University of Toronto Press, Toronto, 264 pp.

Graham, J.J. (1970) Coastal currents of the western Gulf of Maine. ICNAF Res. Bull., 7, 19-31.

Hathaway, J.C. (1971) Data File, Continental Margin Program Atlantic Coast of the United States. Woods Hole Oceanog. Inst. unpublished manuscript 71-15, in cooperation with U.S. Geological Survey, 496 pp.

Hicks, D., A.J. Goodhart and C.W. Iseley (1965) Observations of the tide on the Atlantic continental shelf. J. Geophys. Res., 70(8), 1877-1830.

Inman, D.L. (1949) Sorting of sediments in the light of fluid mechanics. J. Sed. Pet., 19(2), 51-70.

Inman, D.L. (1963) Sediments: physical properties and mechanics of sedimentation. In Shepard, F.P. (ed.), Submarine Geology, Harper and Row, New York, 101-152.

Ippen, A.T. (ed.) (1966) Estuary and Coastline Hydrodynamics. McGraw Hill Book Co., Inc., New York, 744 pp.

Kranck, K. (1972) Tidal current control of sediment distribution in Northumberland Strait, Maritime Provinces. J. Sed. Pet., 42, 596-601.

Maharaj, V.M. and R.C. Beardsley (1973) Spring Runoff in Massachusetts Bay. Massachusetts Institute of Technology Sea Grant Report 74-9, 103 pp.

McCave, I.N. (1972) Transport and escape of fine-grained sediment from shelf areas. In Swift, D.J.P., D.B. Duane, O.H. Pilkey (eds.), Shelf Sediment Transport: Process and Pattern, Dowden, Hutchinson and Ross, Stroudsberg, Pa., 225-249.

Meade, R.H. (1971) The coastal environment of New England. New England River Basins Commission, Boston, Mass., 47 pp.

Miller, R.I., C.S. Albro, J.M. Cohen, and J.F. O'Sullivan (1972) A preliminary study of tidal erosion in Great Harbor at Woods Hole, Massachusetts. Woods Hole Oceanographic Institution unpublished manuscript 72-12.

Oldale, R.N., E. Uchupi and K.E. Prada (1973) Sedimentary framework of the western Gulf of Maine and the southeastern Massachusetts offshore area. U.S. Geological Survey Professional Paper 757, 10 pp.

Parker, Bruce B. (1974) The response of Massachusetts Bay to wind stress. Master's Thesis (unpublished), Massachusetts Institute of Technology, 107 pp.

Pollard, R.T. and R.C. Millard (1970) Comparison between observed and simulated wind-generated inertial oscillations. Deep-Sea Res., 17, 813-821.

Postma, H. (1967) Sediment transport and sedimentation in the estuarine environment. In Lauff, A.H. (ed.), Estuaries, Publ. 83, American Association for the Advancement of Science, New York, 158-179.

Rao, D.B. and T.S. Murty (1970) Calculation of the steady wind-driven circulations in Lake Ontario. Arch. Met. Geoph. Biokl., Ser. A, 19, 195-210.

Redfield, A.C. (1958) The influence of the continental shelf on the tides of the Atlantic coast of the United States. J. Mar. Res., 17, 432-448.

Rhoads, D.C. and D.K. Young (1971) Animal-sediment relations in Cape Cod Bay, Massachusetts II. Reworking by Molpadia oolitica. Mar. Biol., 11, 255-261.

Ryther, J.H., D.W. Menzel and N. Corwin (1967) Influence of the Amazon River outflow on the ecology of the western tropical Atlantic: I. Hydrography and nutrient chemistry. J. Mar. Res., 25, 69-83.

Schlee, J., D.W. Folger, and C.J. O'Hara (1973) Bottom sediments on the continental shelf off northeastern United States — Cape Cod to Cape Ann, Massachusetts. Misc. Geologic Investigations Map I-746, U.S. Geological Survey, Washington, D.C.

Schlee, J.S. and B. Butman (1974) Adjustment of inner shelf sediments to bottom currents off eastern Massachusetts. Memoires de l'Institut de Géologie du Bassin d'Aquitaine, 7, 75-80.

Schureman, P. (1924) A manual of Hamonic Analysis and Prediction of Tides. Spec. Pub. U.S. C&GS #98, Washington, D.C.

Southard, J.B., R.A. Young, and C.D. Hollister (1971) Experimental erosion of calcareous ooze. J. Geophys. Res., 76(24), 5903-5909.

Sternberg, R.W. (1971) Measurements of incipient motion of sediment particles in the marine environment. Marine Geol., 10, 113-119.

Sternberg, R.W. (1972) Predicting initial motion and bedload transport of sediment particles in the shallow marine environment. In Swift, D.P.J., D.B. Duane, O.H. Pilkey (eds.), Shelf Sediment Transport: Process and Pattern. Dowden, Hutchinson and Ross, Inc., Stroudsberg, Pa., 61-82.

Stommel, H. and A. Leetmaa (1972) The circulation on the continental shelf. Proc. Nat. Acad. Sci. U.S., 69, 3380-3384.

Sundborg, A. (1956) The River Klaralven: a study of fluvial processes. Geograf. Ann., 38, 127-136.

Sverdrup, H.U. (1927) Dynamics of Tides on the north Siberian Shelf, results from the Maud Expedition. Geophysiske Publikationer, IV, 5.

Swift, D.J.P., D.B. Duane, O.H. Pilkey, eds. (1972) Shelf Sediment Transport: Process and Pattern. Dowden Hutchinson and Ross, Inc., Stroudsberg, Pa., 656 pp.

Takano, K. (1954) On the salinity and velocity distribution off the mouth of a river. J. Oceanog. Soc. Japan, 10(3), 92-98

Tucholke, B.E., R.N. Oldale, and C.H. Hollister (1972) Map showing echo-sounding survey of Massachusetts Bay and Cape Cod Bays, Western Gulf of Maine. Misc. Geologic Investigations, Map I-716. U.S. Geological Survey, Washington, D.C.

Tucholke, B.E. and C.H. Hollister (1973) Late Wisconsin glaciation of the southwestern Gulf of Maine: new evidence from the marine environment. Geological Society of America Bulletin, 84, 3279-3296.

Uchupi, E. (1968) Atlantic continental shelf and slope of the United States — Physiography. U.S. Geological Survey Professional Paper 529-C. U.S. Govt. Printing Office, Washington, D.C.

UNESCO (1969) Discharge of selected rivers of the world. UNESCO, Place de Fontenoy, 75 Paris-7^e, 70 pp.

Weatherly, G.L. (1972) A study of the bottom boundary layer of the Florida current. J. Phys. Oceanog., 2(1), 54-72.

Welander, P. (1961) Numerical prediction of storm surges. Advan. Geophys., 8, 316-379.

Wimbush, M. and W. Munk (1971) The benthic boundary layer. In Hill, M.N. (ed.), The Sea, V4, Wiley, New York, 731-758.

Wright, L.D. and J.M. Coleman (1971) Effluent expansion and interfacial mixing in the presence of a salt wedge, Mississippi River delta. Jour. Geophys. Res., 76(36), 8649-8661.

APPENDIX A

TABLE A.1

TIME, DEPTH, AND LOCATION OF NEAR BOTTOM CURRENT METER RECORDS

Station and Record	Deployment Start	Stop	Length (Hr)	Inst. Depth	Sta. Depth (m)	Location Lat.	Long.	Comments
BLS2	710601 -	710629	672	25	30	42 20.6	70 45.5	
BLS3	710629 -	710727	667	25	"			
BLS4/1	710727 -	710806	236	25	"			
BLS4/2	710811 -	710913	792	19	"			
BLS5	710914 -	711002	428	21	"			Hit bottom
BLS6	711019 -	711204	1107	21	"			Ship relocated
BLS8	720118 -	720201	334	21	"			
BLS9/1	720211 -	720311	694	21	"			Ship relocated
BLS9/2	720316 -	720401	389	21	"			
BLS10	720404 -	720516	1005	21	"			
BLS11	720516 -	720617	1006	21	"			Direction (?)
A2	711109			82	83	42 37.7	70 31.1	Time base
A3	720319 -	720425	873	84	85	"	"	
B1	711005 -			46	47	42 30.3	70 44.75	Time base
B2	720211 -			46	"	"	"	Time base, partially corrected
B3	720617 -	720716	680	46	"	"	"	
C1	710831 -	710908	175	89	90	42 19.8	70 26.1	Fisherman picked up
C2	720211 -	720318	853	71	72	42 20.5	70 33.6	
C3	720425 -	720527	749	65	66	"	"	
D1	710626 -	710728	780	26	27	42 10.4	70 17.5	
D2	720113 -	720211	694	26	"	"	"	
D3	720605 -	720712	886	26	"	"	"	
E1	710501 -	710527	627	24	25	42 05.45	70 35.75	Compass (?)
E3	711214 -					"	"	Time base
E4	720320 -	720405	388	18	19	"	"	Drifted
F1	710528 -	710625	681	64	65	42 04.6	70 16.8	
F2	710830 -	710907	182	"	"	"	"	Short, timer malfunction
F3/1	720116 -	720122	130	"	"	"	"	Time base, corrected
F3/2	720125 -	720211	408	"	"	"	"	
F4	720425 -	720504	219	"	"	"	"	Short
RP1 (Vertical Array)	720720 -	720727	162	40	60	42 04.6	70 16.8	
RP2	720720 -	720727	162	55	60	"	"	

APPENDIX B

GAUSSIAN FILTER

In this thesis a Gaussian filter is used to filter time series of currents and sea level. The filter is a standard one employed by the Woods Hole Buoy Group (see write-up of program TAPDIS). For data spaced at uniform intervals, the filter is performed as follows in the time domain:

$$U_1(t_i) = \text{original time series},$$

$$U_2(t_i) = \text{filtered time series},$$

$$U_2(t_j) = A \sum_{k_1}^{k_2} U_1(t_k) \exp(-\alpha(t_k - t_j)^2),$$

$$A^{-1} = \sum_{k_1}^{k_2} \exp(-\alpha(t_k - t_j)^2),$$

$$k_1 = j - (N),$$

$$k_2 = j + (N),$$

$$N = \text{number of data points in time } T_{\frac{1}{2}},$$

$$\alpha = \pi^2/4.5 \; T_{\frac{1}{2}}^2 \; .$$

In the frequency domain, by the convolution theorem (Bracewell, 1965), the result of the filtering is to multiply the Fourier transform of the original series by the Fourier transform of the filtering function. In this case the transform of the Gaussian filter in time is also Gaussian in frequency. The transfer function for the Gaussian filter as a function of $T_{\frac{1}{2}}$, the parameter which determines the frequency response at the filter is shown in figure B.1. The half-power point of the filter occurs approximately where $T_{\frac{1}{2}}/T = .275$.

Figure B.1   Transfer function for Gaussian filter.   Half-power
              point indicated.

TRANSFER FUNCTION FOR
GAUSSIAN FILTER
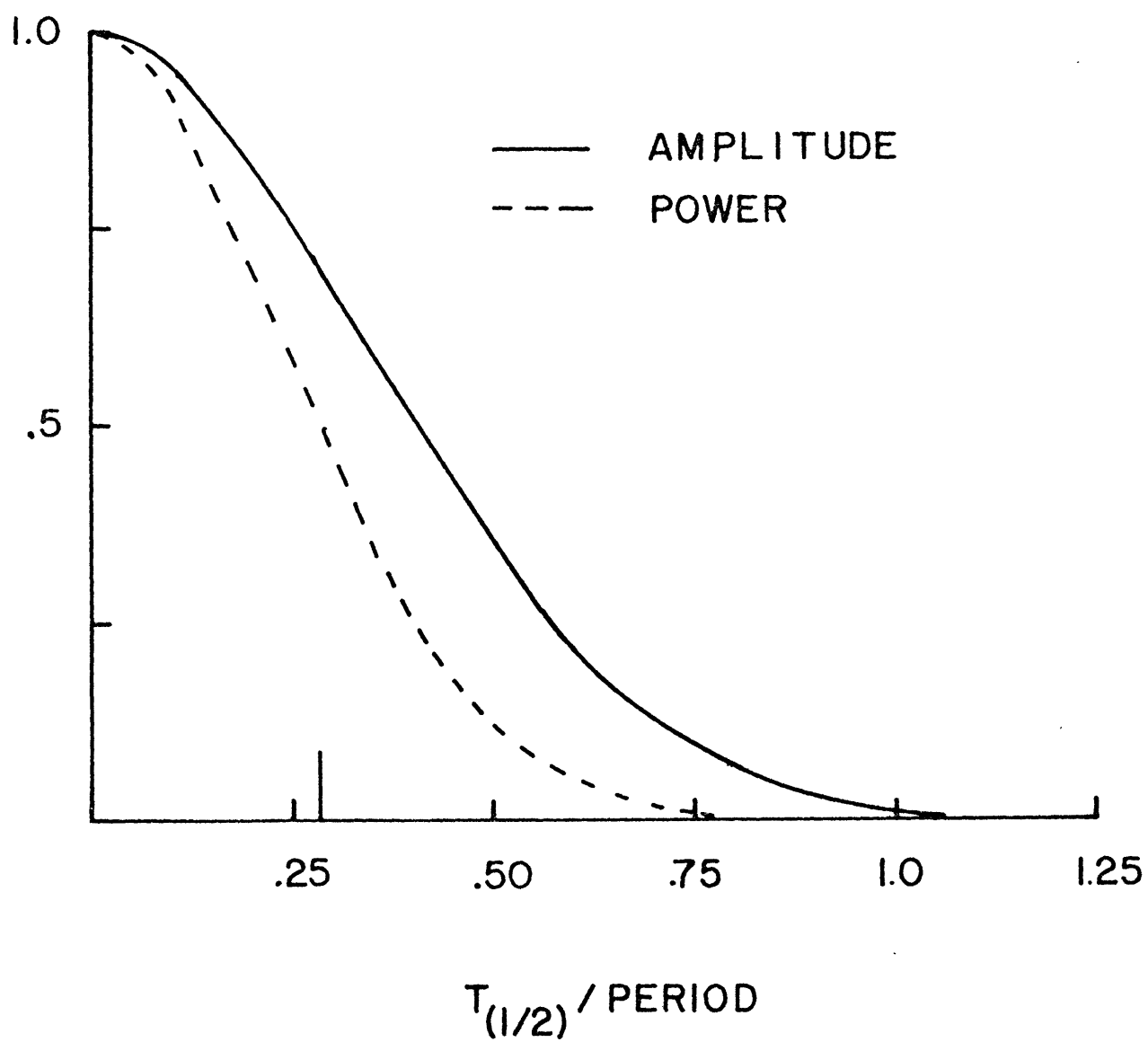

Figure B.1

APPENDIX C

ELLIPSE REPRESENTATION OF CURRENT

A current in two spatial dimensions at one frequency may be represented as two components, as the sum of a clockwise and counter-clockwise rotating vector, or as an ellipse. In each case, four quantities are necessary to specify the current. The component representation is most generally used, where

$$\underset{\sim}{U} = u + iv = \text{vector velocity} , \tag{1}$$

$$u = A_1 \cos\omega t + B_1 \sin\omega t = \text{east-west component} ,$$

$$v = A_2 \cos\omega t + B_2 \sin\omega t = \text{north-south component} .$$

Representing the total complex velocity $\underset{\sim}{U}$ as the sum of a clockwise and counterclockwise rotating current gives:

$$\underset{\sim}{U} = u + iv$$
$$= U_+ e^{i\omega t} + U_- e^{-i\omega t} , \tag{2}$$

$e^{i\omega t}$ = unit vector which rotates counterclockwise ,

$e^{-i\omega t}$ = unit vector which rotates clockwise ,

U_+ and U_- are complex quantities.

Equating (1) and (2) yields

$$\underset{\sim}{U} = (A_1 + iA_2) \cos\omega t + (B_1 + iB_2) \sin\omega t ,$$
$$= (U_+ + U_-) \cos\omega t + i(U_+ - U_-) \sin\omega t , \tag{3}$$

or

$$U_+ = \tfrac{1}{2} [(A_1 + B_2) + i(A_2 - B_1)] \; ,$$

$$U_- = \tfrac{1}{2} [(A_1 - B_2) + i(A_2 + B_1)] \; .$$

(4)

In complex form

$$U_+ = |U_+| e^{i\phi_+} \; ,$$

$$U_- = |U_-| e^{i\phi_-} \; ,$$

(5a)

$$|U_+| = \tfrac{1}{2} [(A_1 + B_2)^2 + (A_2 - B_1)^2]^{\tfrac{1}{2}} \; ,$$

$$|U_-| = \tfrac{1}{2} [(A_1 - B_2)^2 + (A_2 + B_1)^2]^{\tfrac{1}{2}} \; ,$$

(b)

$$\tan \phi_+ = \frac{A_2 - B_1}{A_1 + B_2} \; ,$$

$$\tan \phi_- = \frac{A_2 + B_1}{A_1 - B_2} \; .$$

(c)

The four quantities which specify a current ellipse are (figure C.1):

V = magnitude of major axis ,

rV = magnitude of minor axis ,

θ = ellipse orientation ,

τ = phase of ellipse (where current reaches maximum speed) .

To determine the phase of the current ellipse, we wish the time (relative to $t = 0$) where the velocity vector reaches a maximum. The current magnitude is

$$|\underset{\sim}{U}|^2 = \underset{\sim}{U}\underset{\sim}{U}^* \; ,$$

$$= (U_+ e^{i\omega t} + U_- e^{-i\omega t})(U_+^* e^{-i\omega t} + U_-^* e^{+i\omega t}) \; ,$$

$$= |U_+|^2 + |U_-|^2 + 2|U_+||U_-| \cos (2\omega t + \Delta\phi) \; ,$$

(6)

where

$$\Delta\phi = \phi_+ - \phi_- \; .$$

Figure C.1   Current ellipse showing major and minor axis, orientation, and phase.

CURRENT ELLIPSE

$\omega t = \tau$

rV

V

θ
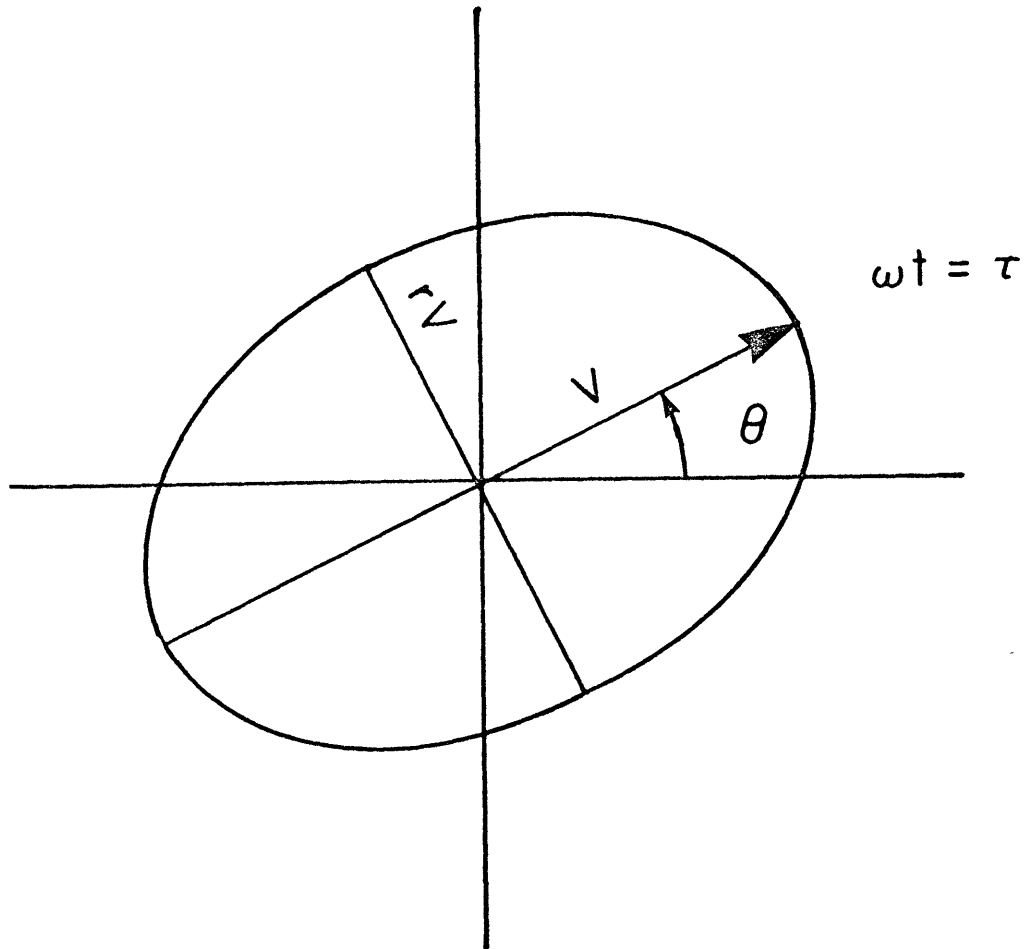
MAJOR AXIS = V

MINOR AXIS = rV

PHASE = τ

ORIENTATION = θ

Figure C.1

The maximum speed is reached where

$$2\omega t + \Delta\phi = 0 \; ,$$

$$\omega t = -\frac{\Delta\phi}{2} \; , \tag{7}$$

$$= \frac{\phi_- - \phi_+}{2} = \tau \; .$$

From (6) the minimum speed occurs where ωt is $\tau + \pi/2$, and is a maximum again at $\omega t = \tau + \pi$. Using (5c) and (7) gives

$$\tan 2\tau = \frac{2(A_1 B_1 + A_2 B_2)}{A_1^2 - B_2^2 + A_2^2 - B_1^2} \; . \tag{8}$$

The amplitude of the major and minor axes is given by (6);

at $\omega t = \tau$, $\left| \underset{\sim}{U} \right| = \left| U_+ \right| + \left| U_- \right|$ = major axis,

$$\tag{9}$$

at $\omega t = \tau + \pi/2$, $\left| \underset{\sim}{U} \right| = \left| U_+ \right| - \left| U_- \right|$ = minor axis.

Finally, to determine the orientation of the ellipse (the angle the major axis makes with respect to the x-axis when $\left| \underset{\sim}{U} \right|$ is maximum) , simply compute $\underset{\sim}{U}$ at $\omega t = \tau$:

$$\underset{\sim}{U}_{max} = \left| U_+ \right| e^{i(\omega t + \phi_+)} + \left| U_- \right| e^{-(i\omega t - \phi_-)} \bigg|_{\omega t = \frac{\phi_- - \phi_+}{2}} \; , \tag{10}$$

$$= (\left| U_+ \right| + \left| U_- \right|)\cos\overline{\phi} + i(\left| U_+ \right| + \left| U_- \right|)\sin\overline{\phi} \; ,$$

where $\overline{\phi} = \frac{\phi_- + \phi_+}{2}$.

The velocity (10) forms an angle θ with the x-axis

$$\tan\theta = \frac{\sin\overline{\phi}}{\cos\overline{\phi}} = \tan\overline{\phi} \; .$$

Using (6c) and (10)

$$\tan 2\theta = \frac{2(A_1 A_2 + B_1 B_2)}{A_1^2 + B_1^2 - (A_2^2 + B_2^2)} \ .$$

(11)

Alternatively, $\overline{\phi}$ can be derived by evaluating the phase of the quantity

$$U_+ U_- = |U_+||U_-| e^{i(\phi_+ + \phi_-)} \ .$$

BIOGRAPHICAL NOTE

Bradford Butman was born October 4, 1947 in Medford, Massachu-
setts. He attended public school in Concord, Massachusetts and
received his B.A. from Cornell University in 1969. After seriously
considering graduate school in city and regional planning, he entered
the Massachusetts Institute of Technology—Woods Hole Oceanographic
Institution Joint Program in Oceanography in 1969. Guided by
interests in science, the environment, the ocean, and by summers
spent on Nantucket Island, he pursued a thesis in coastal oceano-
graphy. The author has accepted a position with the U.S. Geological
Survey in Woods Hole.